

In presenting the dissertation as a partial fulfillment of the requirements for an advanced degree from the Georgia Institute of Technology, I agree that the Library of the Institute shall make it available for inspection and circulation in accordance with its regulations governing materials of this type. I agree that permission to copy from, or to publish from, this dissertation may be granted by the professor under whose direction it was written, or, in his absence, by the Dean of the Graduate Division when such copying or publication is solely for scholarly purposes and does not involve potential financial gain. It is understood that any copying from, or publication of, this dissertation which involves potential financial gain will not be allowed without written permission.

7/25/68

A DETAILED STUDY OF SUBMONOLAYER AND
MULTILAYER ADSORPTION OF KRYPTON ON GRAPHITE

A THESIS

Presented to

The Faculty of the Graduate Division

by


David Sanford Newsome

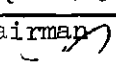
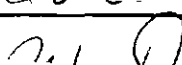
In Partial Fulfillment
of the Requirements for the Degree
Doctor of Philosophy
in the School of Chemistry

Georgia Institute of Technology

January, 1972

A DETAILED STUDY OF SUBMONOLAYER AND
MULTILAYER ADSORPTION OF KRYPTON ON GRAPHITE

Approved: 

Chairman  

Date approved by Chairman: 23 Feb 1972

DEDICATION

I dedicate this thesis to Jane, my wife.

ACKNOWLEDGMENTS

The author expresses his deep appreciation to Dr. Robert A. Pierotti, the director of this research. Dr. Pierotti's help and direction with the experimental and theoretical aspects of the research were a great aid. The author also thanks Mr. John Carden and Mr. Reginald Ramsey for their helpful advice during many conversations on the subject.

TABLE OF CONTENTS

	Page
ACKNOWLEDGEMENTS	iii
LIST OF TABLES	vi
LIST OF ILLUSTRATIONS	viii
GLOSSARY OF ABBREVIATIONS	xi
SUMMARY	xvi
Chapter	
I. INTRODUCTION	1
The Adsorption Isotherm	
Characteristics of the Two-Dimensional State	
Models of the Two-Dimensional State	
Statement of the Problem	
II. DEVELOPMENT OF THE SIGNIFICANT STRUCTURES THEORY OF MULTILAYER ADSORPTION	9
Introduction	
The Multilayer Theory	
Theoretical Isotherms	
III. EXPERIMENTAL APPARATUS	34
Introduction	
Vacuum System	
Dosing System	
Cryostat and Sample Cell	
Pressure Measuring System	
IV. EXPERIMENTAL PROCEDURES	50
Introduction	
Isotherm Temperature Control	
Volume Determinations	
Bake Out of Sample	
Calibration of Capacitance Manometer	
Procedures for Running Isotherms	
Treatment of Data	

TABLE OF CONTENTS (Concluded)

Chapter	Page
V. EXPERIMENTAL DATA	65
Submonolayer Data	
Multilayer Data	
VI. APPLICATION OF THE MULTILAYER SIGNIFICANT STRUCTURES THEORY TO THE KRYPTON-STERLING FT (2700°) SYSTEM. . . .	88
Introduction	
Selection of Theoretical Parameters	
Fit of the Multilayer Theory to the Data	
Discussion of Results	
VII. CONCLUSIONS AND RECOMMENDATIONS	115
APPENDICES	
A. UNCERTAINTIES IN THE THEORETICAL MOLECULAR PARAMETERS .	116
B. EXPERIMENTAL DATA	126
LITERATURE CITED	142
VITA	145

LIST OF TABLES

Table	Page
1. Models of Physical Adsorption	6
2. Adsorption Parameters for Significant Structures Theory as Compared with Some Existing Values	15
3. Molecular Adsorption Parameters Derived from the Multilayer Significant Structures Theory for the Krypton-Sterling FT System at 73.5 K	92
4. Experimental Submonolayer Data for Krypton on Graphite at 69.6 K	127
5. Experimental Submonolayer Data for Krypton on Graphite at 72.4 K	128
6. Experimental Submonolayer Data for Krypton on Graphite at 72.5 K	129
7. Experimental Submonolayer Data for Krypton on Graphite at 73.5 K; Run #1	130
8. Experimental Submonolayer Data for Krypton on Graphite at 73.5 K; Run #2	131
9. Experimental Submonolayer Data for Krypton on Graphite at 74.6 K	132
10. Experimental Submonolayer Data for Krypton on Graphite at 75.6 K	133
11. Experimental Submonolayer Data for Krypton on Graphite at 79.5 K	134
12. Experimental Multilayer Data for Krypton on Graphite at 67.7 K	135
13. Experimental Multilayer Data for Krypton on Graphite at 69.6 K	136
14. Experimental Multilayer Data for Krypton on Graphite at 71.2 K	137
15. Experimental Multilayer Data for Krypton on Graphite at 73.5 K	138

LIST OF TABLES (Concluded)

Table	Page
16. Experimental Multilayer Data for Krypton on Graphite at 74.6 K	140
17. Experimental Multilayer Data for Krypton on Graphite at 77.8 K	141

LIST OF ILLUSTRATIONS

Figure		Page
1.	A Schematic Multilayer Adsorption Isotherm for Krypton on Graphite	3
2.	The Dosing System	37
3.	The Cryostat and Temperature Regulating System	40
4.	The Adsorption System	45
5.	The Capacitance Manometer Head	48
6.	Pierotti's Adsorption of Krypton on Graphite at 74.6°K	66
7.	Submonolayer Adsorption of Krypton on Graphite at 69.6°K	68
8.	Submonolayer Adsorption of Krypton on Graphite at 72.4°K	69
9.	Submonolayer Adsorption of Krypton on Graphite at 72.5°K	70
10.	Submonolayer Adsorption of Krypton on Graphite at 73.5°K; Run I	71
11.	Submonolayer Adsorption of Krypton on Graphite at 73.5°K; Run II	72
12.	Submonolayer Adsorption of Krypton on Graphite at 74.6°K	73
13.	Submonolayer Adsorption of Krypton on Graphite at 75.6°K	74
14.	Submonolayer Adsorption of Krypton on Graphite at 79.5°K	75
15.	Pressure Uncertainties in the 72.4°K Isotherm	79
16.	Pressure Uncertainties in the 72.5°K Isotherm	80
17.	Pressure Uncertainties in the 73.5°K Isotherm; Run I.	81

LIST OF ILLUSTRATIONS (Continued)

Figure		Page
18.	Pressure Uncertainties in the 73.5° K Isotherm; Run II	82
19.	Pressure Uncertainties in the 74.6° K Isotherm	83
20.	Multilayer Adsorption of Krypton on Graphite at 67.7 K, 71.2 K, and 74.6 K	85
21.	Multilayer Adsorption of Krypton on Graphite at 69.6 K, 73.5 K, and 77.8 K	86
22.	Comparison of the Experimental Data to the Significant Structures Multilayer Theory for Krypton on Graphite at 73.5 K; Run I	94
23.	Comparison of the Experimental Data to the Significant Structures Multilayer Theory for Krypton on Graphite at 73.5 K; Submonolayer Region	95
24.	Comparison of the Experimental Data to the Significant Structures Multilayer Theory for Krypton on Graphite at 67.7 K.	96
25.	Comparison of the Experimental Data to the Significant Structures Multilayer Theory for Krypton on Graphite at 69.6° K.	97
26.	Comparison of the Experimental Data to the Significant Structures Multilayer Theory for Krypton on Graphite at 71.2 K	98
27.	Comparison of the Experimental Data to the Significant Structures Multilayer Theory for Krypton on Graphite at 74.6° K	99
28.	Comparison of the Experimental Data to the Significant Structures Multilayer Theory for Krypton on Graphite at 77.8 K	100
29.	Comparison of the Experimental Data to the Significant Structures Multilayer Theory for Krypton on Graphite at 69.6 K; Submonolayer Region	101
30.	Comparison of the Experimental Data to the Significant Structures Multilayer Theory for Krypton on Graphite at 72.4 K; Submonolayer Region	102

LIST OF ILLUSTRATIONS (Concluded)

Figure		Page
31.	Comparison of the Experimental Data to the Significant Structures Multilayer Theory for Krypton on Graphite at 74.6 K; Submonolayer Region . . .	103
32.	Comparison of the Experimental Data to the Significant Structures Multilayer Theory for Krypton on Graphite at 75.6 K; Submonolayer Region	104
33.	Comparison of the Experimental Data to the Significant Structures Multilayer Theory for Krypton on Graphite at 79.5 K; Submonolayer Region . . .	105
34.	Theoretical and Experimental Isosteric Heats of Adsorption for Krypton on Graphite	107
35.	A Simple Model for the Packing of Krypton Atoms on the Graphite Surface in the First and Second Adsorbed Layers	110
36.	The Effect of Changes in U_1 on the Position of the Isotherm	117
37.	The Effect of Changes in U_1 on the Position of the Isotherm; Submonolayer Region	118
38.	The Effect of Changes in ϵ_1 on the Position of the Isotherm	119
39.	The Effect of Changes in ϵ_1 on the Position of the Isotherm; Submonolayer Region	120
40.	Comparison of the Experimental Data to the Theoretical Isotherm After Changing the Packing in the Second and Third Adsorbed Layers	125

GLOSSARY OF ABBREVIATIONS

a	the cell size in the Lennard-Jones and Devonshire cell model
a_f	the free area of a molecule
a_{fi}	the free area of a molecule in the i -th adsorbed layer
A	molar area of the adsorbed phase in McAlpin and Pierotti's significant structures partition function; also the area per molecule in an adsorbed system
A_i	the area per molecule in the i -th layer
A_i^o	the area per molecule when the i -th layer is completed
A_m^o	the area per molecule at monolayer coverage
A_s	the molar area of a two-dimensional solid in McAlpin and Pierotti's partition function
e	the base of the natural logarithms
\exp	the base of the natural logarithms
h	Planck's constant
k	Boltzmann's constant
n_c	the number of moles of gas in V_c
n_d	the number of moles of gas in a dose
n_h	the number of moles of gas in V_h ; also the number of nearest neighbor holes
n_{i+1}	the total number of moles of gas in dose $i + 1$
$n_{g,i}$	the number of moles of gas remaining in gas phase after dose i is added
$n_{s,i}$	the number of moles of gas adsorbed after dose i is added

GLOSSARY OF ABBREVIATIONS (Continued)

$n_{t,i}$	total number of moles of gas in the gas phase and adsorbed after dose i is added
N	Avogadro's number; also the number of molecules adsorbed; also the number of cells in a system
N_i	the numbers of molecules in the i -th layer
N_o	the number of adsorption sites on the adsorbent
P	the pressure
$P_{1,i}$	the true equilibrium gas pressure after dose i is added ($P_{2,i}$ corrected for thermal transpiration)
$P_{2,i}$	the measured equilibrium gas pressure after dose i is added
q_{ig}	the molecular partition function for the gaslike structure in the i -th layer
q_{is}	the molecular partition function for the solidlike structure in the i -th layer
q_{st}	the isosteric heat of adsorption
q_z	the quantum mechanical harmonic oscillator partition function for the vibration of the adsorbed molecule in the z direction normal to the surface
Q	canonical partition function
Q_{ads}	the adsorbed phase partition function in McAlpin and Pierotti's approach
Q_i	the canonical partition function for the i -th adsorbed layer in the multilayer significant structures approach
Q_g	the three-dimensional gaslike partition function
Q_s	the three-dimensional solidlike partition function
Q_{2g}	the two-dimensional gaslike partition function in McAlpin and Pierotti's approach
Q_{2s}	the two-dimensional solidlike partition function in McAlpin and Pierotti's approach

GLOSSARY OF ABBREVIATIONS (Continued)

r	the distance from the cell center to a given molecule in the Lennard-Jones and Devonshire cell model; also the internuclear distance between two atoms
r^*	the internuclear distance at the potential minimum in the Lennard-Jones 6-12 potential equation
R	the gas constant
T	the absolute temperature
T_c	the temperature of the sample
T_r	the room temperature
T_{2c}	the two-dimensional critical temperature
U_o	the gas-surface interaction parameter for submonolayer adsorption
U_i	the molar site energy for an isolated molecule in the i -th layer
v	the volume of a cell
v_f	the free volume of a molecule
V	the volume of a gas; also the molar volume of a liquid
V_{ads}	the volume of gas adsorbed per gram of adsorbent at STP
V_c	the volume of the sample cell bulb and as much of the tube coming to the bulb as is under the liquid coolant level
V_{cm}	the volume of the capacitance manometer between stopcocks 2 and 3 in Figure 5
V_h	the volume of the system from stopcock 1 to stopcock 3, except for that volume contained in V_c as seen in Figure 4
V_m	the volume of adsorbate at STP needed to complete a monolayer
V_s	the molar volume of a solid

GLOSSARY OF ABBREVIATIONS (Continued)

V_{sys}	the apparent volume of the system when the sample is at room temperature; this includes all the volume between stopcocks 1 and 3 in Figure 4
W_i	the molar two-dimensional lattice energy of the adsorbate in the i -th layer
W_0	the molar two-dimensional lattice energy of the adsorbate in submonolayer adsorption
z	the coordination number of the lattice
Z_N	the configurational integral

Greek Symbols:

ϵ	the Lennard-Jones interaction parameter
ϵ_i	the Lennard-Jones interaction parameter in the i -th layer
ϵ_h	the strain energy or the energy a molecule must possess to enter a hole
θ	the experimental fractional surface coverage defined by equation (2); also the theoretical statistical coverage defined by equation (23)
θ_i	the theoretical statistical coverage in the i -th layer defined by equation (21)
Λ	an abbreviation used for $\frac{h}{(2\pi mkT)^{1/2}}$
μ	the chemical potential
μ_g	the chemical potential of the gas phase
μ_g^0	the chemical potential of a gas in its standard state
μ_i	the chemical potential of the i -th adsorbed layer
ν	the vibrational frequency of the adsorbed molecule in the z direction normal to the surface
σ	the molecular hard sphere diameter

GLOSSARY OF ABBREVIATIONS (Concluded)

Subscripts:

ads	adsorbed phase
c	critical; also cold
g	gaslike phase
h	hot
i	layer number
s	solidlike phase

SUMMARY

This work is concerned with the interaction of krypton atoms with graphitized carbon black (Sterling FT(2700°)) in the temperature range from about 67°K to 79°K. Both submonolayer and multilayer work is reported, and the phenomenon of two-dimensional condensation is observed.

The apparatus used in this study is a conventional high vacuum type which measures temperatures, pressures, and volumes. The pressure measuring system consists of a U-tube manometer, a McLeod gauge, and a Granville-Phillips capacitance manometer. The U-tube manometer and McLeod gauge are used to calibrate all volumes and to measure the gas doses. The McLeod gauge is also used to calibrate the capacitance manometer, which in turn is used to measure the equilibrium krypton gas pressures above the graphite sample.

A theory of multilayer adsorption based on the significant structures theory of liquids is developed. Theoretical isotherms and heats of adsorption for the krypton-Sterling FT(2700°) system are obtained from this theory. The theory shows steps in the isotherms with condensation predicted for the first, second, and third adsorbed layers. Molecular adsorption parameters are obtained by a theoretical fit of the experimental data. A two-dimensional critical temperature of about 69.6°K is predicted by this model for the krypton-Sterling FT(2700°) system. This is quite close to our experimentally observed value.

CHAPTER I

INTRODUCTION

The Adsorption Isotherm

When a gas comes in contact with a solid material, a process called adsorption can occur. Two types of adsorption processes are possible: chemisorption and physical adsorption. Chemisorption is a chemical reaction occurring between the solid surface and the gas. Examples of this process are common and numerous, notable examples being oxidation of a metallic surface and the reaction of carbon monoxide with a metal surface. The heats of chemisorption are of the order of those found in normal chemical reactions. Chemisorption will not be considered further in this work. Physical adsorption is characterized by a heat change of the same order of magnitude as that evolved when a gas liquifies, rarely being above 5000 calories per mole. As the name implies, the forces involved in this process are "physical" or "van der Waals" type forces. This work is concerned with the physical adsorption of rare gases on inert solids.

The phase rule for two-dimensional physical adsorption is formulated by de Boer and Broekhoff (1) as

$$V = C - P + 2 - \sum_j (n_j - 1) \quad (1)$$

where V is the variance of the system, C is the number of chemical components, P is the number of distinguishable three dimensional phases, and n_j is the number of two-dimensional phases present at the same surface. This equation is valid for any number of independent, two-dimensional phases stacked on top of each other and adsorbed on a solid substrate. Assume that we have a solid adsorbent with only one type of face, and adsorbed on this solid is one two-dimensional phase. From equation (1) the variance for this system is two; thus, if any two of the thermodynamic variables are fixed, the state of the system is fixed. The usual procedure in surface chemistry is to fix the temperature and the gas phase pressure above the solid adsorbent, thus determining the total state of the system. It is then common to report the results as the amount of gas adsorbed as a function of gas pressure at a given temperature; this is called an adsorption isotherm.

Characteristics of the Two-Dimensional State

Surface chemists usually separate physical adsorption into two classes: submonolayer and multilayer adsorption. Adsorption limited to one molecular layer or less is known as submonolayer adsorption, while multilayer adsorption is the adsorption of more than one molecular layer.

A schematic multilayer isotherm for krypton adsorbed on graphitized carbon black is shown in Figure 1. Here θ is defined as

$$\theta = \frac{V_{\text{ads}}}{V_m} \quad (2)$$

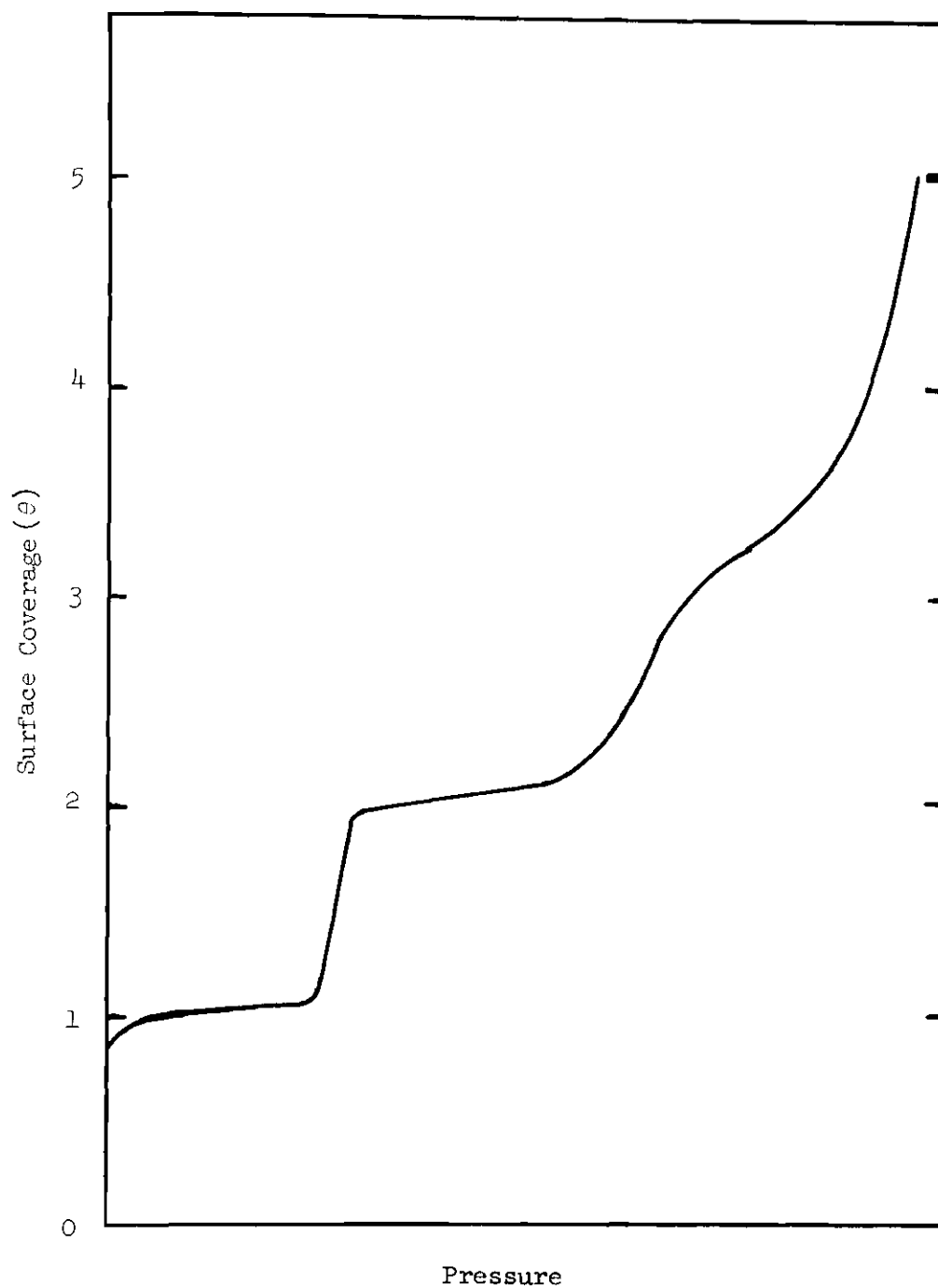


Figure 1. A Schematic Multilayer Adsorption Isotherm for Krypton on Graphite.

where V_{ads} is the volume of the gas adsorbed at STP, and V_m is the volume of the adsorbate at STP which is necessary to form a complete surface layer.

Steps are clearly visible in the isotherm in Figure 1. It can be seen that the steps, taken as being successive adsorbed layers, begin and end at near integral values of θ . The height of each step is about equal, and represents the amount of gas needed to complete that particular layer.

We have already seen that the phase rule applies to the adsorbed state. In fact, a whole class of classical thermodynamics for physical adsorption has been developed by several workers, and adsorption phenomena are often interpreted in this manner. Other thermodynamic behavior usually only thought of as applying to ordinary three-dimensional systems has been seen or predicted for adsorbed two-dimensional systems. Such behavior includes phase changes on the surface, two-dimensional critical temperatures in the adsorbed layers, and two-dimensional triple points. Davis and Pierce (2), who studied adsorption of polyatomic molecules on Sterling MT, a graphitized carbon black, summarized the behavior of the stepwise isotherm as follows:

1. The height of the vertical region in a step decreases with temperature.
2. The pressure at which the vertical region occurs in a step increases with temperature.
3. Above a critical temperature, the vertical region in a step disappears.

Other workers (3) have made similar observations. The occurrence of

phase transitions and triple points have also been seen in computer generated two-dimensional fluids (4).

Models of the Two-Dimensional State

Historically, physical adsorption has been divided into the submonolayer and multilayer regions for theoretical and experimental study. Let us begin this section with some models of submonolayer adsorption.

Submonolayer Adsorption

This region of adsorption has received a great deal of theoretical attention and consequently is much better understood than multilayer adsorption. In attempting to explain the adsorption process, some workers (5,6) in the past have devised kinetic mechanisms of adsorption and arrived at isotherm equations. Another method of arriving at an isotherm equation is to transform a three-dimensional equation of state into two-dimensional form by using the "Gibbs adsorption isotherm" derived from classical thermodynamics. Table 1 shows some of these isotherm equations. These kinetic and thermodynamic models are useful in that they are simple and give some insight into the adsorption process. With the exception of the van der Waals equation, however, these models give no information of the adsorption process on a molecular level.

To obtain a detailed molecular interpretation of adsorption one must apply the methods of statistical mechanics. A very good theory of submonolayer physical adsorption based on statistical mechanics is a theory devised by McAlpin and Pierotti (7,8) called the

Table 1. Models of Physical Adsorption

Model	Isotherm Equation
Mobile film with no lateral interaction in the adsorbed layer (Volmer Equation)	$P = k \left(\frac{\theta}{1 - \theta} \right) \exp \left(\frac{\theta}{1 - \theta} \right)$
Two-dimensional van der Waals equation	$P = k \left(\frac{\theta}{1 - \theta} \right) \exp \left(\frac{\theta}{1 - \theta} - \frac{2\alpha\theta}{kT\beta} \right)$
Localized film with no lateral interactions (Langmuir Equation)	$P = k \left(\frac{\theta}{1 - \theta} \right)$
Localized film with interaction	$P = k \left(\frac{\theta}{1 - \theta} \right) \exp \left(- \frac{cw\theta}{kT} \right)$

significant structures theory of adsorption. The isotherm equation for this model can be written (9)

$$\ln P = - \frac{\mu_g^0}{kT} - 2\theta \ln \left[\left(\frac{B\theta}{C} \right) \left(1 + z \left\{ \frac{1 - \theta}{\theta} \right\} \right) \right] + \frac{5\theta^2}{z - (z-1)\theta} - \ln \left(\frac{C}{\theta} \right) + 1. \quad (3)$$

This theory will be discussed in much greater detail in Chapter II. For now, it will suffice to say that equation (3) predicts two-dimensional condensation, critical temperatures, and isotherm temperature dependence, all in terms of intermolecular potential.

Multilayer Adsorption

Of the very few theories of multilayer adsorption existing at the present time, the BET theory (10) is the most discussed, and accounts of it are given in almost any book dealing with adsorption. The BET theory has no doubt stimulated a great deal of research and thought in surface chemistry. Despite this, the model is extremely crude, being based on the Langmuir model, and it gives no information on a molecular level.

Pace (11) has developed a statistical model of multilayer adsorption based on the lattice vacancy theory, and this work has been further extended by Pierotti (12). The heats of adsorption predicted by the model are in good agreement with experiment for argon-like molecules adsorbed on graphitized carbon. The theoretical isotherms which the model predicts are not as realistic, however.

Pierotti and Thomas (12) have outlined some other approaches

to the multilayer problem.

Statement of the Problem

The purpose of this work is to investigate the physical adsorption of krypton on graphitized carbon black over a fairly wide temperature range around the two-dimensional critical temperature. Sterling FT (2700[°]) is the type of carbon black used and both submonolayer and multilayer regions are investigated. This Kr-Sterling FT system has been studied very little previously, and there is some doubt in our mind as to the validity of some of the work which has been done on this system. Of particular interest to us are two-dimensional condensation, critical temperatures, and the dependence of the isotherms on temperature.

The apparatus which was used to make these measurements is a modification of a volumetric apparatus previously used by Pierotti (13) and Levy (14).

A theory to treat adsorption in all ranges, both submonolayer and multilayer, is developed. This theory is a statistical thermodynamic theory based on the significant structures theory of liquids. The resulting isotherm equation is tested with the data obtained for the krypton - Sterling FT system and molecular parameters are obtained for the system.

This work will now be presented in the following pages, beginning with the development of the theoretical model in Chapter II.

CHAPTER II

DEVELOPMENT OF THE SIGNIFICANT STRUCTURES

THEORY OF MULTILAYER ADSORPTION

Introduction

The direct evaluation of the classical configurational integral for a real liquid is not possible. Cell theories of the liquid state are merely a way of dividing the configurational integral into N solvable integrals, where N is the number of cells in the system. The partition function is then a product of the N identical configurational integrals for each cell.

In the cell theory, each molecule is assumed to be confined to a certain region of space in the entire volume, V , of the liquid. These regions of space, or cells, are formed by the nearest neighbors of the molecule. If there are N such cells, then each cell has a volume $v = V/N$. If we assume there are no intermolecular forces between molecules, then the configurational integral, Z_N , is (15)

$$Z_N = v^N. \quad (4)$$

If however, there is an intermolecular potential between the molecules in the cells, as a function of position in the cell, then the total volume of the cell is no longer available to the central molecule.

There is instead a "free" volume through which the molecule can move.

The configurational integral is now

$$Z_N = v_f^N \quad (5)$$

where v_f is the "effective" or "free" volume. By assuming some sort of intermolecular potential, Z_N can thus be found.

The most successful of the cell theories is the so called significant structures theory, originally developed by Eyring and co-workers (16) and later modified by Henderson (17). The theory is a logical extension of the original cell model, with the idea of an empty cell, or hole, being added. As the theory is based partly on experimental evidence and partly on intuition, the lack of rigor in its development is the most frequently used argument against it. Its success in accounting for the properties of fluids is, however, excellent.

X-ray data show that the nearest neighbor distance in liquids, such as argon, is not greatly different from the nearest neighbor distance in the solid. The molar volume of the liquid is, however, about 12 per cent greater than that of the solid. Short range order is also known to exist in a liquid. These facts suggest that a fluid could possibly be represented by a pseudo-lattice structure in which the lattice sites are either molecules or holes. According to Eyring (18), these holes contribute gaslike properties to the fluid and the fluid therefore has solidlike qualities from the filled cells and

gaslike qualities from the holes. Another degree of freedom which must be considered is the positional degeneracy due to the presence of vacant sites in the solidlike lattice. In significant structures theory one chooses these three structures as the important ones which characterize the liquid state and ignores all other structures. In writing a partition function for a significant structures fluid, one must include

1. Solidlike degrees of freedom
2. Positional degeneracy degrees of freedom due to the presence of holes
3. Gaslike degrees of freedom.

A partition function which satisfies these requirements is (19)

$$Q = \left\{ Q_s \left[1 + n_h \exp \left(- \frac{\epsilon_h}{RT} \right) \right] \right\}^{\frac{V_s N}{V}} \left[Q_g \right]^{\frac{(V-V_s)N}{V}} . \quad (6)$$

Q_s is the solidlike partition function and Q_g is the gaslike partition function. The term multiplying Q_s in equation (6) is the total number of positions available to a molecule in the fluid. This is the positional degeneracy factor spoken of earlier. Here n_h is proportional to the number of holes available to a solidlike molecule and ϵ_h is the so called strain energy, or the energy a molecule must possess to enter a hole, thus excluding its competing neighbors. The fraction V_s/V of the degrees of freedom should be solidlike, where V and V_s are the molar volumes of the liquid and of the solid,

respectively. $(V - V_s)/V$ is the fraction of the degrees of freedom of the fluid which should be gaslike.

Any suitable partition functions desired can be used for Q_s and Q_g . Eyring (18) chose to use the ideal gas partition function for Q_g and the Einstein solid partition function for Q_s .

McAlpin and Pierotti (7,8) were the first workers to treat physical adsorption with the significant structures theory. They pointed out that a two-dimensional adsorbed phase is a better candidate for treatment by a lattice or hole theory than its three-dimensional counterpart. The idea of filled sites and empty sites, or holes, has long been accepted in surface chemistry, whereas in liquids the idea of a hole seems somewhat artificial. By assuming that the strain energy was zero, McAlpin and Pierotti (7,8) arrived at a two-dimensional partition function for adsorption limited to one molecular layer. Their partition function is

$$Q_{\text{ads}} = \left[Q_{2s} \right]^{\frac{NA_s}{A}} \left[Q_{2g} \right]^{\frac{N(A - A_s)}{A}} \quad (7)$$

where Q_{ads} , Q_{2s} , and Q_{2g} are the partition functions for the adsorbed phase, the two-dimensional solidlike structure, and the two-dimensional gaslike structure. A_s is the molar area of the two-dimensional solid, and A is the molar area of the adsorbed phase. N is the number of molecules adsorbed. McAlpin and Pierotti (7) used the Einstein crystal

model for the solidlike degrees of freedom and the ideal gas model for the gaslike degrees of freedom. Their results were in good agreement with experiment. McAlpin (8,9) also used the cell model of Devonshire for the solidlike degrees of freedom. This is probably a better choice than the Einstein model since the results are expressed in terms of ϵ , the Lennard-Jones interaction parameter, instead of the less interesting Einstein characteristic temperature. The complete canonical partition function for the adsorbed film is (12)

$$Q_{\text{ads}} = \left[\Lambda^{-2} q_z \exp\left(\frac{U_0}{RT}\right) \right]^{\theta N_m} \left[a_f \left(\exp\left(\frac{W}{NkT}\right) \right) \left(1 + \frac{z(1-\theta)}{\theta} \right) \right]^{\theta^2 N_m} \quad (8)$$

$$\times \left[\frac{A_m^0}{\theta} \right]^{\theta N_m (1-\theta)}$$

and the resulting isotherm equation is (9)

$$\ln P = - \frac{\mu_g^0}{kT} - 2\theta \ln \left[\left(\frac{B\theta}{C} \right) \left(1 + z \left(\frac{1-\theta}{\theta} \right) \right) \right] + \frac{5\theta^2}{z - (z-1)\theta} - \ln\left(\frac{C}{\theta}\right) + 1 \quad (9)$$

where

$$B = D \left(\frac{2\pi mkT}{h^2} \right) a_f \exp\left(\frac{W}{RT}\right)$$

$$C = D \left[\left(\frac{2\pi mkT}{h^2} \right) e^{\frac{\mu_g^0}{RT}} A_m^0 \right]$$

$$D = \left(\frac{e^{-\frac{h\nu}{2kT}}}{1 - e^{-\frac{h\nu}{kT}}} \right) e^{\frac{U_0}{RT}}$$

μ_g^0 = standard chemical potential of the gas phase

z = coordination number of the assumed lattice

a_f = free area of the adsorbate

W = molar two-dimensional lattice energy of the adsorbate

A_m^0 = area per molecule adsorbed at monolayer capacity

ν = vibrational frequency of the adsorbate normal to the surface

U_0 = molar gas-surface interaction parameter

and all the other symbols have their common meanings. This equation has been used successfully to describe a great deal of adsorption phenomena. Table 2 shows some parameters predicted by this theory as compared to some existing values.

The agreement with existing values is good. The significant structures theory predicts somewhat lower two-dimensional critical temperatures than does either the cell model of Devonshire (22) or the two-dimensional van der Waals theory. Our experience indicates that the two-dimensional critical temperatures predicted by significant structures theory are much more in line with experiment, at least in

Table 2. Adsorption Parameters for Significant Structures Theory as Compared with Some Existing Values

System	U_o (cal/mole)	$\nu \times 10^{-12}(\text{sec}^{-1})$	$\epsilon/k(^{\circ}\text{K})$	A_m^o ($\text{\AA}^2/\text{molecule}$)
Ar - C	2204 ^a	2.13 ^a	110 ^a	14.6 ^e
	2200 ^b	1.28 ^c	96 ^b	15.4
	2120 ^c	2.3-2.7 ^c		
Ar - BN	1900 ^a	1.16 ^a	112 ^a	14.6 ^e
	1950 ^d			15.4

a. Significant structures theory value (Reference 9)

b. Reference 20

c. Reference 21

d. Reference 13

e. Obtained from liquid densities

the systems we have studied.

Considering the success of the significant structures theory in the area of submonolayer adsorption, we have extended the theory into the multilayer region. The multilayer partition function and isotherm equations will now be developed, and the resulting equations will then be tested with experimental data in Chapter VI.

The Multilayer Theory

The Model

The model used here is one where two-dimensional liquidlike layers adsorb on a structureless, energetically uniform surface. The surface imposes no structure on the adsorbed layers. Each layer is thus assumed to be in a hexagonal close-packed, or triangular, configuration. The number of sites for adsorption in the i^{th} adsorbed layer is N_{i-1} , where N_{i-1} is the number of molecules adsorbed in the $(i-1)$ layer. The number of adsorption sites on the surface is N_0 .

The energy of a molecule in a layer is made up of two contributions: 1) site energy and 2) lateral interaction energy. The site energy is the energy an isolated molecule in the i^{th} layer derives from the surface interaction and also from its interaction with all the molecules in the $(i-1)$ layers beneath the i^{th} layer. The adsorbate-adsorbate interaction, or lateral interaction, in any layer is assumed to follow a Lennard-Jones 6-12 potential and is assumed to be pairwise additive. Molecular vibrations in the z direction normal to the surface are assumed to be the same in every layer. A quantum mechanical harmonic oscillator model is used to describe these vibrations in the

z direction. Just as in the submonolayer case, each adsorbed layer is assumed to have three significant structures, or degrees of freedom: a solidlike degree of freedom, a configurational degeneracy of the solidlike degree of freedom due to the presence of holes, and a gaslike degree of freedom. The strain energy in this model is assumed to be zero.

The Partition Function

The canonical partition function for the i^{th} adsorbed layer of the model can be written as

$$Q_i = q_{is}^{N_i \left(\frac{N_i}{N_{i-1}} \right)} q_{ig}^{N_i \left(\frac{N_{i-1} - N_i}{N_{i-1}} \right)} \quad (10)$$

where q_{is} is the molecular partition function for the solidlike structure in the i^{th} layer and q_{ig} is the corresponding molecular partition function for the gaslike structure. N_i is the number of molecules in the i^{th} layer, and N_{i-1} is the number of molecules in the $(i-1)$ layer. The N_{i-1} molecules are also the number of adsorption sites available to the N_i molecules in the i^{th} layer. The expression for Q_i is seen to have the right limits. When the i^{th} layer approaches completion, (N_i/N_{i-1}) approaches 1 and $(N_{i-1}-N_i/N_{i-1})$ approaches 0. The solidlike degrees of freedom then dominate and this is certainly expected. When the i^{th} layer is just beginning to fill, the opposite is true, and the gaslike degrees of freedom dominate Q_i . This also is the correct behavior.

For q_{is} we use the partition function for the cell model as given by Devonshire (22), which also includes a term for the configurational degeneracy. The partition function for the solidlike degrees of freedom in the i^{th} layer is then

$$q_{is} = (\Lambda^{-2} a_{fi}) \left[\exp \left(\frac{U_i + W_i}{RT} \right) \right] (1 + n_h) \times q_z. \quad (11)$$

The first term on the right of equation (11) is the partition function for a Lennard-Jones and Devonshire two-dimensional fluid, where a_{fi} is the free area in the i^{th} layer and is given by

$$a_{fi} = \pi a^2 \int_0^{\frac{1}{4}} \exp \left[\left(\frac{6\epsilon_i}{kT} \right) \{ 2m_s(y) - l_s(y) \} \right] dy \quad (12)$$

where

a is the diameter of the cell containing the molecule

ϵ_i is the Lennard-Jones interaction parameter in the i^{th} adsorbed layer

$m_s(y)$, $l_s(y)$ are polynomials whose form is given by Lennard-Jones and Devonshire

$y = (r/a)^2$ where r is the distance from the cell center to molecule

The second term in equation (11) is a correction for energy

zero, which is taken as a molecule at rest infinitely removed from the surface. U_i is the molar adsorptive potential, or the molar site energy for an isolated molecule in the i -th layer. U_i includes both an adsorbate-adsorbent interaction term and the interaction of the molecule with all the molecules in the $(i-1)$ layers below the i -th layer. W_i is the molar two-dimensional lattice energy of the adsorbate in the i^{th} adsorbed layer. W_i is obtained by assuming pairwise interactions hold and summing the Lennard-Jones 6-12 potential function over the assumed lattice. More will be said of this in Chapter VI.

The third term in equation (11) is the degeneracy factor for the strained solid state. Eyring (23) expresses n_h as

$$n_h = \frac{n(V - V_s)}{V_s} \quad (13)$$

where n is a proportionality constant. The other terms have been defined previously. Following McAlpin (9) we let n_h be expressed as

$$n_h = \frac{z(A_i - A_i^o)}{A_i^o} \quad (14)$$

where z is the coordination number (6 for triangular lattice), A_i is the area per molecule in the i -th layer, and A_i^o is the area per molecule in the i -th layer when the i -th layer is filled to capacity.

The last term in equation (11) is the quantum mechanical harmonic oscillator partition function for the vibration in the z direction normal to the surface. It is assumed to be the same in all layers and is written as

$$q_z = \frac{\exp\left(\frac{-h\nu}{2kT}\right)}{1 - \exp\left(\frac{-h\nu}{kT}\right)} \quad (15)$$

where ν is the vibrational frequency.

The molecular partition function for the gaslike structure in the i^{th} adsorbed layer is

$$q_{ig} = q_z \left\{ \exp\left(\frac{U_i}{RT}\right) \right\} (\Lambda^{-2} A_i e). \quad (16)$$

The meaning of the symbols has been explained previously. The first term on the right side of equation (16), q_z , is a gas-solid interaction term where the molecules in the i^{th} layer are vibrating in a parabolic potential well whose minimum is U_i calories per mole below the energy zero. The last term on the right side of equation (16) is the partition function for an ideal, two-dimensional gas molecule.

The expressions for q_{ig} and q_{is} , equations (16) and (11), are now combined with equation (10) to find Q_i . Substituting in the expression for n_h in equation (14) we find that

$$Q_i = \left[\Lambda^{-2} a_{fi} \left\{ \exp\left(\frac{U_i + W_i}{RT}\right) \right\} q_z \left(1 + \frac{z(A_i - A_i^o)}{A_i} \right) \right]^{N_i \left(\frac{N_i}{N_{i-1}} \right)} \quad (17)$$

$$\times \left[q_z \left\{ \exp\left(\frac{U_i}{RT}\right) \right\} \Lambda^{-2} A_i e \right]^{N_i \left(\frac{N_{i-1} - N_i}{N_{i-1}} \right)}.$$

Combining terms we find that

$$Q_i = \left[\Lambda^{-2} q_z \exp\left(\frac{U_i}{RT}\right) \right]^{N_i} \left[a_{fi} \left\{ \exp\left(\frac{W_i}{RT}\right) \right\} \left(1 + \frac{z(A_i - A_i^o)}{A_i^o} \right) \right]^{N_i \left(\frac{N_i}{N_{i-1}} \right)} \quad (18)$$

$$\times \left[A_i e \right]^{N_i \left(\frac{N_{i-1} - N_i}{N_{i-1}} \right)}.$$

The total partition function, Q , for all i adsorbed layers is

$$Q = \prod_i Q_i \quad (19)$$

or

$$\ln Q = \sum_i \ln Q_i. \quad (20)$$

This partition function for our multilayer model is now used to

compute theoretical adsorption isotherms.

Theoretical Isotherms

Introduction

Theoretical isotherms are determined by finding the chemical potential for the adsorbed molecules in each layer and equating these to each other and to the chemical potential of the gas phase. This procedure yields i equations in i unknowns, where i is the number of layers assumed. The i unknowns are the ratios of $N_i/(N_{i-1})$, $N_{i-1}/(N_{i-2})$, . . . , N_1/N_0 . In the multilayer significant structures theory, we define the coverage in the i^{th} layer, θ_i , as

$$\theta_i = \frac{N_i}{N_{i-1}} \quad \text{for } i = 1, 2, 3, \dots \quad (21)$$

A set of θ_i 's are then the solution of the theoretical isotherm equations. The total statistical coverage, θ , is

$$\theta = \left(\frac{1}{N_0} \right) \sum_{i=1}^{\infty} N_i \quad (22)$$

or

$$\theta = \left(\frac{1}{N_0} \right) \sum_{i=1}^{\infty} N_{i-1} \theta_i. \quad (23)$$

The statistical coverage, θ , is one parameter which will be used in comparing the theory to experiment. The experimental coverage has

already been mentioned in equation (2); this coverage is really an adjustable parameter since the capacity of a full layer is rather uncertain.

The other parameter which will be used in comparing the theory to experiment is the gas phase pressure, P . In the multilayer significant structures theory, if one arbitrarily sets the pressure in the gas phase, a whole set of θ_i 's can be determined from the set of i equations. By then varying P at a given temperature one can generate a theoretical multilayer isotherm.

Equation (20) can be expanded as

$$\ln Q = \ln Q_1(N_0, N_1) + \ln Q_2(N_1, N_2) + \ln Q_3(N_2, N_3) + \dots + \quad (24)$$

$$\ln Q_i(N_{i-1}, N_i) .$$

From equation (17) it is obvious that the logarithm of the partition function for each layer is a function of the number of molecules in that layer and also the number of molecules in the layer directly beneath, as shown in equation (24). The chemical potential of the molecules in the i^{th} layer is given by

$$\frac{\mu_i}{kT} = - \left(\frac{\partial \ln Q}{\partial N_i} \right)_{N_{k \neq i}, T} . \quad (25)$$

It should be noted that the chemical potential in the i^{th} layer is found by differentiating the total assembly partition function and not the i^{th} layer partition function. From the last two equations it can be seen that

$$\frac{\mu_i}{kT} = - \left[\left(\frac{\partial \ln Q_i}{\partial N_i} \right) + \left(\frac{\partial \ln Q_{i+1}}{\partial N_i} \right) \right]_{N_{k \neq i}, T} \quad (26)$$

If the gas phase is taken to be an ideal monatomic gas, the chemical potential is (24)

$$\frac{\mu_g}{kT} = - \ln \left[\left(\frac{2\pi m k T}{h^2} \right)^{\frac{3}{2}} kT \right] + \ln P. \quad (27)$$

These last two equations are the ones which will be used to find the theoretical isotherm equations.

The One Layer Case

We will now consider the case of limiting adsorption to one molecular layer. This is the simplest of all possibilities and a good way to begin a test of the model. For one layer it is seen from equation (20) that

$$\ln Q = \ln Q_1. \quad (28)$$

Let us now make the following definitions:

$$X_i = \Lambda^{-2} q_z \exp\left(\frac{U_i}{RT}\right) \quad (29)$$

$$Y_i = a_{fi} \left[\exp\left(\frac{W_i}{RT}\right) \right] \left[1 + \frac{z(A_i - A_i^O)}{A_i^O} \right] \quad (30)$$

$$Z_i = A_i e \quad (31)$$

For one layer we can now write

$$\ln Q = N_1 \ln X_1 + \frac{(N_1)^2}{N_0} \ln Y_1 + N_1 \ln Z_1 - \frac{(N_1)^2}{N_0} \ln Z_1. \quad (32)$$

Both Y_i and Z_i contain A_i , the area per molecule in the i^{th} layer.

A_i can also be written as

$$A_i = \frac{A_i^O N_{i-1}}{N_i}. \quad (33)$$

Using equation (26) along with the expression for A_i in equation (33),

we can determine the chemical potential of the adsorbed layer to be

$$\begin{aligned}
 \left(\frac{\partial \ln Q}{\partial N_1} \right)_{N_0, T} &= - \frac{\mu_1}{kT} = \ln \left[\Lambda^{-2} q_z \exp \left(\frac{U_1}{RT} \right) \right] + \frac{2N_1}{N_0} \ln \left[a_{f1} \exp \left(\frac{W_1}{RT} \right) \right] \quad (34) \\
 &+ \frac{2N_1}{N_0} \ln \left[1 + 6 \left(\frac{N_0 - N_1}{N_1} \right) \right] - \frac{6N_1}{6N_0 - 5N_1} + \ln \left(\frac{A_1^0 N_0}{N_1} \right) \\
 &- \frac{2N_1}{N_0} \ln \left(\frac{A_1^0 N_0}{N_1} \right) - \frac{N_1}{N_0} .
 \end{aligned}$$

Equating this chemical potential to that of the gas phase as given by equation (27), we obtain,

$$\begin{aligned}
 \ln P &= - \ln \Lambda + \ln(kT) - \ln q_z - \frac{U_1}{RT} - \frac{2N_1}{N_0} \ln \left(\frac{a_{f1}}{A_1^0} \right) \quad (35) \\
 &- \left(\frac{2W_1}{RT} \right) \left(\frac{N_1}{N_0} \right) - \frac{2N_1}{N_0} \ln \left(6 - \frac{5N_1}{N_0} \right) + \frac{6N_1}{6N_0 - 5N_1} - \ln A_1^0 \\
 &+ \ln \left(\frac{N_1}{N_0} \right) + \frac{N_1}{N_0} .
 \end{aligned}$$

Using the definitions of θ as given in equations (21), (22), and (23) we find that

$$\begin{aligned} \ln P = & -\ln \Lambda + \ln(kT) - \ln q_z - \frac{U_1}{RT} - 2\theta \ln\left(\frac{a_{f1}}{A_1^o}\right) \\ & - \left(\frac{2W_1}{RT}\right) \theta - 2\theta \ln(6-5\theta) + \left[\frac{6\theta}{(6-5\theta)}\right] - \ln A_1^o \\ & + \ln \theta + \theta. \end{aligned} \quad (36)$$

Equation (36) is the isotherm equation for our multilayer model with adsorption restricted to one layer. This isotherm equation is identical to the equation developed by Pierotti and McAlpin which is equation (9) in this chapter.

Two Layer Case

This is, of course, the simplest possible case for multilayer adsorption and a good place to begin with a theory of multilayer adsorption. First, let us determine from the model partition function the chemical potential in each layer. For the first layer (the one next to the surface) we find using equation (26) that

$$-\frac{\mu_1}{kT} = \left(\frac{\partial \ln Q_1}{\partial N_1}\right)_{N_0, N_2, T} + \left(\frac{\partial \ln Q_2}{\partial N_1}\right)_{N_0, N_2, T}. \quad (37)$$

Then using the expression for Q_1 as given by equation (17) we find that

$$-\frac{\mu_1}{kT} = \ln \left[q_z \Lambda^{-2} \exp \left(\frac{U_1}{RT} \right) \right] + \frac{2N_1}{N_0} \ln \left[\frac{a_{f1}}{A_1^o} \exp \left(\frac{W_1}{RT} \right) \right] + \frac{2N_1}{N_0} \ln \left(6 - \frac{5N_1}{N_0} \right) \quad (38)$$

$$- \left(\frac{6N_1}{6N_0 - 5N_1} \right) + \ln \left(\frac{A_1^o N_0}{N_1} \right) - \frac{N_1}{N_0} - \left(\frac{N_2}{N_1} \right)^2 \ln \left[\frac{a_{f2}}{A_2^o} \exp \left(\frac{W_2}{RT} \right) \right]$$

$$- \left(\frac{N_2}{N_1} \right)^2 \ln \left(6 - \frac{5N_2}{N_1} \right) + \frac{6(N_2)^2}{N_1(6N_1 - 5N_2)} + \frac{N_2}{N_1} .$$

Recalling the definition of θ_1 this last equation is rewritten as

$$-\frac{\mu_1}{kT} = \ln \left[\Lambda^{-2} q_z \exp \left(\frac{U_1}{RT} \right) \right] + 2\theta_1 \ln \left[\frac{a_{f1}}{A_1^o} \exp \left(\frac{W_1}{RT} \right) \right] + 2\theta_1 \ln (6 - 5\theta_1) \quad (39)$$

$$- \left(\frac{6\theta_1}{6 - 5\theta_1} \right) + \ln A_1^o - \ln \theta_1 - \theta_1 - (\theta_2)^2 \ln \left[\frac{a_{f2}}{A_2^o} \exp \left(\frac{W_2}{RT} \right) \right]$$

$$- (\theta_2)^2 \ln (6 - 5\theta_2) + \left[\frac{6(\theta_2)^2}{6 - 5\theta_2} \right] + \theta_2 .$$

For the second layer, equation (26) shows that if only two layers are considered then

$$-\frac{\mu_2}{kT} = \left(\frac{\partial \ln Q_2}{\partial N_2} \right)_{N_0, N_1, T} \quad (40)$$

Using the expression for Q_1 , equation (17), we find that

$$-\frac{\mu_2}{kT} = \ln \left[\Lambda^{-2} q_z \exp \left(\frac{U_2}{RT} \right) \right] + 2\theta_2 \ln \left[\frac{a_{f2}}{A_2^o} \exp \left(\frac{W_2}{RT} \right) \right] \quad (41)$$

$$+ 2\theta_2 \ln(6 - 5\theta_2) - \left(\frac{6\theta_2}{6-5\theta_2} \right) + \ln A_2^o - \ln \theta_2 - \theta_2.$$

By now letting

$$\frac{\mu_1}{kT} = \frac{\mu_2}{kT}$$

and

$$\frac{\mu_2}{kT} = \frac{\mu_g}{kT}$$

where μ_g is given by equation (27), we obtain the isotherm equations for the two layer case of adsorption. The equations are

$$\frac{U_1}{RT} - \frac{U_2}{RT} + 2\theta_1 \ln \left[\frac{a_{f1}}{A_1^o} \exp\left(\frac{W_1}{RT}\right) \right] + 2\theta_1 \ln (6-5\theta_1) - \left(\frac{6\theta_1}{6-5\theta_1} \right) \quad (42)$$

$$- \ln \theta_1 - \theta_1 = (\theta_2)^2 \ln \left[\frac{a_{f2}}{A_2^o} \exp\left(\frac{W_2}{RT}\right) \right] + (\theta_2)^2 \ln (6-5\theta_2) - \left[\frac{6(\theta_2)^2}{6-5\theta_2} \right]$$

$$+ 2\theta_2 \ln \left[\frac{a_{f2}}{A_2^o} \exp\left(\frac{W_2}{RT}\right) \right] + 2\theta_2 \ln (6-5\theta_2) - \left(\frac{6\theta_2}{6-5\theta_2} \right) - \ln \theta_2 - 2\theta_2$$

and

$$\ln P = -\ln A + \ln (kT) - \ln q_2 - \frac{U_2}{RT} - 2\theta_2 \ln \left(\frac{a_{f2}}{A_2^o} \right) \quad (43)$$

$$- 2\theta_2 \ln (6-5\theta_2) + \ln \theta_2 - \ln A_2^o - \left(\frac{2W_2}{RT} \right) \theta_2$$

$$+ \left[\frac{6\theta_2}{(6-5\theta_2)} \right] + \theta_2 .$$

Equations (42) and (43) taken together form the two layer significant structures isotherm equations. One could just as easily have equated

μ_g/kT to μ_1/kT instead of to μ_2/kT as we have done. This procedure, however, would have put both θ_1 and θ_2 in the equation involving the pressure. Using our method, only θ_2 is involved in the pressure equation and this is computationally more desirable.

Three Layer Case

This is the largest number of layers which will be considered in the present multilayer treatment. The procedure for finding the isotherm equations is exactly the same as in the two layer case. First, one finds the chemical potentials of the molecules in all three layers using equations (26) and (17). Then the isotherm equations can be found by letting

$$\frac{\mu_1}{kT} = \frac{\mu_2}{kT}$$

$$\frac{\mu_2}{kT} = \frac{\mu_3}{kT}$$

and

$$\frac{\mu_3}{kT} = \frac{\mu_g}{kT}.$$

The equations determined in this way are

$$\frac{U_1}{RT} - \frac{U_2}{RT} + 2\theta_1 \ln \left[\frac{a_{f1}}{A_o} \exp\left(\frac{W_1}{RT}\right) \right] + 2\theta_1 \ln (6-5\theta_1) - \ln \theta_1 \quad (44)$$

$$- \left(\frac{6\theta_1}{6-5\theta_1} \right) - \theta_1 = \left[2\theta_2 + (\theta_2)^2 \right] \ln \left[\frac{a_{f2}}{A_o} \exp\left(\frac{W_2}{RT}\right) \right]$$

$$+ \left[2\theta_2 + (\theta_2)^2 \right] \ln (6-5\theta_2) - \left[\frac{6(\theta_2)^2}{6-5\theta_2} \right] - \left[\frac{6\theta_2}{6-5\theta_2} \right]$$

$$- 2\theta_2 - \ln \theta_2 + \left[\frac{6(\theta_3)^2}{6-5\theta_3} \right] - (\theta_3)^2 \ln \left[\frac{a_{f3}}{A_o} \exp\left(\frac{W_3}{RT}\right) \right]$$

$$- (\theta_3)^2 \ln (6 - 5\theta_3) + \theta_3,$$

$$\frac{U_2}{RT} - \frac{U_3}{RT} + 2\theta_2 \ln \left[\frac{a_{f2}}{A_o} \exp\left(\frac{W_2}{RT}\right) \right] + 2\theta_2 \ln (6-5\theta_2) - \left(\frac{6\theta_2}{6-5\theta_2} \right) \quad (45)$$

$$- \ln \theta_2 - \theta_2 = - \left[\frac{6(\theta_3)^2 + 6\theta_3}{6 - 5\theta_3} \right] + \left[2\theta_3 + (\theta_3)^2 \right] \ln \left[\frac{a_{f3}}{A_o} \exp\left(\frac{W_3}{RT}\right) \right]$$

$$+ \left[2\theta_3 + (\theta_3)^2 \right] \ln (6-5\theta_3) - \ln \theta_3 - 2\theta_3,$$

and

$$\ln P = -\ln \Lambda + \ln(kT) - \ln q_z - \frac{U_3}{RT} - 2\theta_3 \ln\left(\frac{a_{f3}}{A_3^o}\right) \quad (46)$$

$$- 2\theta_3 \ln(6-5\theta_3) + \ln \theta_3 - \ln A_3^o - \left(\frac{2W_3}{RT}\right) \theta_3$$

$$+ \left(\frac{6\theta_3}{6-5\theta_3}\right) + \theta_3.$$

Equations (44), (45), and (46) taken together form the three layer isotherm equations for our model. The equation containing the gas pressure, equation (46), has only parameters from the third adsorbed layer. Equation (45) contains parameters from the second and third layers. Equation (44) contains parameters from all three adsorbed layers. So the equations go from simple to complex, which will prove useful in the actual solution of these equations, as will be seen in Chapter VI.

CHAPTER III

EXPERIMENTAL APPARATUS

Introduction

Any volumetric adsorption apparatus does basically three things: it measures temperatures, pressures, and volumes. The range and precision of the measurements desired determine the particular instrument design.

The instrument used in this work is a conventional volumetric high vacuum apparatus built entirely of pyrex glass and mounted on a Flexaframe rack. High vacuum stopcocks are employed as valves, using Apiezon N grease. This instrument is very similar to the BET apparatus described by Young and Crowell (25) which is used to make surface area determinations.

The isotherm pressure range one has in mind determines the pressure measuring equipment used. This particular instrument is designed to measure isotherm pressures at about 1 micron Hg, or below. The basic apparatus was initially built by Pierotti (13), and was then used by Levy (14). Both workers used the apparatus primarily to study multilayer isotherms, which is fairly high pressure work. It was then decided to look at submonolayer adsorption of krypton on Sterling FT (2700°). The original equipment was not designed for such low pressure measurements; thus, the author's task was to redesign the equipment. The main parts of the system and the order in which they

will be discussed are the vacuum system, the dosing system, the cyrostat and sample cell, and the pressure measuring system.

Vacuum System

As mentioned before, the ultimate vacuum attainable with this system is between 10^{-6} mm Hg and 10^{-7} mm Hg. As pointed out by Pierotti and Thomas (12), the greater the surface area of the sample, the less rigid are the vacuum requirements for a system. Since this system has a sample size of 0.2482 g, which corresponds to a sample surface area greater than 2.5 m^2 , the residual pressure of 10^{-6} mm Hg should be more than adequate.

The pumping system consists of a three stage mercury diffusion pump and a Welch Duo-Seal mechanical pump. A trap is positioned between the diffusion pump and the rest of the system to prevent mercury vapors from passing into the system. Either dry ice or liquid nitrogen is used as the coolant for this trap.

Another Welch Duo-Seal mechanical pump is used to operate an auxilliary low pressure manifold. This manifold's purpose is to regulate the various mercury levels in the main system, such as the McLeod gauge, the Toeppler pump, and the gas buret; it is otherwise completely independent of the main system.

Dosing System

The purpose of the dosing system is to introduce a known volume of gas at a known temperature into the sample cell containing the Sterling FT (2700°). Since an isotherm is a plot of the quantity of gas adsorbed versus equilibrium pressure at a constant temperature, it

is essential to know very exactly the amount of gas introduced into the sample cell. The dosing system is diagrammed in Figure 2.

The gas samples in Figure 2 are assayed-reagent grade gases with individual mass spectronic analysis run to insure purity. The three gases on this system are krypton, helium, and argon; they come in glass flasks provided with a breakoff seal. The flasks are fused directly to the system, and gas is introduced to the system by means of stopcocks 1, 2, and 3 in Figure 2.

If, for instance, a dose of krypton is desired, the gas is first introduced into the Toeppler pump by opening stopcock 4, which, along with stopcock 5, is a two-way stopcock. Now by opening stopcock 4 in the other direction, the krypton gas can go from the Toeppler pump into the gas buret. The Toeppler pump is used to store the gas of interest. The pressure of the gas inside the Toeppler pump can be varied by changing the mercury level inside the top bulb of the Toeppler pump. The pressure of a dose can then be varied when the Toeppler pump is used in conjunction with the gas buret.

Figure 2 shows the gas buret to be a series of four glass bulbs with stopcock 5, a two-way stopcock, situated on one end of the buret, and a mercury reservoir situated on the other end. Four gas volumes are attainable with the buret by simply placing the mercury level at any of the four positions directly below each bulb. Valve 6 in Figure 2 is a Nupro bellows valve which is used in conjunction with the auxiliary low pressure manifold to control the mercury level inside the gas buret.

Pierotti (13) calibrated each of the four volumes of the gas buret

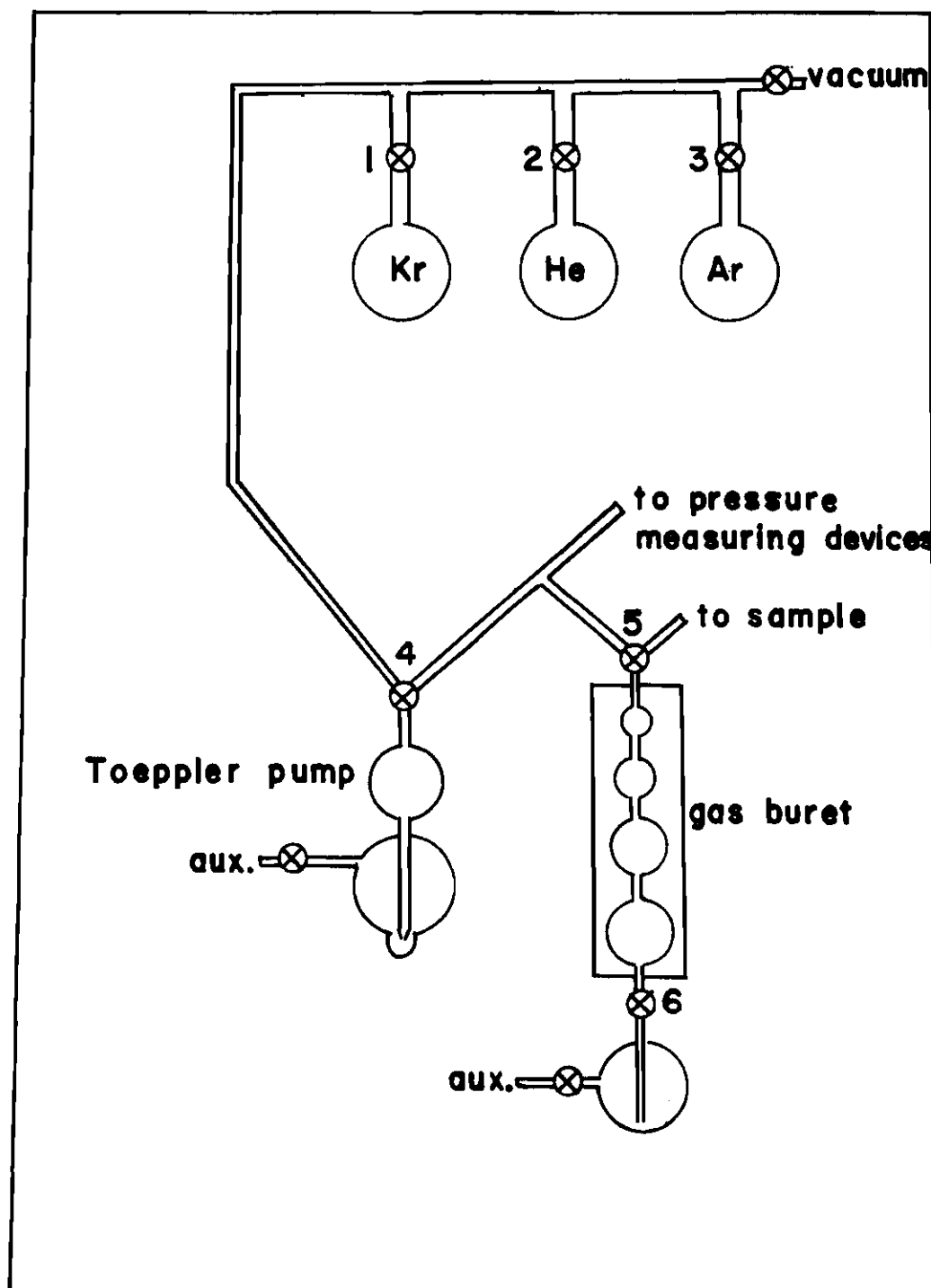


Figure 2. The Dosing System.

previously. These volumes were calibrated outside the system using a mercury weighing technique.

The gas buret is surrounded by a water jacket to minimize temperature fluctuations. A mercury thermometer which can be read to 0.01° C is used to measure the temperature of the water bath, and thus the temperature of the dose.

As an example of how the gas buret works, suppose a dose of about 1×10^{-4} moles of gas is desired. The mercury level in the gas buret is placed on the mark between the top bulb and the second bulb. Stopcock 5 is opened to the Toeppler pump and to the pressure measuring devices. Since this volume in the buret is 10.667 cc, the pressure of gas desired is given by

$$P = \frac{n RT}{V} = \frac{1 \times 10^{-4} \times 82.05 \times 298}{10.667}$$

$$P = 174 \text{ mm Hg.}$$

Thus enough gas should be released from the Toeppler pump so that the pressure is about 174 mm Hg. Stopcock 5 is now closed and 1×10^{-4} moles of gas is trapped in the gas buret. By opening stopcock 5 to the sample cell, the 1×10^{-4} moles of gas can be introduced into the sample cell. This is accomplished by opening valve 6 and running the mercury level to the top of stopcock 5. A great variety of dose sizes

are attainable by using different combinations of pressure and buret volumes.

The dose pressures are measured either by an ordinary mercury U-tube manometer or a high precision McLeod gauge. Ordinarily, gas pressures of 1 cm Hg or greater are measured by the mercury U-tube manometer, and pressures below 1 cm Hg are measured with the McLeod gauge. The McLeod gauge is usually used to measure dose pressures, since small doses are normally used. The McLeod gauge is also used in other capacities, which will be discussed later.

Cryostat and Sample Cell

The purpose of any cryostat on an adsorption apparatus is to obtain and maintain a particular sample temperature within acceptable limits. Since the cryostat is one of the most important of all components on the adsorption apparatus, great care and thought should go into its construction. Figure 3 shows the sample cell and cryostat arrangements. This cryostat is relatively simple in design, but is highly reliable. Liquid nitrogen, liquid oxygen, or a mixture of the two is placed in the Dewar flask which surrounds the sample cell. Any temperature from about 65°K to 90°K can be obtained with this cryostat and in addition can be maintained at $\pm 0.05^{\circ}\text{K}$ or better. One is also able to come back to this temperature after a shutdown, which is very important for isotherms that require more than one day to run.

Figure 3 shows the sample cell containing the Sterling FT (2700°) sample. This sample cell is a flat bottomed glass bulb whose design was first suggested by Clark (26). The sample, which is 0.2482

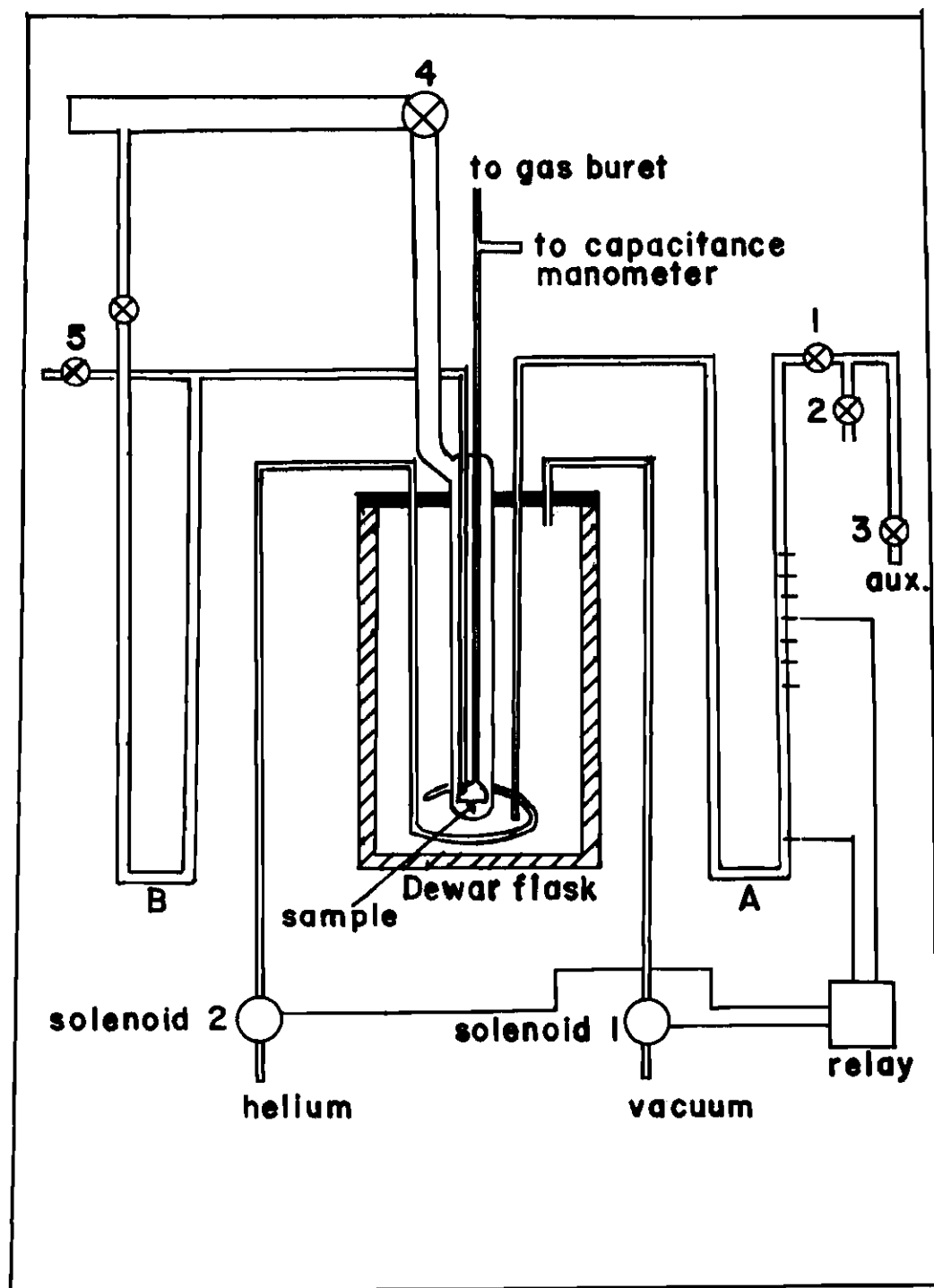


Figure 3. The Cryostat and Temperature Regulating System.

grams in size, is spread over the flat bottom, allowing more rapid equilibrium times during an isotherm run.

Two glass tubes go to the sample bulb. Both of these enter through the top of the vacuum jacket surrounding the sample cell, forming an air tight seal with the jacket. One tube is a 4 mm I.D. glass tube which comes from the gas buret and also goes to the capacitance manometer. The purpose of this tube is to deliver the krypton doses from the gas buret to the sample. The other tube also goes into the sample bulb, but it is sealed off inside the sample bulb - this is, it does not open into the sample bulb. This tube is part of a closed system of argon gas which acts as a vapor pressure thermometer. The argon vapor pressure thermometer will be discussed in detail later.

The sample cell and the tubes coming into it are all surrounded by a vacuum jacket, which is simply a tapered ground glass joint, sealed on with Apiezon N grease. The vacuum jacket is thus easily removed, exposing the sample cell and thus enabling one to bake out or remove the sample. The vacuum jacket is connected to the main manifold of the system through stopcock 4 in Figure 3. By opening stopcock 4, the jacket is evacuated. About 1 mm of helium gas is then put into the jacket and stopcock 4 is closed. The vacuum jacket, with the low gas pressure, acts as an insulator for the sample cell against short term temperature fluctuations in the Dewar flask during isotherm runs. The bath temperature inside the Dewar flask is controlled in such a way that it is always oscillating up and down. The sample cell, however, does not see as much oscillation due to the low pressure inside the vacuum jacket.

Cryostat temperature control will now be discussed. Figure 3 shows three tubes which go into the cryostat through the Plexiglas plate. The two tubes which go to solenoid valves 1 and 2 are made from copper and are attached to the Plexiglas plate by means of Swagelok fittings. The other tube is glass and goes to manometer B. This glass tube is sealed to the Plexiglas plate with Apiezon Q wax. The Dewar flask is also sealed to the Plexiglas plate using Apiezon Q wax. By pumping on the coolant inside the Dewar flask with a mechanical pump through solenoid valve 1, the temperature of the coolant, and thus the sample, is lowered.

The tube which goes to manometer B in Figure 3 is parallel to the vacuum jacket and extends into the coolant as far as the bottom of the vacuum jacket. The tube is sealed on its lower end and is filled with argon gas. At the temperatures used in this study, argon exists as a solid. The solid argon vapor pressure is a function only of bath temperature. Therefore, when one pumps on the bath through solenoid 1 and lowers the bath temperature, the vapor pressure of the solid argon decreases. The mercury level in the right arm of U-tube manometer B then comes down until it breaks contact with the relay in Figure 3. The right arm of manometer B has metal pins extending through the glass wall which come in contact with the mercury and is thus able to complete the circuit on the relay. However, when the argon vapor pressure decreases, as discussed above, contact can be broken and when this happens the relay closes solenoid valve 1. This stops the pumping action in the bath, and the temperature of the bath immediately begins increasing, raising the vapor pressure of the solid argon until

finally contact is made again with the right arm of manometer B. The relay then opens solenoid valve 1 in the pump line and the cycle starts again. In this manner the temperature of the bath is maintained constant.

Solenoid valve 2 connects a helium tank to the bath. The line from solenoid 2 goes into the cryostat and coils around at the bottom of the cryostat. This copper coil has several pin-holes which allow helium gas to bubble up through the coolant. When pump solenoid 1 is in the on, or pump, position, helium solenoid 2 is in the off, or closed position. But when pump solenoid 1 is in the off position, helium solenoid 2 is in the on position. Thus a small amount of helium gas is allowed to bubble through the coolant in the Dewar flask, but the helium flow is stopped when pumping begins. The purpose of the helium is to keep the coolant stirred and prevent temperature gradients inside the bath, and also to help cool the bath, as will be discussed next.

The one drawback of the above system is that it is inadvisable to pump on liquid oxygen. In such cases one may omit the pumping and use a method suggested by Lythe and Stoner (27). Here helium gas is bubbled through the coolant, which can be either liquid oxygen or liquid nitrogen. The coolant evaporates into the gas bubbles. This evaporation lowers the temperature of the bath and trips the relay in the same way as above, closing the solenoid valve in the helium line, thus stopping the helium flow. The bath then heats up and the cycle starts anew. The bath is also stirred by the helium bubbles. This method is simple, but surprisingly effective considering that the bath

temperature can be lowered as much as 10°K below the normal boiling temperature. Both this method and the pumping method of cooling were used in obtaining the data in this work.

The argon vapor pressure thermometer was mentioned previously while discussing the sample cell. This is used in actually determining isotherm temperatures. The argon vapor pressure thermometer consists of manometer A in Figure 3 and the tube going from manometer A into the sample bulb. This tube is filled with about 65 cm of argon gas at room temperature. When the temperature of interest is reached in the sample cell, the argon in the probe will be a solid. Thus, a measure of the solid argon vapor pressure on U-tube manometer A tells the temperature of the solid argon. This is also the sample temperature since the argon probe is actually inside the sample cell. The solid argon vapor pressure data of Clark, Din, and Robb (28) is used in determining sample temperatures.

Pressure Measuring System

Gas pressure measuring devices are a fundamental part of any adsorption apparatus, the particular type of isotherm studies one wishes to make determining the particular type of device. The apparatus used in this research is designed to measure extremely small gas pressures, one micron or less, although it is capable of measuring gas pressures of several millimeters of mercury just as easily. It is thus possible with this apparatus to measure isotherms from sub-monolayer coverage up to the completely saturated state. The pressure measuring devices are two mercury U-tube manometers, one McLeod gauge, and one capacitance manometer, all shown in Figure 4.

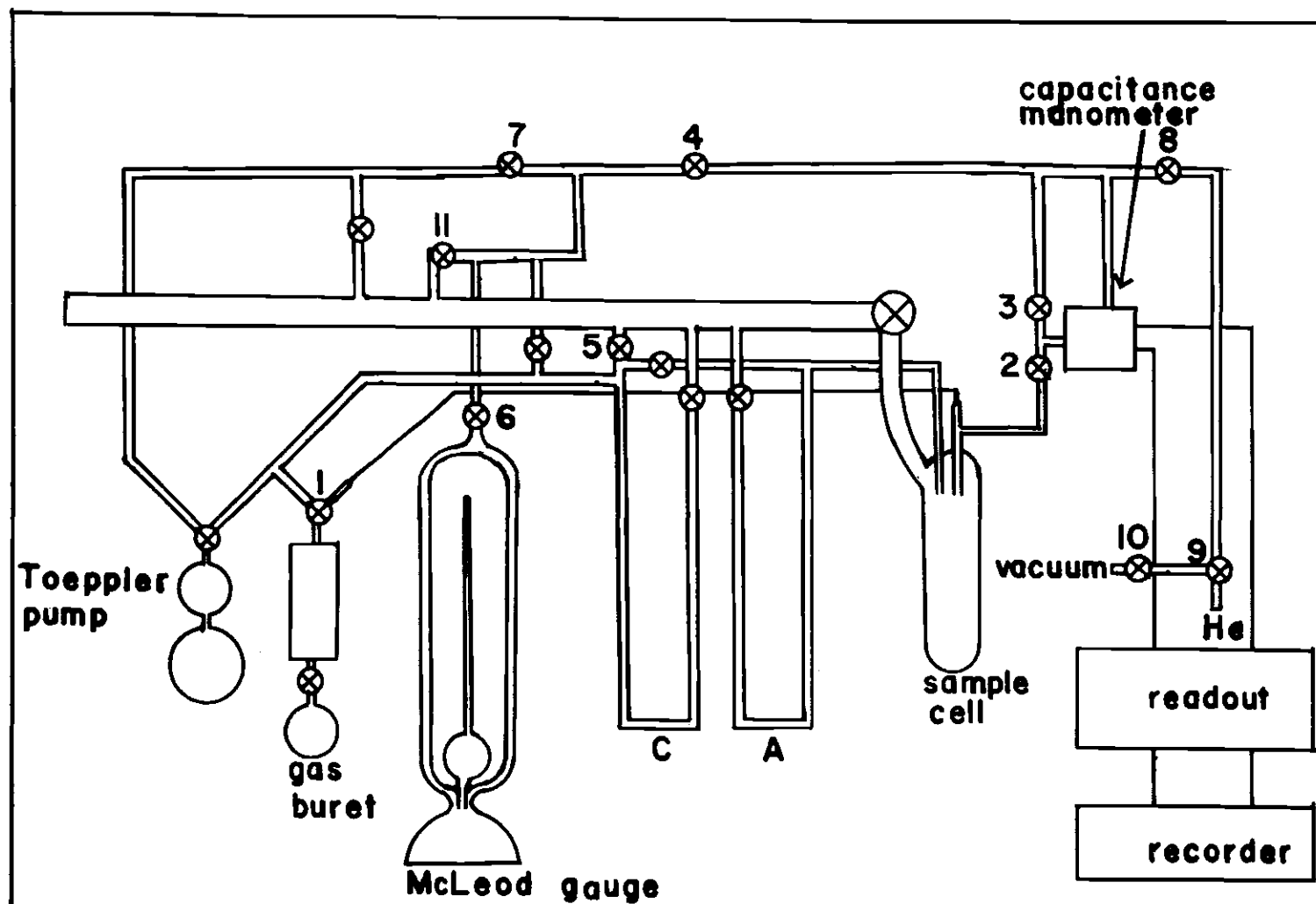


Figure 4. The Adsorption System.

U-tube Manometers

Both mercury U-tube manometers have already been mentioned. Manometer A in Figure 4 is used solely as the argon vapor pressure thermometer, while manometer C is used to measure dose pressures in the gas buret of 1 cm mercury or more and also in the calibration of the sample cell volume. The calibration will be discussed thoroughly in Chapter 4.

Both U-tube manometers can handle gas pressures up to one atmosphere. The bore of the manometer tubing is wide enough to prevent capillary depressions of the mercury. The mercury levels in these manometers and in the McLeod gauge are read with a Gaertner Universal Cathetometer, Number 72730, purchased from Central Scientific Company.

McLeod Gauge

The McLeod gauge on this system has three purposes: 1) to measure dose pressures, 2) to calibrate the capacitance manometer as a direct readout instrument, and 3) to measure isotherm equilibrium pressures that are greater than about 100 microns.

The McLeod gauge was built and calibrated by Pierotti (13). The instrument calibration was then checked against a CVC McLeod gauge by McAlpin (9), and the agreement between the two gauges was found to be within experimental error in all ranges.

The McLeod gauge is a precision pressure measuring instrument. For example, it can be shown that a gas pressure of 0.5 microns can be measured to within 1 per cent with this McLeod gauge, assuming that the precision of the cathetometer is ± 0.05 mm. It should be

pointed out here that all manometer readings taken with the cathetometer, including the McLeod gauge readings, are corrected for temperature and gravity effects. The McLeod gauge also has a capillary correction.

Figure 4 shows the McLeod gauge in relation to the rest of the system. A good discussion of McLeod gauges and U-tube manometers is found in Ross and Olivier (29).

Capacitance Manometer

A capacitance manometer is used either as a differential pressure measuring device, or when calibrated, as a direct pressure measuring device. The manometer head, shown in Figure 5, contains a thin metal diaphragm and a probe. If the pressure on one side of the diaphragm exceeds the pressure on the other side, the diaphragm is displaced relative to the probe. The movement of the diaphragm changes the electrical capacitance between the probe and the diaphragm, resulting in an AC signal which is amplified and displayed on an indicator meter. A recorder is attached to this meter and the signal is recorded.

The capacitance manometer used in this work is a Granville-Phillips Series 212, Model 03. This instrument has five pressure ranges of 1X, 0.3X, 0.1X, 0.03X, and 0.01X, where X indicates the full scale differential pressure in mm Hg on the readout meter. This simply means that on the 0.01X range, a pressure differential of 0.01 mm Hg across the metal diaphragm will deflect the readout meter by 200 units, which is full scale.

The capacitance manometer is used to measure the equilibrium

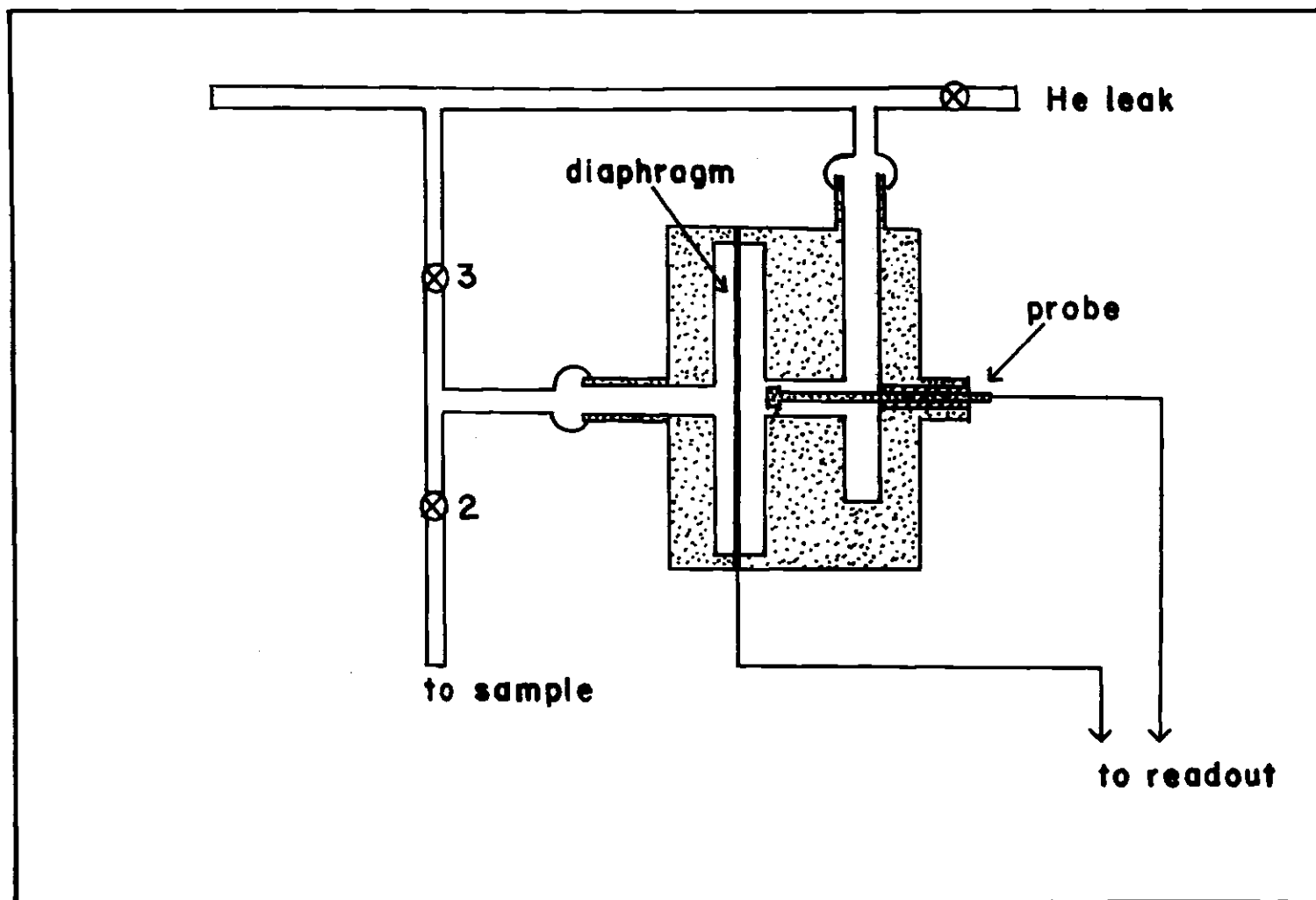


Figure 5. The Capacitance Manometer Head.

krypton pressure above the graphite sample. Since the instrument is linear on all scales but the LX, the capacitance manometer is calibrated against the McLeod gauge and is used as a direct readout instrument for pressures from about 0 to 100 microns. For isotherm gas pressures above 100 microns, the capacitance manometer is used as a null instrument and the isotherm pressures are measured on the McLeod gauge. In either case, the McLeod gauge and the capacitance manometer are linked together. The calibration and use of the capacitance manometer and McLeod gauge will be discussed in detail in the next chapter.

CHAPTER IV

EXPERIMENTAL PROCEDURES

Introduction

In this work, two types of experiments are performed: submonolayer adsorption and multilayer adsorption. Different techniques are used in obtaining the data in each type of experiment, these differences arising primarily in the isotherm pressure measurements. There are, however, certain preliminary procedures which must be followed prior to running both submonolayer and multilayer isotherms which will now be discussed in the order in which they occur experimentally.

Isotherm Temperature Control

When an isotherm run is contemplated, the first thing considered is at what temperature the measurements will be made. Then by using the data of Clark, Din, and Robb (28), the vapor pressure which solid argon will exhibit at that temperature is determined. Suppose, for example, that a sample temperature of 75°K is desired. The pressure in the argon vapor pressure thermometer, manometer A in Figures 3 and 4, should be 127 mm. The coolant, in this case pure liquid nitrogen, is added to the Dewar flask surrounding the sample cell. The temperature of the sample cell is now somewhat over 77°K , the normal boiling point of liquid nitrogen, and the bath temperature must therefore be lowered. The relay in Figure 3 is now connected to a

set of leads on manometer B, making contact through the mercury and opening solenoid valve 1 to a vacuum pump. The pump lowers the pressure above the nitrogen bath and the bath temperature begins falling. This temperature is allowed to fall until the pressure in manometer A is about 127 mm, indicating a temperature of about 75° K. At the moment the desired temperature is reached, stopcock 3 is closed and stopcock 1 is opened on manometer B. Air is leaked into the right arm of manometer B through leak valve 2, causing the mercury to just break contact with the top lead of the relay. This closes solenoid valve 1 and stops the pumping action. The bath temperature then stops falling. At this moment leak valve 2 is closed and stopcock 1 is closed and the desired bath temperature of about 75° K has now been obtained. This temperature can be maintained as explained in the cryostat section of Chapter III. The sample cell can be brought up to room temperature and returned to the set temperature as often as desired so long as the air pressure in the right arm of manometer B is not changed.

Volume Determinations

When a gas is introduced into the sample cell, part of the gas is adsorbed on the surface of the adsorbent, and part of the gas remains in the gas phase above the sample. Everything else being constant, the amount of gas remaining in the gas phase above the sample depends on the volume available to the gas phase. It is necessary to know this volume to find how much of a gas is adsorbed and how much remains in the gas phase.

Helium is employed as the calibrating gas to determine the volumes. Helium is particularly suited for this since it is not adsorbed appreciably at temperatures greater than 30° K (30).

The first volume which is determined is V_{sys} , the apparent volume of the system when the sample is at room temperature. This is the volume of the tubing between stopcocks 1 and 3 in Figure 4 and it includes the sample and one side of the capacitance manometer. First the size of a dose of helium gas is determined as discussed in Chapter III. This dose should be large enough so that the U-tube manometer can be used. Stopcock 3 is closed and 2 is opened; the helium is then forced from the gas buret into the sample cell by running the mercury level in the gas buret to the top of stopcock 1 in Figure 4. The capacitance manometer is used as a null instrument. That is, when the gas pressure on one side of stopcock 3 is equal to the gas pressure on the other side of stopcock 3, the capacitance manometer readout indicates zero pressure differential. Closing stopcocks 6, 7 and 11 and opening stopcocks 4, 5 and 8, helium gas is leaked into manometer C in Figure 4 through leak valve 9. This is continued until the capacitance manometer readout indicates zero pressure differential across stopcock 3. The pressure of the gas in V_{sys} is now read from manometer C. Then

$$V_{\text{sys}} = \frac{n_d RT_r}{P} \quad (47)$$

where n_d equals the number of moles in the dose, T_r is the room temperature, and P is the pressure as read from U-tube manometer C.

V_{sys} should remain constant so long as the system is not altered.

The coolant is now added to the Dewar flask surrounding the sample cell and the previously set temperature is obtained. Let V_c be the volume of the sample cell bulb and as much of the tube coming to the bulb as is under the liquid coolant level. This volume is at temperature T_c , where T_c is the sample temperature. V_h is defined as all the volume of the system from stopcock 1 to stopcock 3, except for that volume contained in V_c . Thus

$$V_{\text{sys}} = V_h + V_c. \quad (48)$$

Since we are dealing with a rare gas at extremely low pressures, the ideal gas law is a good approximation. We can then write the last equation as

$$V_{\text{sys}} = \frac{n_h RT_h}{P} + \frac{n_c RT_c}{P} \quad (49)$$

where n_h equals the number of moles of gas in V_h , and n_c equals the number of moles of gas in V_c . Obviously

$$n_c + n_h = n_d \quad (50)$$

where n_d equals the number of moles of the dose. Equations (49) and (50) can be combined to give

$$\frac{n_d RT_h}{P} - \frac{n_c RT_h}{P} + \frac{n_c RT_c}{P} = V_{\text{sys}} \quad (51)$$

A known dose of helium, n_d , is introduced into the sample cell which is now at temperature T_c . The capacitance manometer is zeroed, indicating zero pressure differential across stopcock 3 in Figure 4. The pressure of the gas is read on manometer C giving P in equation (51); n_c is now found from equation (51), and n_h is found from equation (50). V_h and V_c are now determined by using the ideal gas law. That is

$$V_h = \frac{n_h RT_h}{P} \quad \text{and} \quad V_c = \frac{n_c RT_c}{P}. \quad (52)$$

It will later be shown how V_h and V_c are used to find the number of moles of krypton gas remaining in the gas phase during an isotherm.

Another volume of interest is the volume of the sample side of the capacitance manometer. This is designated V_{cm} , where V_{cm} equals the volume of the capacitance manometer between stopcocks 2 and 3 in Figure 4. V_{cm} is seen more clearly in Figure 5. It includes all the volume from stopcocks 2 and 3 up to the metal diaphragm. V_{cm} is part

of V_{sys} and is determined when V_{sys} is determined. After V_{sys} has been determined, stopcock 2 is closed and 3 is opened in Figure 4. Stopcocks 4, 7 and 8 are also opened and V_{cm} is evacuated. After evacuation is complete, stopcock 3 is closed and stopcock 2 is opened. The capacitance manometer is now rezeroed, and the new pressure inside V_{sys} is obtained from manometer C. Let the new pressure be P_2 and let the pressure inside V_{sys} before V_{cm} is evacuated be P_1 . The number of moles of helium which remain in V_{sys} after V_{cm} is evacuated is

$$n = \frac{P_2 V_{\text{sys}}}{RT_r} . \quad (53)$$

Thus $(n_d - n)$ is the number of moles pumped from V_{cm} . Thus

$$V_{\text{cm}} = \frac{(n_d - n)RT_r}{P_1} . \quad (54)$$

The use of V_{sys} , V_h , V_c , and V_{cm} in determining an adsorption isotherm will be explained later in this chapter.

Bake Out of Sample

The next step toward running an adsorption isotherm is the sample bake out. Sterling FT (2700°) outgasses readily at room temperature and a sample bake out is probably not necessary. However, a sample

bake out at 250° C for at least 12 hours is always made before each isotherm run; this is done to ensure that the graphite surface is the same for each isotherm. A cylindrical heater fits around the sample cell to outgas the sample. The capacitance manometer is also usually baked out at the same time as the sample. A temperature of about 300° C is used to bake out the capacitance manometer, a heating tape being used for this purpose. During bake out procedures all stopcocks coming to the capacitance manometer and sample cell are opened to the diffusion pump. Bake out is not considered complete until a stick vacuum (at least 10^{-6} mm) is observed on the McLeod gauge.

Calibration of Capacitance Manometer

The capacitance manometer is used as a null instrument when measuring gas pressures of about 100 microns or more. This use of the capacitance manometer has been referred to previously and will now be explained in more detail with the aid of Figure 4. Assume that the pressure on the sample side of stopcock 3 is 150 microns, and the pressure on the vacuum side is zero (10^{-6} mm Hg). The capacitance manometer has been previously zeroed, meaning that the readout is zero on all ranges for zero pressure differential across stopcock 3. Stopcocks 11, 5 and 7 are now closed, and stopcocks 8, 4 and 6 remain open. The capacitance manometer readout is placed on the 1X range and the readout needle immediately deflects to the right. The idea is to add enough helium gas to the vacuum side of stopcock 3 to bring the readout back to zero pressure differential. So on the 1X range, helium is leaked slowly into the system using leak valve 9 until the

readout returns to zero. If too much gas is leaked in, it can be removed with leak valve 10. After zeroing on the 1X range is complete, the capacitance manometer is switched to the 0.1X range and is now zeroed on this more sensitive range using the same procedure as on the 1X range. Finally the readout is switched to the 0.01X range, the most sensitive range, and again is zeroed; the pressure differential across stopcock 3 is now assumed to be zero. Thus the pressure in the McLeod gauge (or U-tube manometer) is assumed to be equal to the pressure on the sample side of stopcock 3.

On all scales but the 1X range, the capacitance manometer readout is linear in pressure which means that any pressure below about 100 microns is directly proportional to the capacitance manometer readout. Therefore, in principle one should be able to zero the manometer, add doses of gas to the sample cell, and read the equilibrium pressures directly from the readout, after some kind of calibration procedure. In practice, however, this procedure is not successful. On all the readout ranges, particularly the 0.01X range, there is a continual drift of the capacitance manometer readout. This means that the position of the readout needle for zero pressure differential across stopcock 3 in Figure 4 changes continually with time.

What is needed is a method of rezeroing the capacitance manometer during an isotherm run. This can be done as will now be explained with the aid of Figure 4. Suppose a gas pressure of, say, 2 microns is on the sample side of stopcock 3, with zero (10^{-6} mm Hg) pressure on the vacuum side of stopcock 3. The capacitance manometer

readout is placed on the 0.01X range, and the readout is adjusted to read zero pressure differential. This is just a convenient reference point on the readout. A recorder with a 5 mv full scale range is attached to the readout. A baseline is established on the recorder. Stopcock 2 in Figure 4 is now closed and stopcock 3 is opened. The capacitance manometer readout immediately defects to the left by an amount directly proportional to the pressure which was contained in V_{cm} . This deflection is observed and recorded on the recorder. With higher gas pressures other readout ranges and recorder scales can be used. What remains is to determine how the recorded capacitance manometer deflection is proportional to the pressure in V_{cm} . Once the proportionality is known, this method of finding pressures can be used in isotherm determinations.

The method of calibrating the capacitance manometer as a direct pressure measuring device will now be discussed with the aid of Figure 4. First of all, the scales one wishes to calibrate are set on both the capacitance manometer readout and on the recorder. Such scales might be the 0.01X range with the 5 mv range of the recorder, the 0.01X and 10 mv range, or the 0.1X and 10 mv range. All combinations of scales which could possibly be used during an isotherm run should be calibrated. After a set of scales are decided on, stopcocks 2, 7, 5 and 11 in Figure 4 are closed and stopcocks 8, 3, 4 and 6 remain open. A small dose of helium is admitted through leak valve 9. After this gas has equilibrated throughout the system, stopcock 3 is closed. The pressure of the gas is measured using the McLeod gauge. This is the same pressure as that of the gas trapped in V_{cm} between

stopcocks 2 and 3. The vacuum side of stopcock 3 is then pumped out. The capacitance manometer readout is adjusted to read zero pressure differential and a baseline is established with the recorder. Stopcock 3 is now opened, instantly pumping out V_{cm} . A deflection is observed on the capacitance manometer readout and is recorded on the recorder. The magnitude of the deflection is directly proportional to the gas pressure in V_{cm} . Thus

$$P = KD \quad (55)$$

where P equals the pressure as read from the McLeod gauge, D equals the deflection of the recorder in units of chart paper, and K is a proportionality constant.

A number of determinations gives an average value of K . All possible scales of the capacitance manometer and recorder which might be used in an isotherm should be calibrated.

Procedures for Running Isotherms

The sample temperature has been set, all volumes determined, and the capacitance manometer has been calibrated. An isotherm run may now be begun.

Monolayer Isotherm

Approximately 15 data points are desired for each submonolayer isotherm. If V_m , the volume of a monolayer, is assumed to be 3.15 cc (STP) per gram (31) of adsorbent for Sterling FT (2700°), then each dose for our sample should be about 0.053 cc (STP), or about 2.3×10^{-6}

moles. This dose size is easily obtained using the gas buret and McLeod gauge. Referring to Figure 4, stopcock 2 is opened and 3 is closed. The vacuum side of stopcock 3 is at zero pressure (10^{-6} mm Hg). Dose 1 is now introduced into the sample cell. The capacitance manometer readout deflects greatly at first, but within minutes the readout is back near its original position. Thus the adsorption process can be followed on the capacitance manometer. A sufficient period of time is allowed to ensure equilibrium of the krypton gas with the solid adsorbent. The pressure in the argon vapor pressure thermometer is now measured using the cathetometer and this reading is recorded under dose 1. One can now measure the isotherm pressure. After the proper range selections on the readout and recorder are made, the capacitance manometer readout is set to zero and a base line is established on the recorder. Stopcock 2 in Figure 4 is closed, isolating V_{cm} from the sample cell. Then stopcock 3 is opened, V_{cm} is pumped out, and the capacitance manometer readout and recorder deflects by an amount proportional to the pressure in V_{cm} . This deflection, along with the room temperature, is recorded. Stopcock 3 is closed and 2 is opened. One point on the isotherm has now been completed. It should be noted that the capacitance manometer is calibrated in exactly the same way isotherm pressures are measured. The equilibrium krypton pressure is found from equation (55).

This process is repeated for doses 2, 3, 4, etc., until V_m is reached.

Multilayer Isotherm

A multilayer isotherm here is taken to be one which begins with

a surface coverage of one molecular layer of krypton. The size of the doses used is about the same as in the monolayer work, or about 2×10^{-6} moles. A very different procedure is used, however, to measure the equilibrium krypton pressures. Assume that the sample temperature is set and enough krypton has previously been added so that the sample coverage is greater than a monolayer. Stopcock 2 is closed and 3 is opened in Figure 3. Stopcocks 2 and 3 have been in this configuration since the last pressure measurement was made. A new dose of krypton gas is now added. The capacitance manometer, which still has zero pressure on both sides, is zeroed on all ranges. Then stopcock 3 is closed and 2 is opened. After enough time to ensure equilibrium of the krypton gas, the capacitance manometer is rezeroed in conjunction with the McLeod gauge. The pressure is then measured with the McLeod gauge and at the same time the argon vapor pressure reading is taken. The room temperature is noted, and one point on the multilayer isotherm is complete. Stopcock 2 is now closed and then stopcock 3 is opened. The capacitance manometer is on the 0.01X range. Any deflection of the readout when stopcock 3 is opened is noted and used as a correction to the pressure measured on the McLeod gauge, since any deflection indicates that the rezeroing was not exact. A new dose is now added to the sample cell, and the process is repeated.

Treatment of Data

The desired result of any series of isotherm measurements is the amount of gas adsorbed as a function of equilibrium gas pressure at

a given temperature. The raw data must now be treated to reach this end. For each krypton dose added, the raw data consists of the following quantities: dose size, room temperature, equilibrium pressure, and a sample temperature. The first step is to correct the measured isotherm pressures for an effect called thermal transpiration, which will now be discussed briefly.

When two parts of a closed system of gas connected by a capillary are held at different temperatures, a pressure differential develops across the capillary; this phenomenon is known as thermal transpiration. Thus, the pressure measured in an isotherm is not the true equilibrium pressure, but must somehow be corrected for thermal transpiration in order to determine the true equilibrium pressure.

Two regions of thermal transpiration are fairly well understood: the Knudsen region and the normal region. The Knudsen region is the region when the amount of gas in the system is so small that gas-gas interactions are unimportant compared to gas-wall interactions. The normal region occurs at higher gas pressures when no pressure differential develops across the temperature boundary.

The transition region between these two extremes is very difficult to understand. This difficult region is the one where some isotherm measurements are made. Miller (32) has developed an equation which is used to correct the measured pressure for thermal transpiration. Miller's equation is

$$\frac{1 - \left(\frac{P_1}{P_2}\right)}{1 - \left(\frac{T_1}{T_2}\right)^{\frac{1}{2}}} = \left[0.0300 y^2 + 0.245 y + \frac{(1 + 2.5y)}{(1 + 2y)} \right]^{-1} \quad (56)$$

where P_2 equals measured isotherm pressure, P_1 equals corrected isotherm pressure, T_2 equals room temperature, T_1 equals sample temperature, y equals $(P_2 d \sigma^2 / 2.33T) \times 10^3$, d equals inside diameter of tube crossing temperature boundary, σ equals molecular hard sphere diameter, and T equals $(T_1 + T_2)/2$. P_2 , T_2 , and T_1 are known quantities, and P_1 is calculated from equation (56).

Therefore, the experimentally measured pressure for submonolayer or multilayer data is corrected using equation (56). To find the amount of gas adsorbed on the surface of the Sterling FT (2700°) for each dose, one needs to know how much gas remains in the gas phase above the sample after each dose. Recalling that V_h is the part of V_{sys} at room temperature, and that V_c is the part of V_{sys} at sample temperature, let $n_{t,i}$ equal the total number of moles of krypton in the gas phase and adsorbed on the surface after dose i is added. If dose i is the last dose entered in the system, then there are $n_{t,i}$ total number of moles in the gas phase and adsorbed on the surface. The number of moles of gas adsorbed on the surface is $n_{s,i}$ where

$$n_{s,i} = n_{t,i} - n_{g,i} \quad (57)$$

or

$$n_{s,i} = n_{t,i} - \frac{P_{1,i}V_c}{RT_1} - \frac{P_{2,i}V_h}{RT_2} \quad (58)$$

where $n_{s,i}$ equals the total number of moles of krypton adsorbed on the adsorbent after dose i is added, $n_{g,i}$ equals the total number of moles of krypton remaining in the gas phase after dose i is added, $P_{2,i}$ equals the measured equilibrium krypton gas pressure after dose i is added, and $P_{1,i}$ equals the corrected equilibrium krypton gas pressure by equation (56) after dose i is added. Thus the corrected equilibrium pressure and total number of adsorbed moles, $n_{s,i}$, are determined for dose i from equations (56) and (58). But in determining $P_{2,i}$, V_{cm} is pumped out as explained previously. The loss of krypton from V_{cm} is taken into account for $n_{t,i+1}$ by

$$n_{t,i+1} = n_{t,i} + n_{i+1} - \frac{P_{2,i}V_{cm}}{RT_2} \quad (59)$$

where $n_{t,i+1}$ equals the total number of moles of krypton in the gas phase and adsorbed on the adsorbent after dose $(i+1)$ is added, n_{i+1} equals the total number of moles of krypton gas in dose $(i+1)$, and $P_{2,i}V_{cm}/RT_2$ equals the number of moles of krypton gas pumped from V_{cm} in determining $P_{2,i}$.

One now has for a given T_2 a group of $n_{s,i}$'s and corresponding $P_{1,i}$'s, which is the desired result.

CHAPTER V

EXPERIMENTAL DATA

Submonolayer Data

There is some uncertainty about the submonolayer krypton isotherms on graphitized carbon black as found in the literature. Ross and Winkler (33) estimated the two-dimensional critical temperature for krypton on P-33 (2700°) to be about 85°K . They measured an isotherm at 77.8°K and found a vertical region of constant pressure but upon measuring another isotherm at 90.1°K , found no vertical region. On the basis of this work the two-dimensional critical temperature of krypton adsorbed on P-33 (2700°K) does seem to be somewhere around 85°K . Clark (26) also found that krypton adsorbed on P-33 (2700°) at 70°K shows evidence of a two-dimensional phase transition in both the first and second adsorbed layers.

Pierotti was the first worker to find a discrepancy in the krypton data. He measured an isotherm of krypton on P-33 (2700°) at 74.6°K and found no region of vertical discontinuity in the first layer (14). In the course of his work Levy (14) also measured isotherms of krypton on P-33 (2700°) at 74.56°K and 76.91°K but saw no sign of a vertical region of constant pressure.

Pierotti's isotherm is shown in Figure 6. It is obvious that no vertical region of two-dimensional condensation exists in this isotherm.

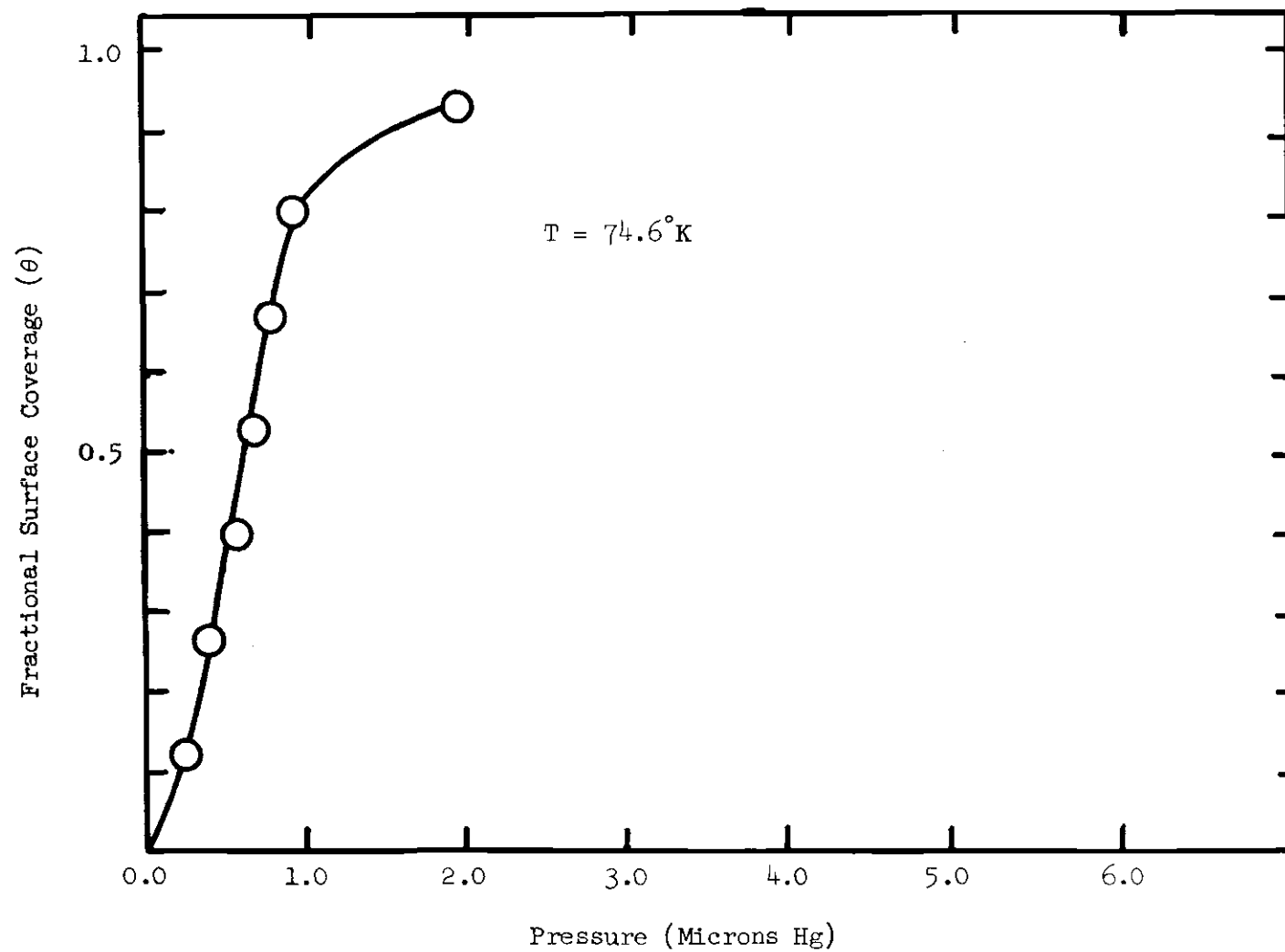


Figure 6. Pierotti's Adsorption of Krypton on Graphite at 74.6°K .

One of the purposes of this submonolayer work is thus to study the adsorption of krypton on graphitized carbon over a number of different temperatures in order to determine the two-dimensional critical temperature. The sample used is Sterling FT (2700°) obtained from Godfrey L. Cabot Inc., Boston. Prenzlöw and coworkers (34) have shown that Sterling FT (2700°) and P-33 (2700°) are virtually identical. Our data can thus be compared to any taken on the P-33 (2700°) system. The submonolayer data obtained is shown at six different temperatures in Figures 7 through 14 as plots of the volume of gas adsorbed per gram of adsorbent at STP versus the equilibrium gas pressure in microns of mercury.

On looking at the data it is immediately obvious that the system is passing through a two-dimensional critical region; it is not so very obvious, however, exactly where the critical region occurs. The isotherms at 74.6°K , 75.6°K , and 79.5°K seem to be definitely above the critical temperature; the isotherm at 69.6°K has a definite vertical region of constant pressure indicating that this isotherm is below the two-dimensional critical temperature. The isotherms at 72.4°K , 72.5°K , and 73.5°K may or may not have vertical risers. At any rate the isotherms at these three temperatures appear to be very close indeed to the critical temperature. These temperatures, however, are very far from the values of T_{2c} usually quoted in the literature of between about 82°K and 85°K (33).

It is necessary, then, to examine the results obtained in this research more closely and to try to determine the maximum error in the measurements to see if this could in some manner be responsible

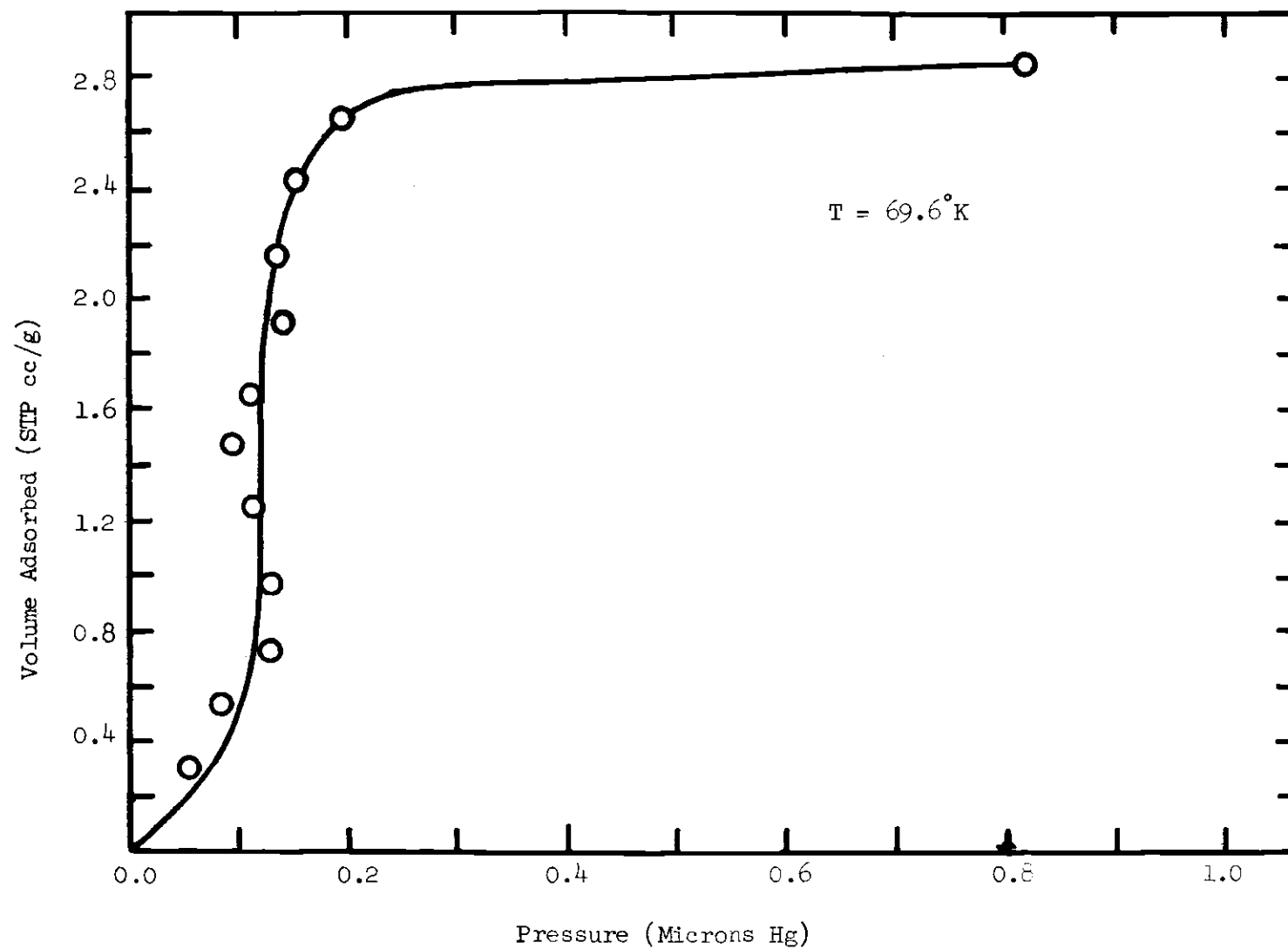


Figure 7. Submonolayer Adsorption of Krypton on Graphite at 69.6°K .

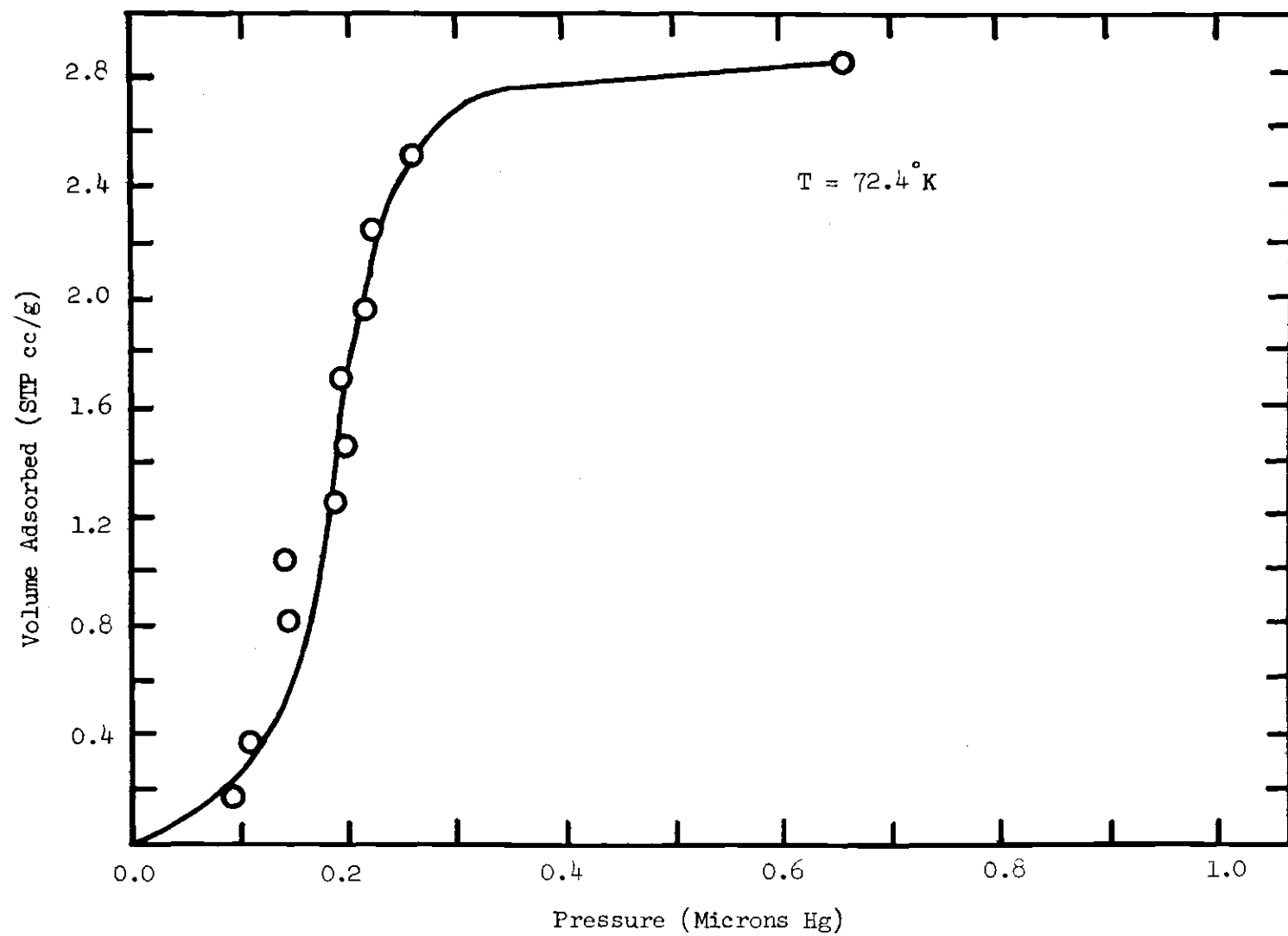


Figure 8. Submonolayer Adsorption of Krypton on Graphite at 72.4°K .

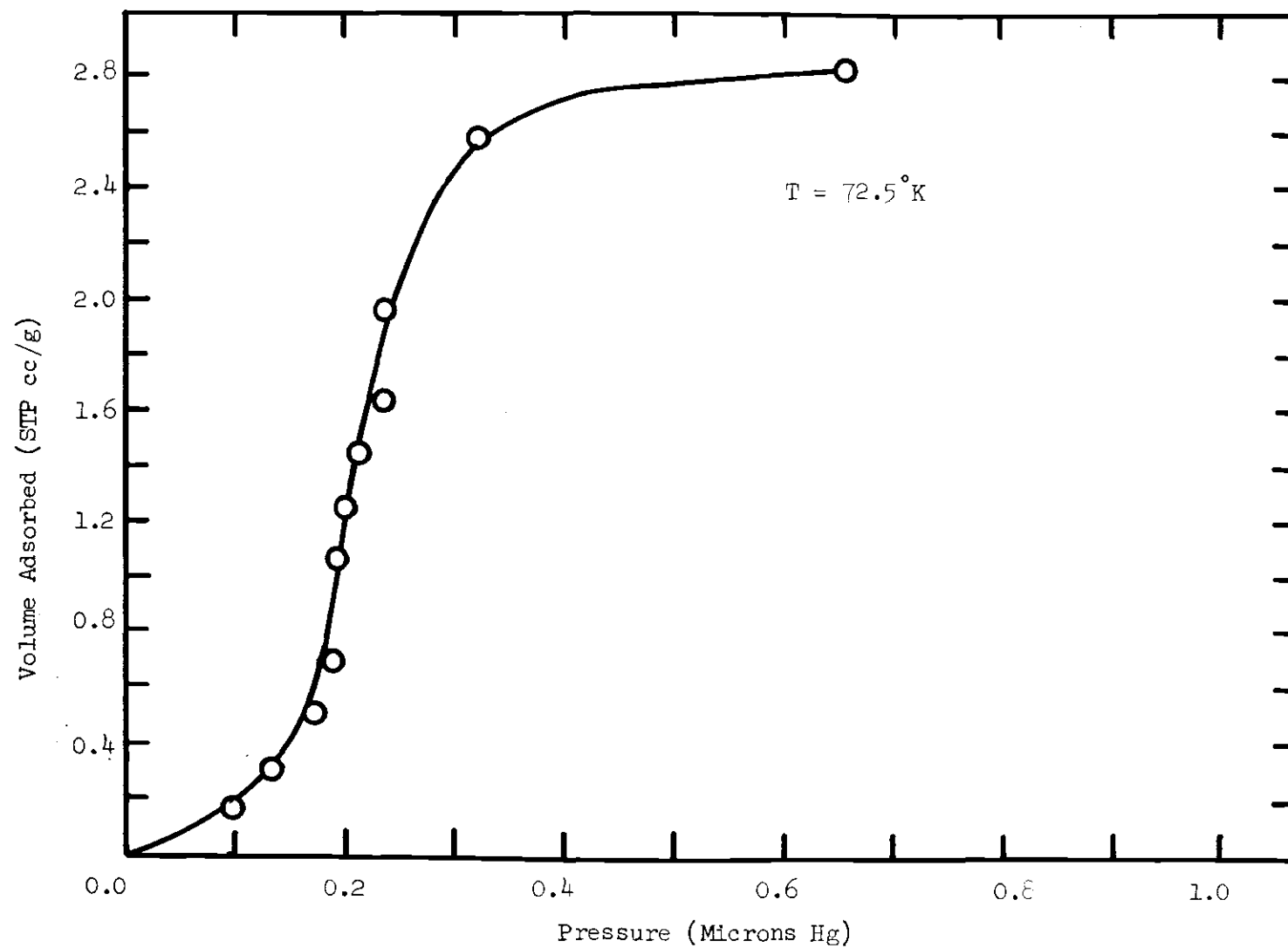


Figure 9. Submonolayer Adsorption of Krypton on Graphite at 72.5°K.

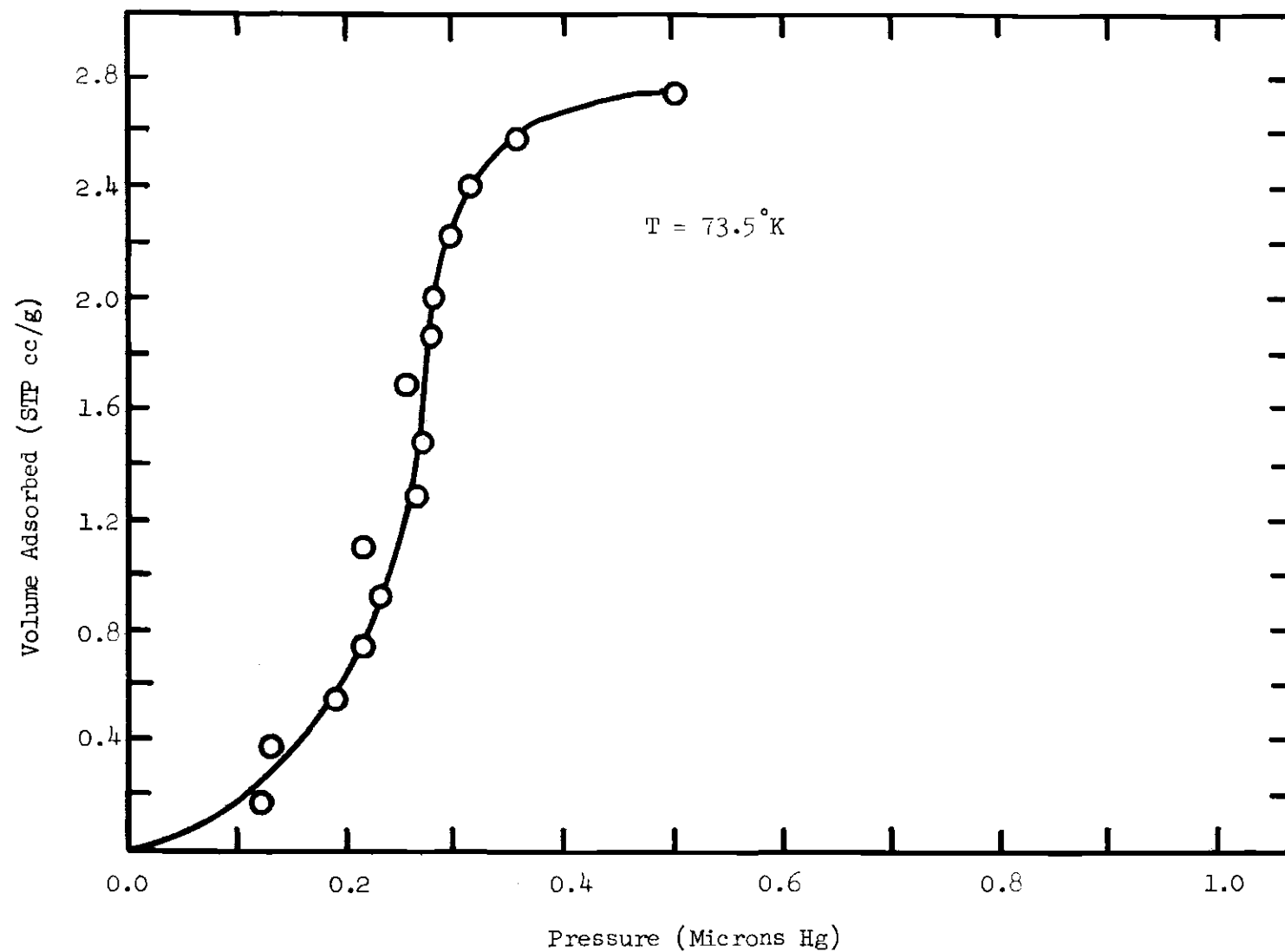


Figure 10. Submonolayer Adsorption of Krypton on Graphite at 73.5°K ; Run I.

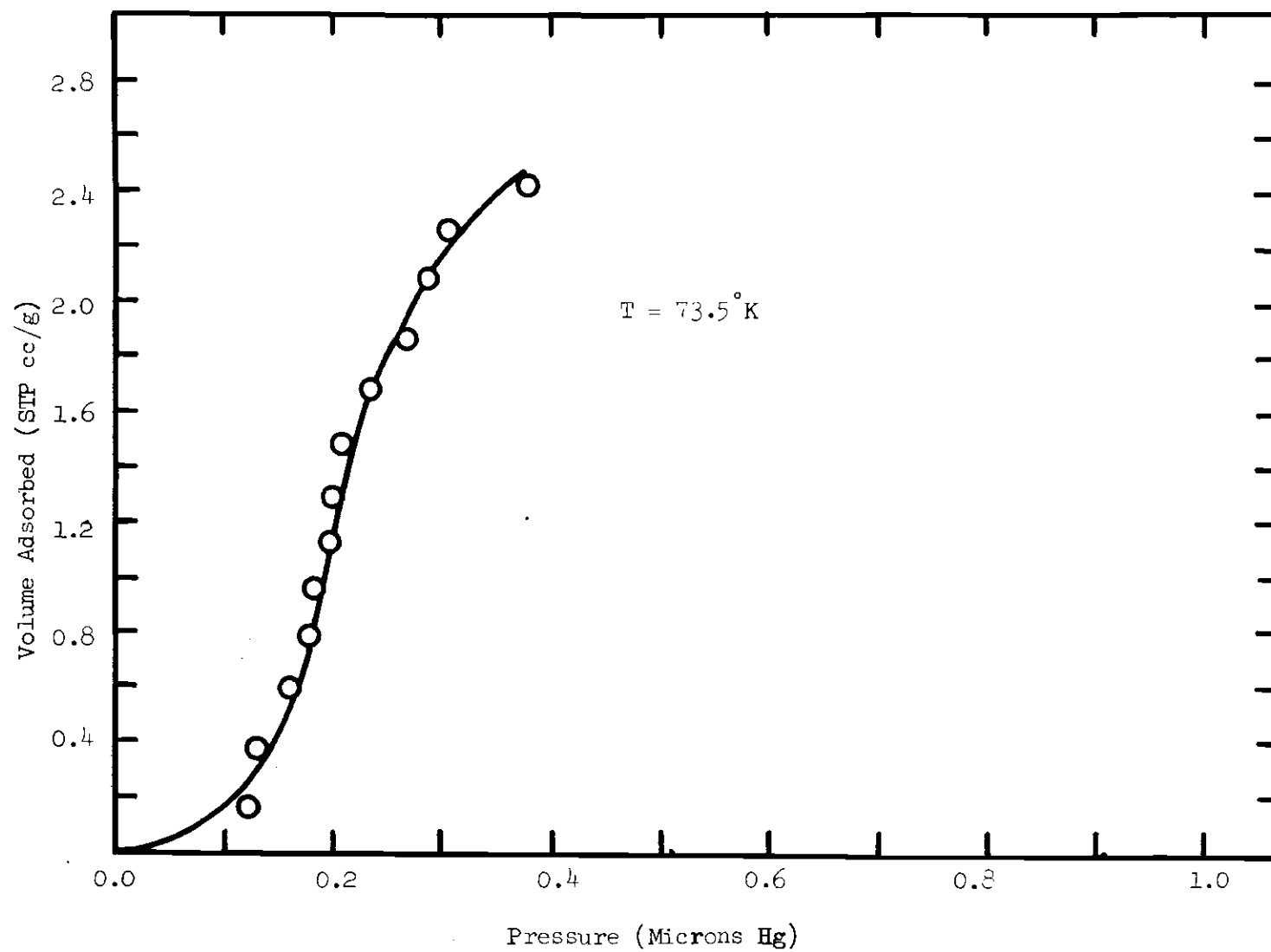


Figure 11. Submonolayer Adsorption of Krypton on Graphite at 73.5° K; Run II.

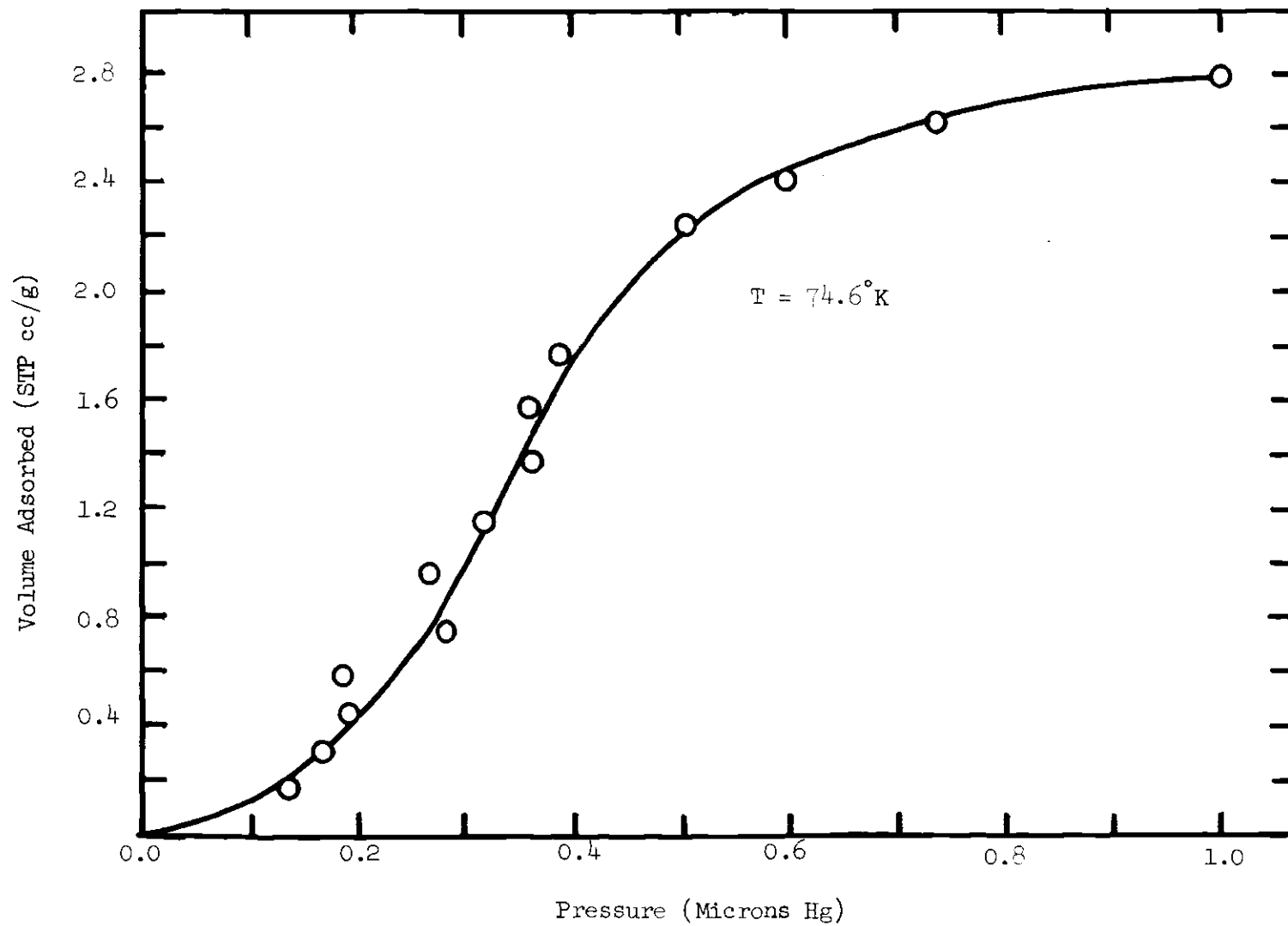


Figure 12. Submonolayer Adsorption of Krypton on Graphite at 74.6°K .

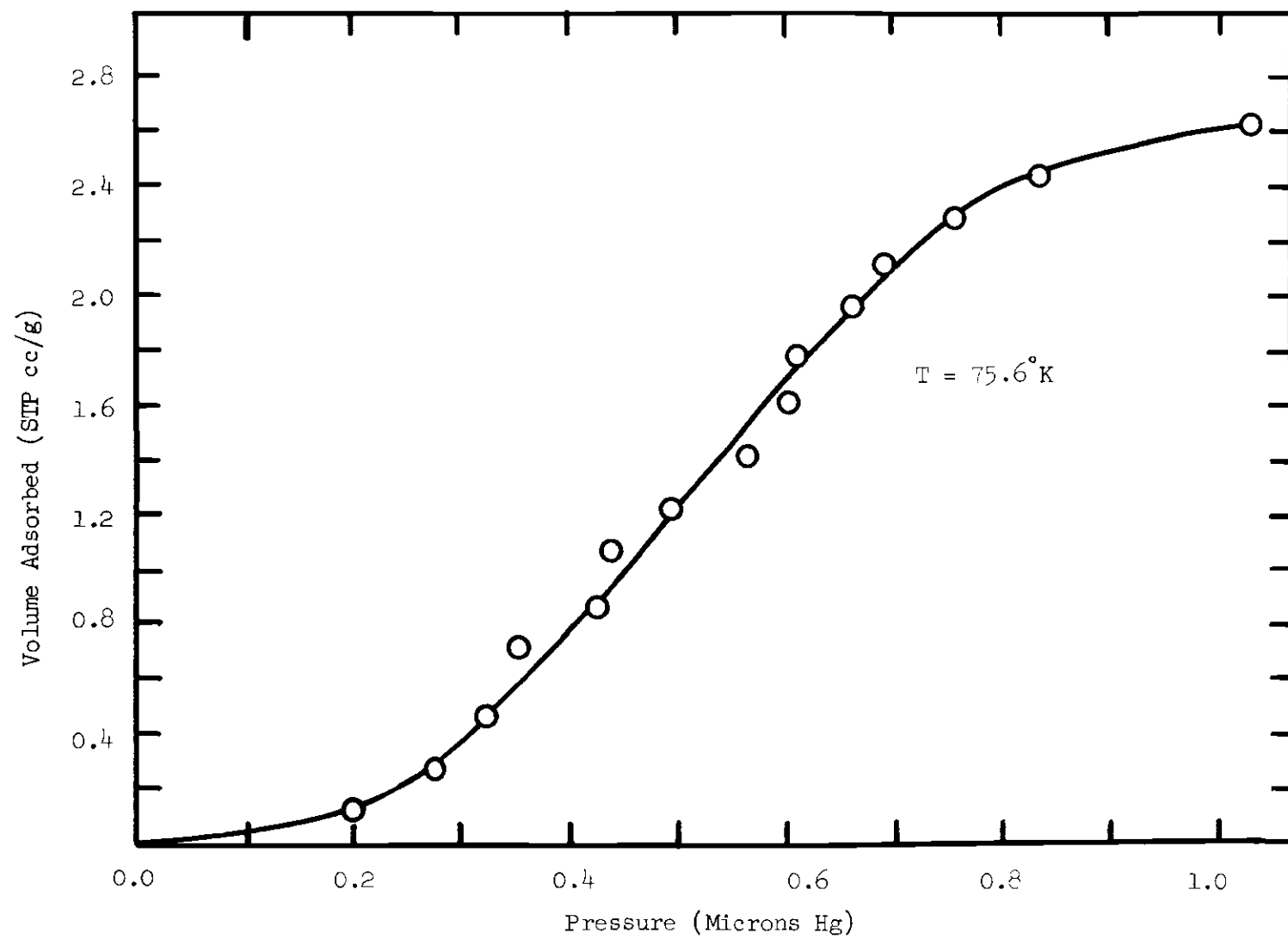


Figure 13. Submonolayer Adsorption of Krypton on Graphite at 75.6°K .

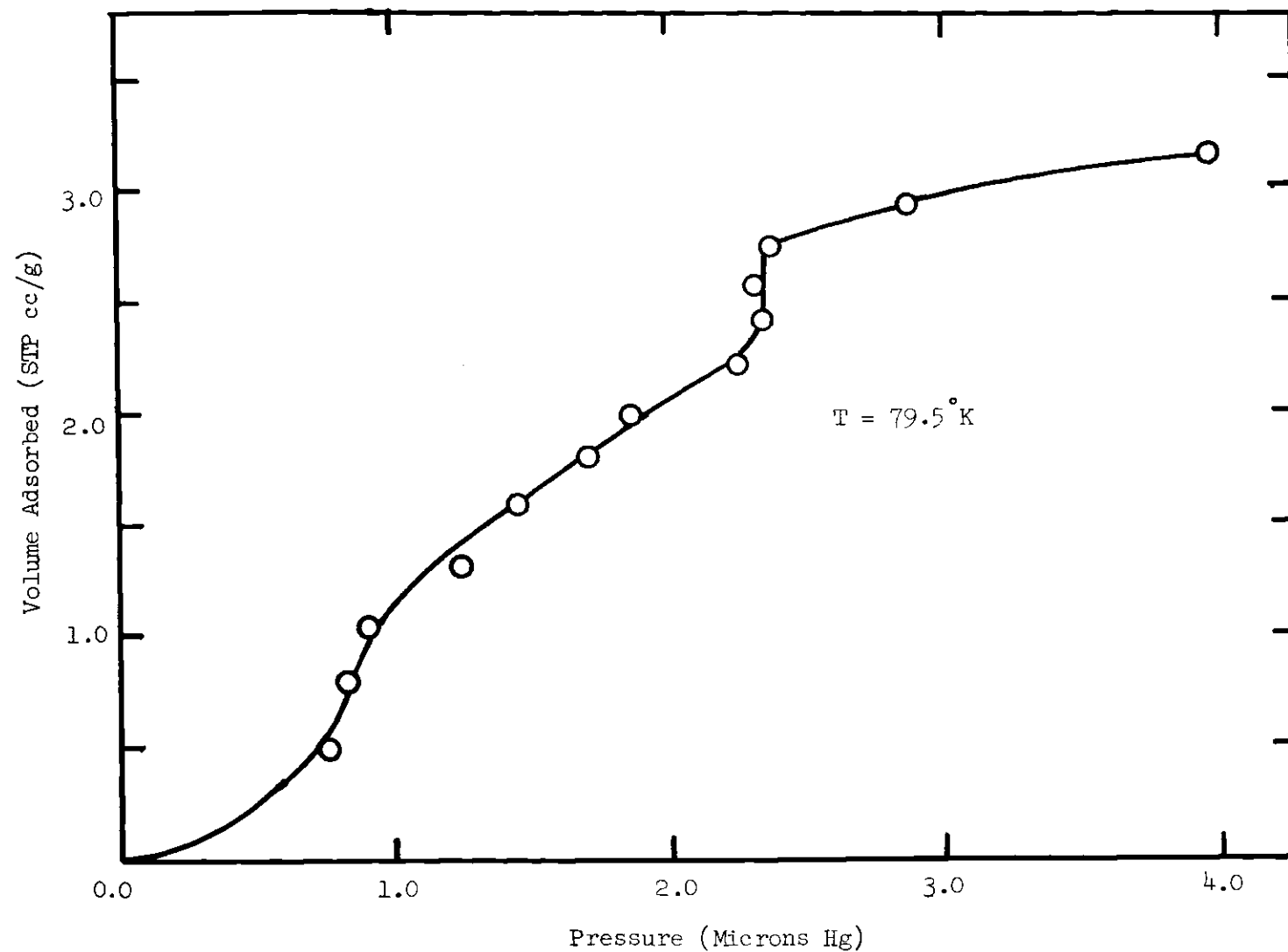


Figure 14. Submonolayer Adsorption of Krypton on Graphite at 79.5°K .

for the discrepancies. First, assume that the volume of gas adsorbed, V_{ads} , is correct as given in the data. Errors in this variable are not important in the determination of T_{2c} ; rather the isotherm temperatures and pressures are the important quantities.

The method of determining isotherm pressures is given in Chapter IV. By using equation (55), which is the calibration equation for the capacitance manometer, submonolayer isotherm pressures are determined. Uncertainties in the pressure are introduced by

1. errors in the calibration of the capacitance manometer which lead to errors in the absolute value of the pressure
2. temperature fluctuations in the sample
3. errors in the reading of the capacitance manometer readout meter.

Errors in the calibration of the capacitance manometer come from a number of sources, including the McLeod gauge, the catheotometer, and the reading of the capacitance manometer output meter. The actual, absolute isotherm pressure values are not important, however, in the determination of T_{2c} . The isotherm pressure uncertainty, ΔP , is the important quantity to consider. This uncertainty is brought about by factors (2) and (3) above, which will now be discussed.

The temperature of the sample fluctuates just from the design of the cryostat, since an on-off type of control is used. As pointed out in Chapter III, however, these fluctuations are greatly minimized by the vacuum jacket surrounding the sample. In taking the isotherm data, it should be emphasized that the sample temperatures were taken just before each isotherm pressure measurement. It was found that the

sample temperature never varied in any isotherm more than 0.05°K ; in most cases, in fact, the sample temperature never drifted more than about 0.02°K . Using a similar cryostat, Pierotti (13) found that the sample temperature could be maintained to within $\pm 0.05^{\circ}\text{K}$. Therefore, in trying to establish ΔP we let the temperature uncertainty, ΔT , be 0.05°K . A Clapeyron type expression, equation (60), is used to determine how ΔP is affected by ΔT .

$$\frac{\Delta P}{P} = \frac{q_{st} \Delta T}{RT^2} \quad (60)$$

where P equals the isotherm pressure, T equals the isotherm temperature, and q_{st} equals the isosteric heat of adsorption. The isosteric heat is both a function of temperature and sample coverage. Amberg, Spencer, and Beebe (35) found by calorimetric studies that q_{st} for low values of sample coverage is about 4000 calories per mole for krypton on P-33 (2700°). This value is probably high, but for our purposes is a good value of q_{st} to establish maximum errors in the data. At 70°K and at a pressure of 0.2 microns, this error is about 0.004 microns, an amount considered as quite small.

Another error contributing to ΔP is the uncertainty in the recorded capacitance manometer output which determines D in equation (55). Any error here is lessened greatly when the pressure is corrected for thermal transpiration effects. We estimate that the recorder chart can be read to within two of its smallest units, which

corresponds to a pressure uncertainty of about ± 0.025 microns; this is by far the major contribution to ΔP . This error is added to that contributed from ΔT as given by equation (60) and the isotherms at 72.4°K , 72.5°K , 73.5°K , and 74.6°K are shown in Figures 15 through 19 with the total uncertainty ΔP included.

Even with the uncertainties included, the isotherm at 74.6°K , Figure 19, is definitely above the critical temperature. Figures 15, 16, 17, and 18, the isotherms at 72.4°K , 72.5°K , and 73.5°K , could be taken as being either supercritical or subcritical. We believe, however, that these isotherms are supercritical and conclude that the two-dimensional critical temperature for krypton on Sterling FT (2700 $^\circ$) is about 69.6°K .

There is, therefore, a difference of 10°K or more between our critical temperature and that of Ross and Winkler (33). We feel that with the data presented here and with the work done by Pierotti and Levy (14), we can only conclude that our critical temperature is considerably closer to being correct.

The isotherm at 79.5°K , Figure 14, deserves special attention. One can see that this isotherm begins very much like the isotherms at 74.6°K and 75.6°K . That is, it is above the two-dimensional critical temperature and the pressure increases throughout the isotherm. However, up near 2.55 cc (STP) adsorbed, a very strange phenomenon occurs - a small but definite vertical region appears in the isotherm. This means that a phase transition is occurring on the surface, but a different type of phase transition than the one which occurs at 69.6°K . A phase transition such as the one occurring at 79.5°K has been predicted

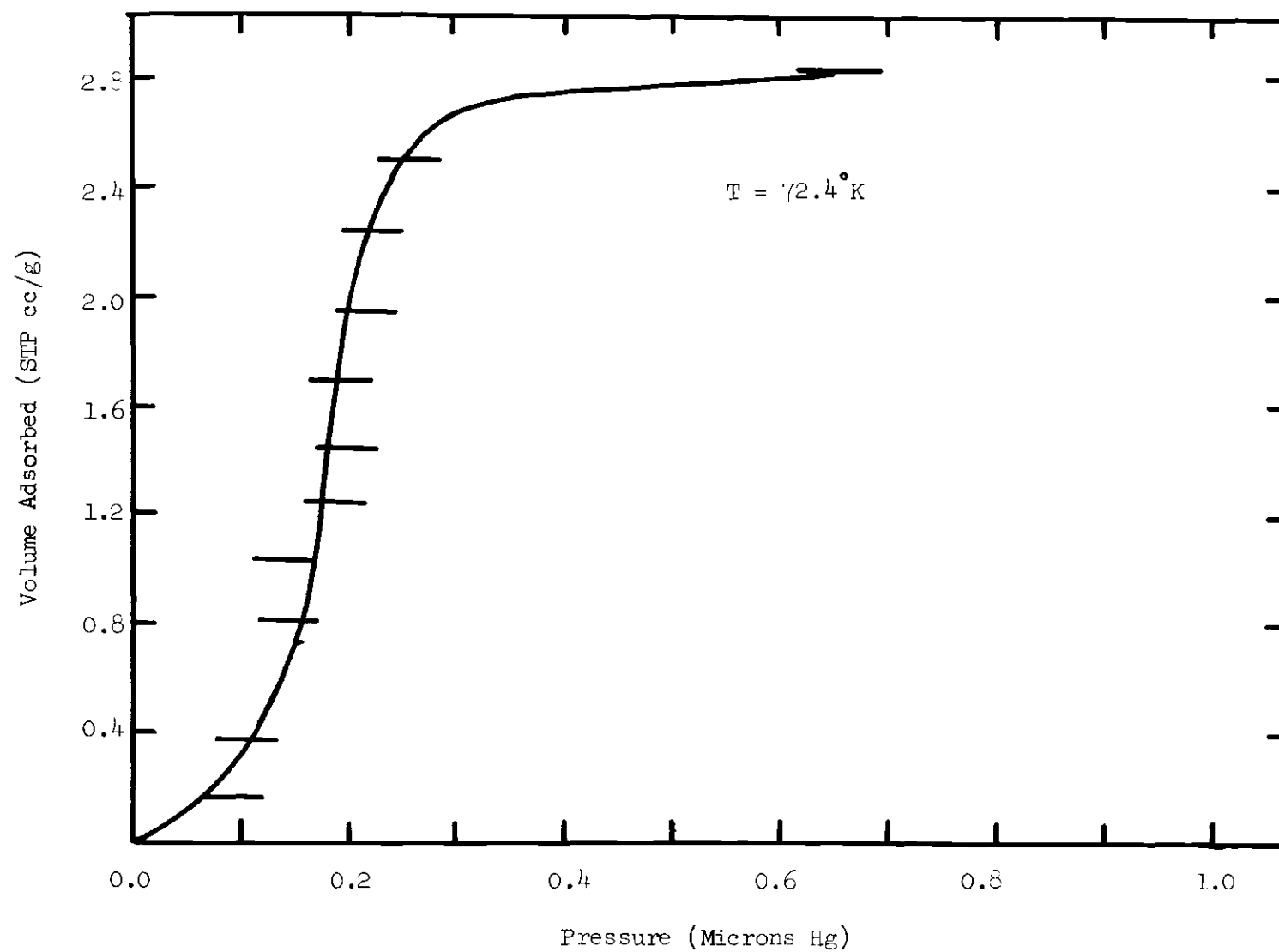


Figure 15. Pressure Uncertainties in the 72.4° Isotherm.

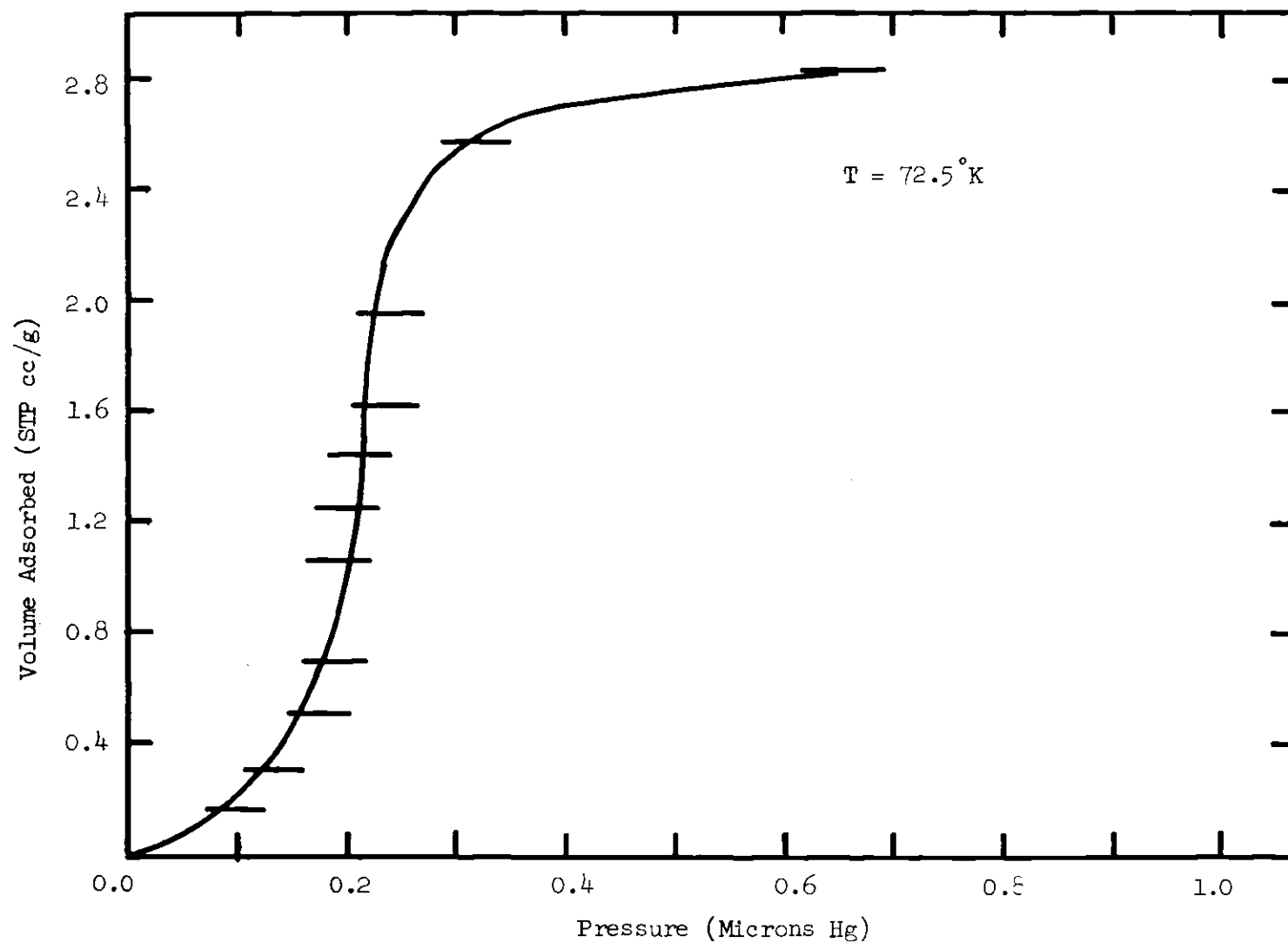


Figure 16. Pressure Uncertainties in the 72.5°K Isotherm.

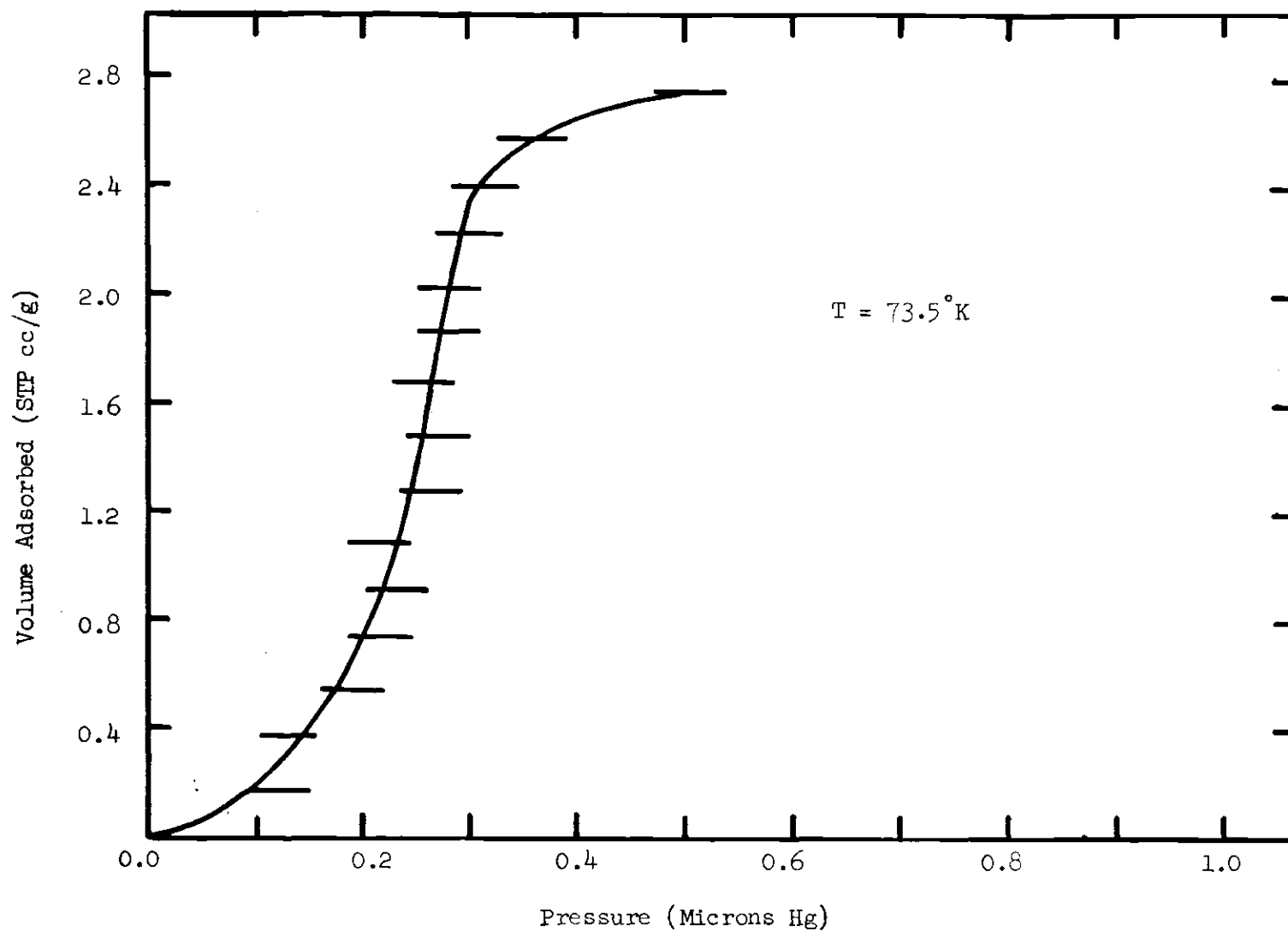


Figure 17. Pressure Uncertainties in the 73.5°K Isotherm; Run I.

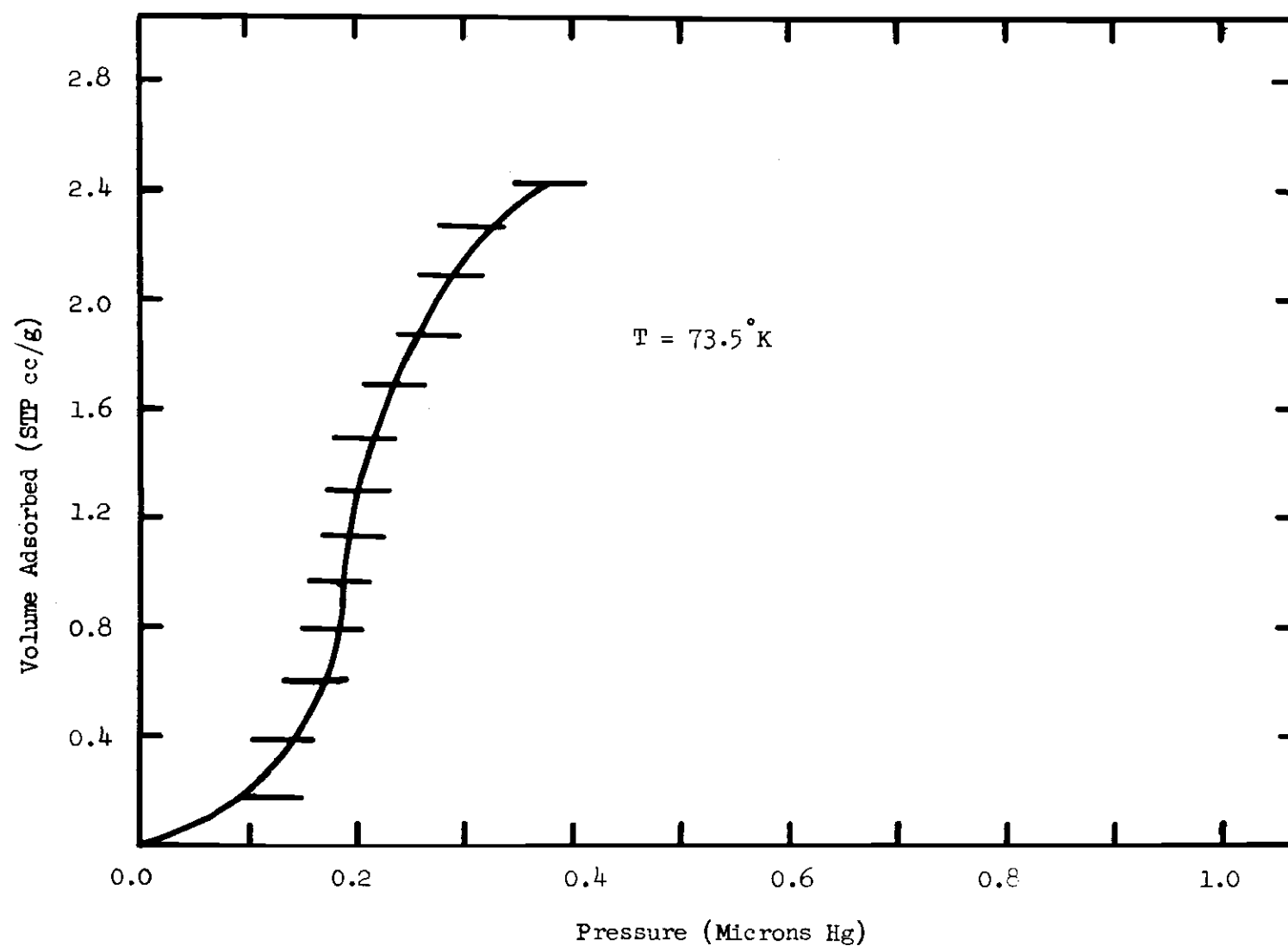


Figure 18. Pressure Uncertainties in the 73.5°K Isotherm; Run II.

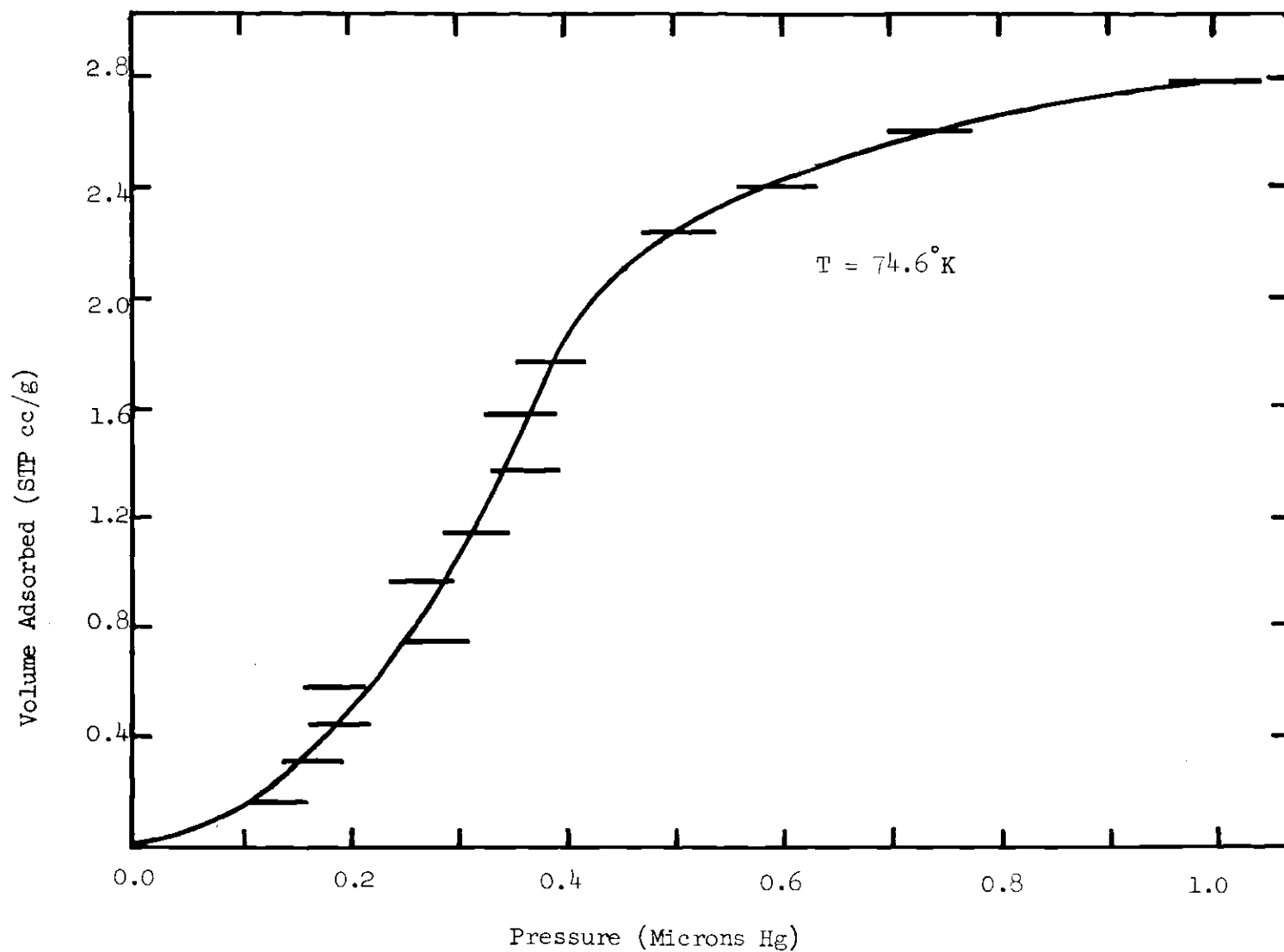


Figure 19. Pressure Uncertainties in the 74.6°K Isotherm.

theoretically by Tsien and Halsy (36). On studying systems of krypton adsorbed on exfoliated graphite, Duval and Thomy (37) have observed a considerable amount of this particular type of phase transition.

The phase transition which occurs at 69.6°K is usually thought of as a gaslike to liquidlike transition on the surface. Hence we speak of the critical temperature, just as in three-dimensional systems critical temperatures are associated with gas-liquid phase transitions. The behavior seen in the 79.5°K isotherm is probably due to a liquidlike to solidlike transition on the surface. Supposedly one could find an isotherm where the gaslike-liquidlike-solidlike phases are all in equilibrium on the surface. This would be the two-dimensional triple point, which Duval and Thomy (37) claim to have found in their system. This area of surface chemistry deserves a great deal more attention.

Multilayer Data

Multilayer adsorption isotherms for krypton on Sterling FT (2700°) were run at six temperatures between 67.7°K and 77.8°K . These isotherms are seen in Figures 20 and 21 as plots of volume adsorbed per gram in cubic centimeters at STP versus the equilibrium gas pressure in microns of mercury. Let us first examine the second adsorbed layer, which occurs between about 3cc (STP) and 7cc (STP) in Figures 20 and 21. The features of the second layer are very much like the first layer. The height of the second layer is almost the same as the height of the first layer. Assuming that the first layer is complete somewhere on the first plateau, or about 3.2cc (STP), the second layer is seen to end at about the corresponding place on the second plateau, or about 6.4cc (STP).

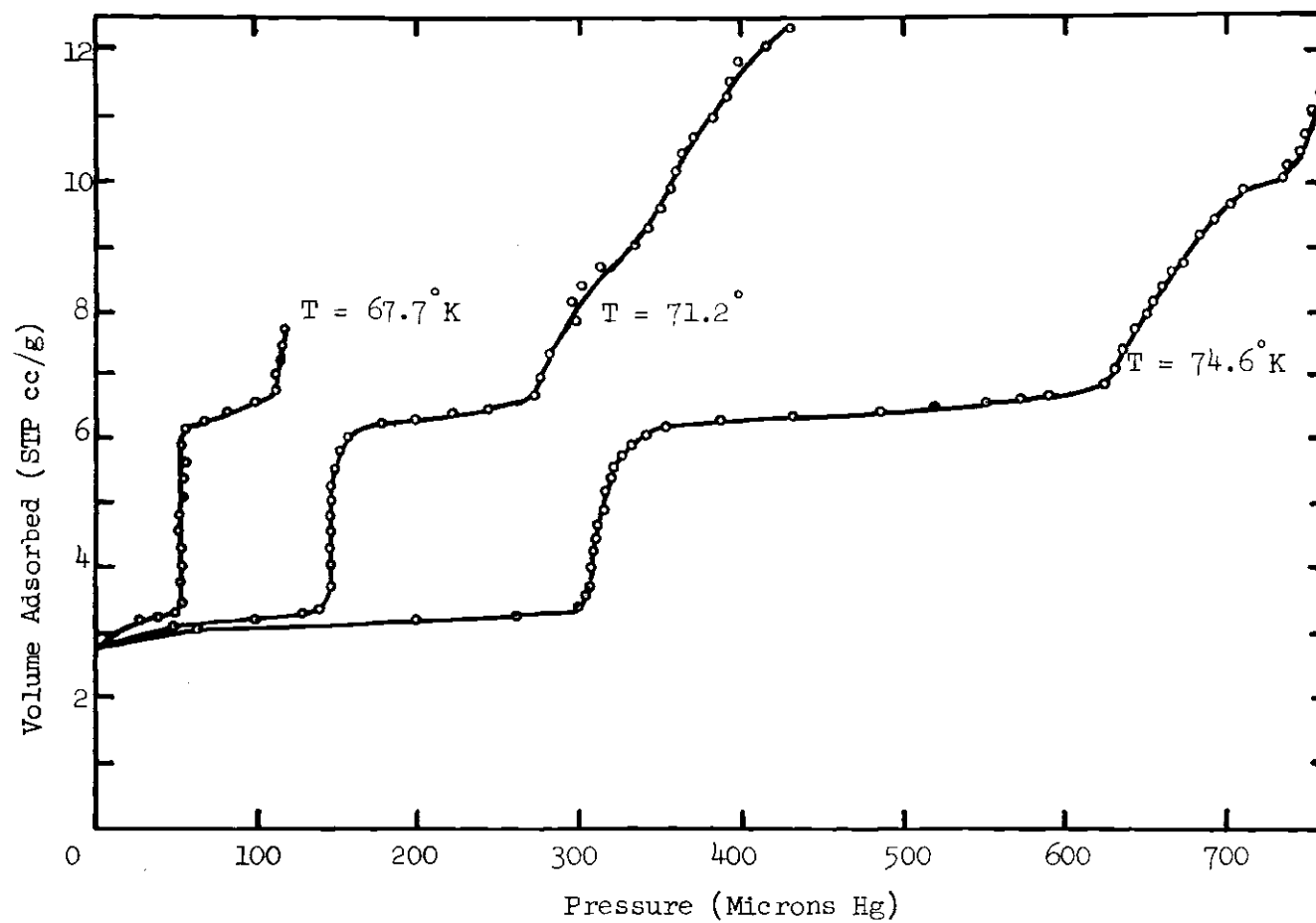


Figure 20. Multilayer Adsorption of Krypton on Graphite at 67.7° K, 71.2° K, and 74.6 K.

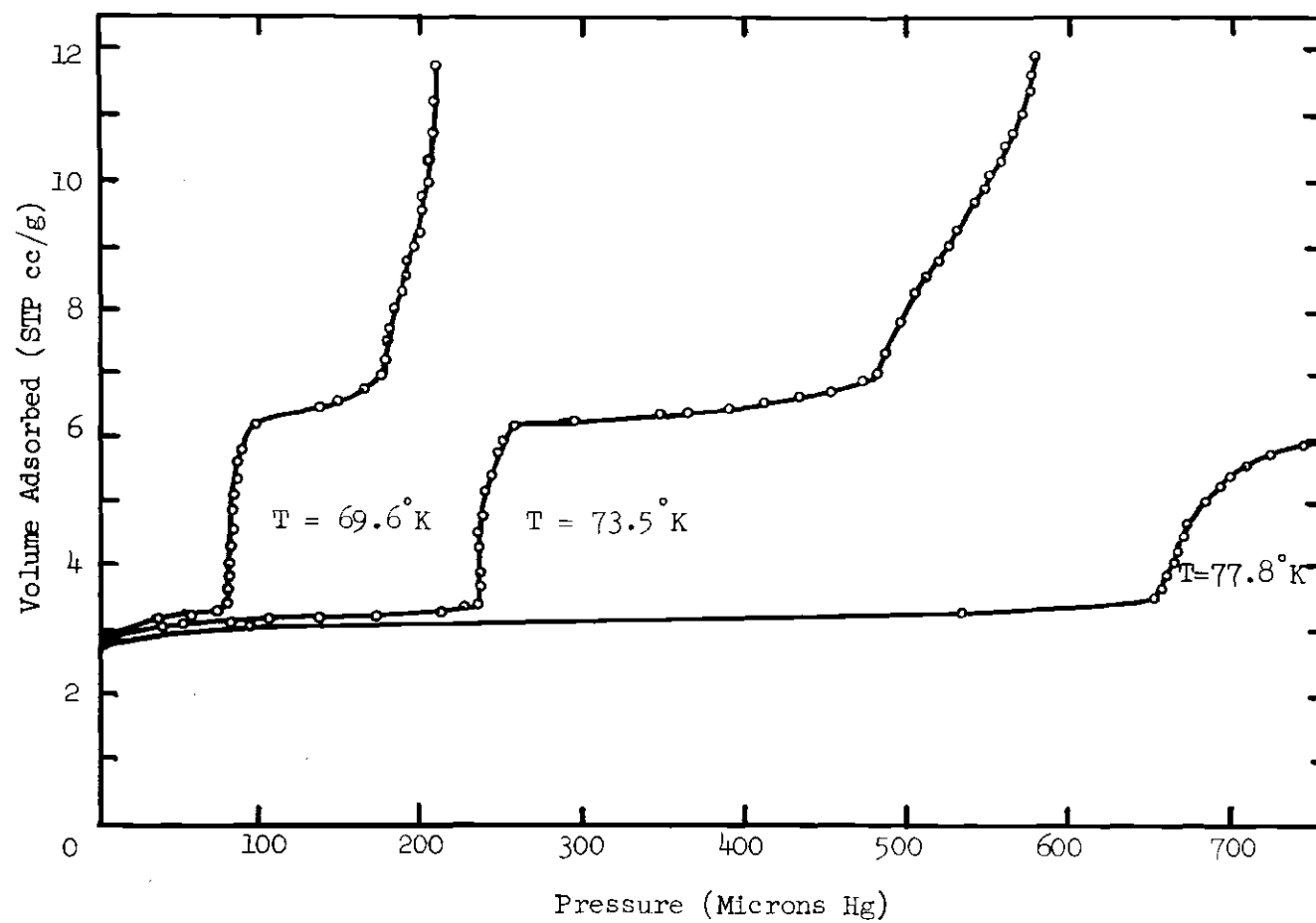


Figure 21. Multilayer Adsorption of Krypton on Graphite at 69.6° K, 73.5 K, and 77.8° K.

This corresponds to approximately the same amount of krypton to complete each layer.

It is interesting how sharply each of the plateaus end, especially the first one. As the temperature increases the top of the vertical riser in the second layer becomes more and more rounded off. This indicates higher layer formation is occurring before the second layer is complete. Higher layer formation occurs readily in multilayer adsorption since the energy differences between layers is not great.

The second layer seems to be passing through a phase transition. The isotherms at 73.4°K and below have definite vertical regions, whereas the isotherms at 74.6°K and 77.8°K have no vertical region in the second layer. The two-dimensional critical temperature in the second adsorbed layer is then about 74°K . The fact that the critical temperature in the second layer is higher than in the first layer is theoretically not surprising since the lateral interaction energy between the molecules in a given layer is expected to increase with layer number. This is another reason we believe that the critical temperature value for submonolayer adsorption given by Ross and Winkler (33) of between 82°K and 85°K is not correct. Our data seems to be consistent on this point.

The data will now be analyzed in terms of the multilayer significant structures theory as developed in Chapter II.

CHAPTER VI

APPLICATION OF THE MULTILAYER SIGNIFICANT
STRUCTURES THEORY TO THE KRYPTON - STERLING FT (2700°) SYSTEMIntroduction

The multilayer significant structures theory is developed in Chapter II. In this chapter the equations of the multilayer significant structures theory are applied to our data on the krypton-Sterling FT adsorption system. Only the "Three Layer Case" will be used in this treatment, which is given by equations (44), (45), and (46) in Chapter II. It should be emphasized that the total adsorption process can be described with the "Three Layer Case". No distinction is made between the submonolayer and multilayer regions in the theory; that is, the same model applies to all regions of adsorption. When equations (44), (45), and (46) are solved simultaneously, the solution is the total isotherm from zero coverage up to three layers.

To demonstrate how a solution to these three equations is determined, first assume that values for all the molecular parameters are known for the equations. Then using equation (46), the pressure P is varied and a corresponding set of θ_3 's is determined. This set of θ_3 's is then substituted into equation (45) to find the set of corresponding θ_2 's. Finally the set of $\theta_3 - \theta_2$'s so obtained is substituted into equation (44) to find the corresponding θ_1 's. The total statistical coverage θ is found from equation (23). In this case

$$\theta = \theta_1 + \theta_1\theta_2 + \theta_1\theta_2\theta_3. \quad (61)$$

This procedure yields a set of pressures with a corresponding set of coverages at a given temperature and molecular parameter values. This is the theoretical isotherm which will be compared to the data.

Selection of Theoretical Parameters

In order to determine a solution for the theoretical isotherm equations, a set of molecular parameters need to be known. The method used here to find the parameters involves specifying one particular set of parameters which apparently give a best fit of one particular isotherm, namely that at 73.5°K. This set of parameters is then used throughout varying only the temperature to observe how well the theory predicts the other isotherms. The values of our molecular parameters are then compared to values from outside sources or theories to perhaps determine the validity of the approach.

Each parameter needed in the "Three Layer Case" will now be considered to find how it is obtained for the isotherm at 73.5°K. The following parameters are needed in order to fit the 73.5°K isotherm: A_1^0 , v , $(\epsilon/k)_1$, a_{f1} , W_1 , and U_1 .

Area Per Molecule

The area per molecule when the i -th layer is filled to capacity, A_i^0 , is assumed to be the same in each layer and is taken to be 19.5\AA^2 . This is a previously used value for krypton (38).

Vibrational Frequency

The vibrational frequency in the z direction is taken to be the same in each layer and is obtained by a method outlined by McAlpin (9). In this method equation (9) is used and a plot is made of the quantity $\ln(C) - 2\ln(T)$ versus $1/T$ for the submonolayer data. This results in a straight line and the vibrational frequency is determined from the intercept. This method results in a value of $0.8 \times 10^{-12} \text{ sec}^{-1}$ for the vibrational frequency for the krypton-Sterling FT system.

Adsorbate-Adsorbate Interaction Parameter

The Lennard-Jones interaction parameter $(\epsilon/k)_i$ for the adsorbate-adsorbate interaction in the i -th layer is not a function of temperature, but is a function of layer number. Theoretically the interaction should increase as the layer number increases. As will be shown later, $(\epsilon/k)_i$ determines the shape of the theoretical isotherm in the i -th layer; that is, the critical properties are determined by $(\epsilon/k)_i$. In this work $(\epsilon/k)_1$ is given a value of 130°K . This value is chosen to give the theoretical isotherm the best shape in the first layer. For the second and third layers, $(\epsilon/k)_2$ and $(\epsilon/k)_3$ are given the gas phase values of 171°K (39). This is probably a fairly good choice for the second and third layer values since the gas-surface interaction is relatively weak in these layers.

Free Areas

After the values of $(\epsilon/k)_i$ have been chosen, finding the free area in each layer, a_{fi} , is simply a matter of solving equation (12). The free areas are a function of temperature and are slightly different for each isotherm.

Lattice Energy

The molar two-dimensional lattice energy in the i -th layer, W_i , is obtained by assuming pairwise interactions hold and summing the Lennard-Jones 6-12 potential over the assumed triangular lattice. In this work the summation is performed directly over the first 36 nearest neighbors of a central molecule and then the potential equation is integrated over the rest of the plane. The final result is that W_i is $6.72 (\epsilon/k)_i$ calories per mole.

Molar Site Energy

The molar site energy, U_i , for an isolated molecule in the i -th layer includes both an adsorbate-adsorbent term and a term for the interaction of the molecule with all the molecules in the $(i-1)$ layers below the i -th layer. U_i determines the relative position of the i -th step in the theoretical isotherm. Values of U_i in this work are chosen to best fit the positions of the steps in the isotherm at 73.5°K. U_i is not a function of temperature.

Table 3 shows the values of the parameters used to fit the 73.5°K isotherm. It will be recalled that the experimental coverage, θ , is the ratio of the volume of krypton adsorbed to the volume of a complete monolayer, V_m . A value of 3.22cc (STP) per gram is used for V_m to obtain the best overall fit of the experiment and theory. This is a very typical value of V_m for krypton on graphitized carbon, falling very close to the value used by Singleton and Halsey (31).

Table 3. Molecular Adsorption Parameters Derived from the Multilayer Significant Structures Theory for the Krypton-Sterling FT System at 73.5 K

Parameter	Value
ν	$0.8 \times 10^{12} \text{ sec}^{-1}$
A_1^0, A_2^0, A_3^0	19.5 \AA^2
$(\epsilon/k)_1$	130° K
$(\epsilon/k)_2, (\epsilon/k)_3$	171° K
a_{f1}	0.2062 \AA^2
a_{f2}, a_{f3}	0.1620 \AA^2
W_1	874 cal/mole
W_2, W_3	1149 cal/mole
U_1	2910 cal/mole
U_2	1670 cal/mole
U_3	1625 cal/mole
V_m	3.22 cc (STP)/g

Fit of the Multilayer Theory to the Data

Adsorption Isotherms

The isotherm at 73.5°K will first be discussed, since this is the isotherm used to find the parameters in Table 3. Figure 22 shows the experimental points and the theoretical curve for this temperature. The submonolayer region is at such a low pressure that it lies on the θ axis of Figure 22. Figure 23 shows the submonolayer region expanded so that the detail can be seen.

The theoretical first layer curve, Figure 23, is seen not to be vertical, just as the data points are not vertical. The second layer, Figure 22, is vertical in both the theory and the data. The theoretical third layer is vertical as a result of a van der Waals type loop. This loop is not shown in Figure 22, or in any of the subsequent isotherms, where only the equal areas vertical line is seen. The loop in the third layer is the result of arbitrarily limiting adsorption in the theoretical model to three layers, making the third layer a closed system. It should be emphasized that a loop is seen only in the third layer and that any vertical region in the theoretical first or second layers is not the result of a van der Waals type loop.

The parameters in Table 3 are now used to predict the isotherms at the other temperatures used in this study. Figures 24 through 33 show the experimental data points and the resulting theoretical isotherm curves. The submonolayer scales are again expanded in order to see the detail.

The behavior of the first layer seems to be predicted most accurately by this theory as the theoretical curves coincide very

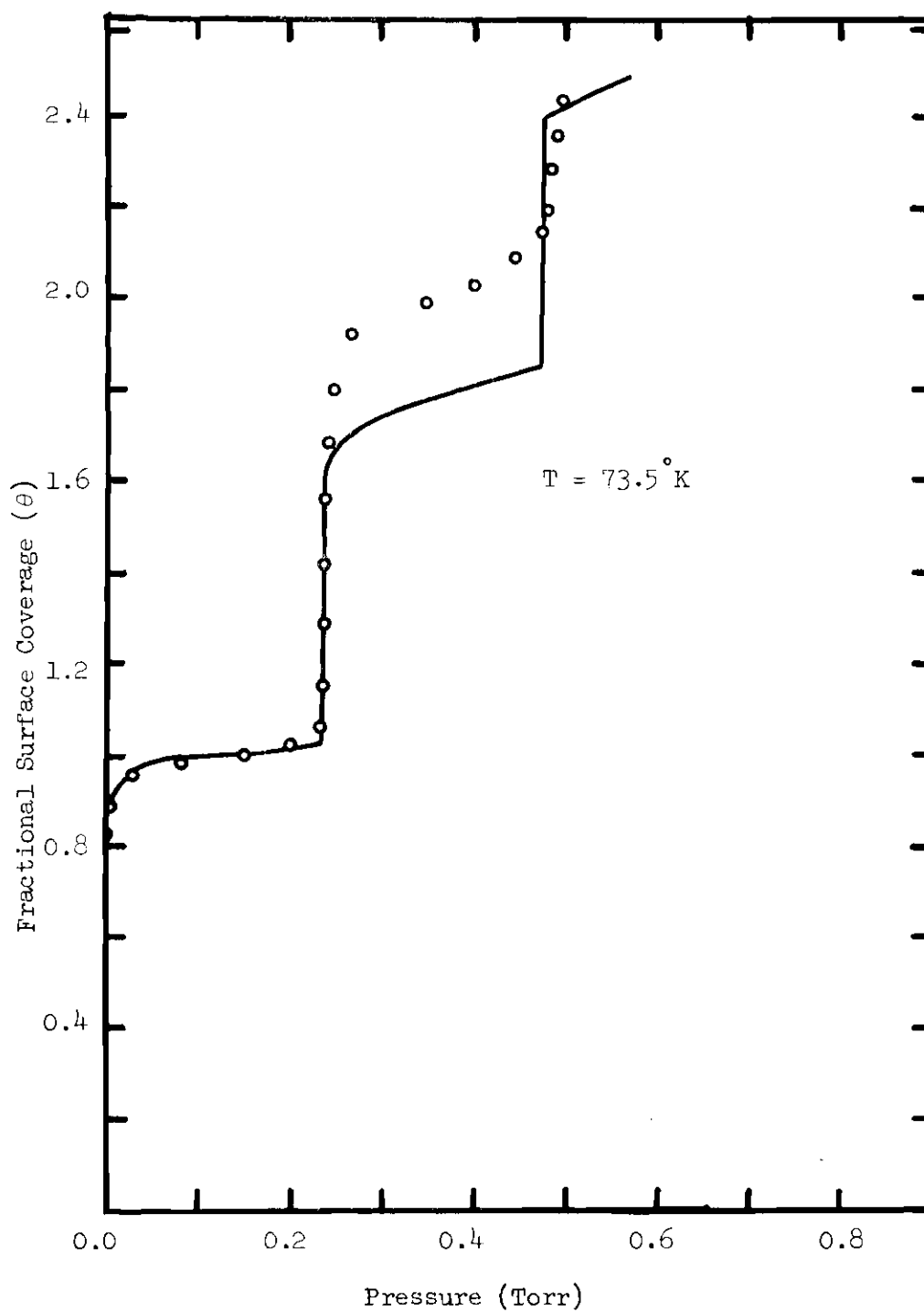


Figure 22. Comparison of the Experimental Data to the Significant Structures Multilayer Theory for Krypton on Graphite at 73.5 K; Run I.

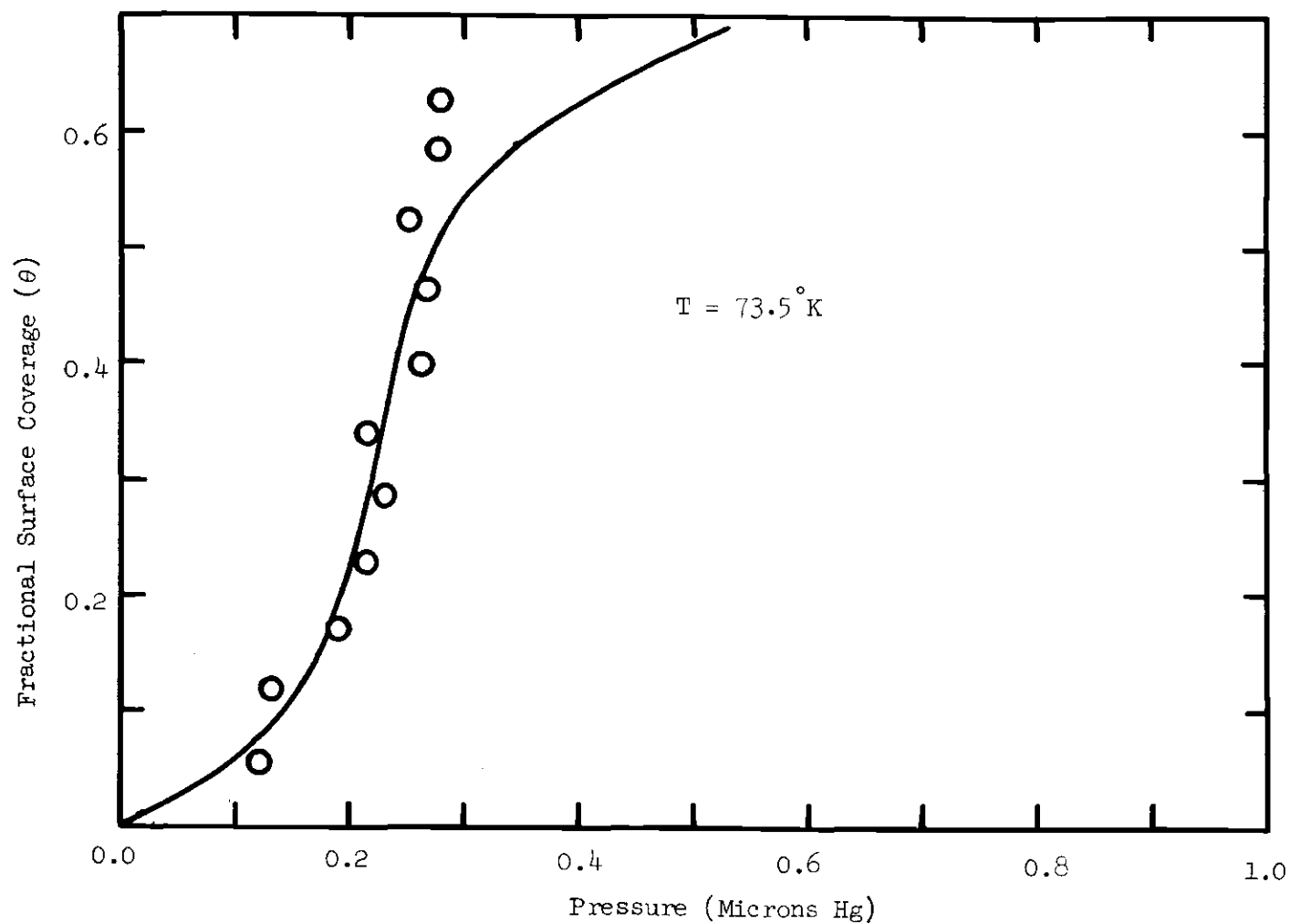


Figure 23. Comparison of the Experimental Data to the Significant Structures Multilayer Theory for Krypton on Graphite at 73.5 K; Submonolayer Region.

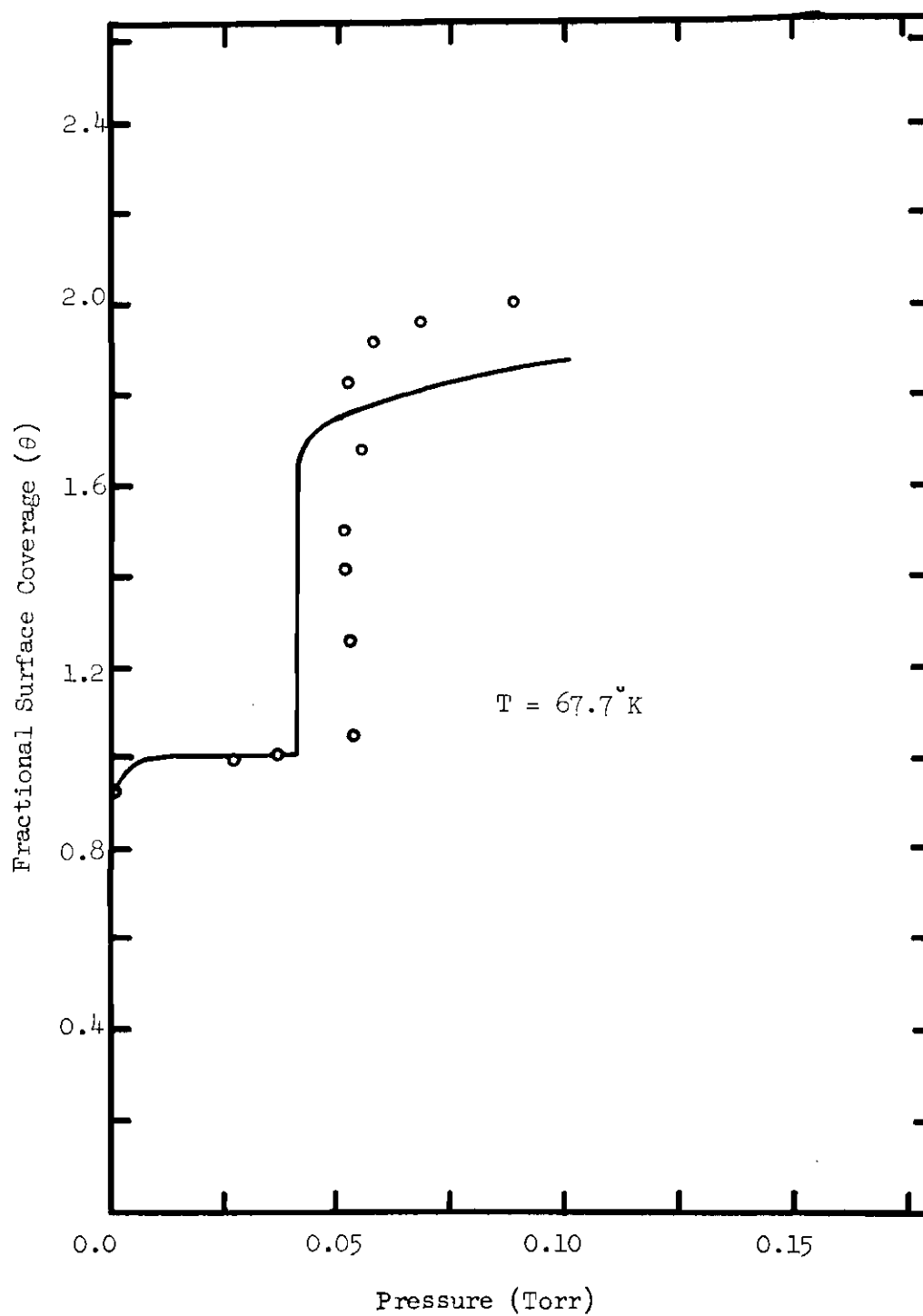


Figure 24. Comparison of the Experimental Data to the Significant Structures Multilayer Theory for Krypton on Graphite at 67.7 K.

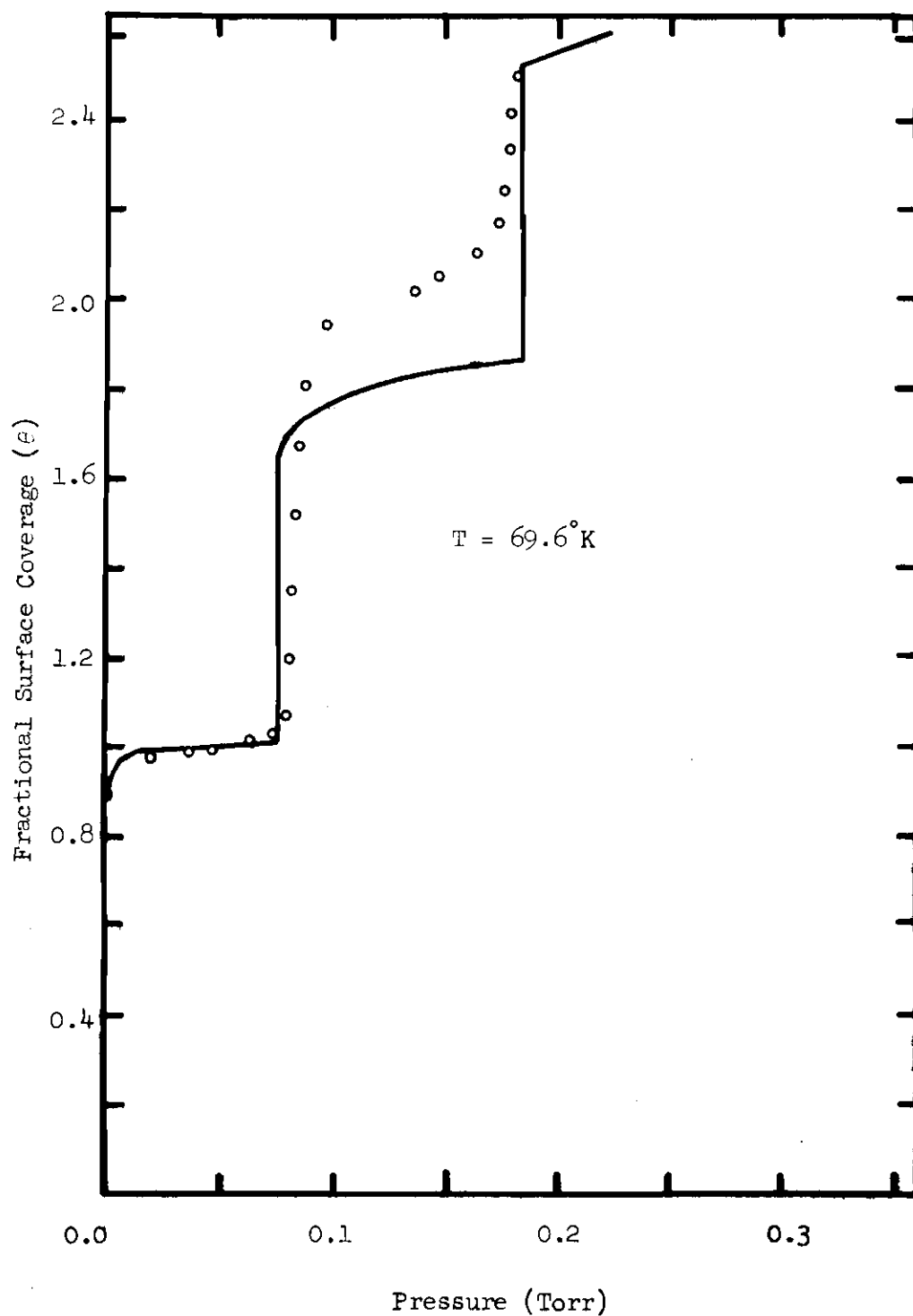


Figure 25. Comparison of the Experimental Data to the Significant Structures Multilayer Theory for Krypton on Graphite at 69.6 K.

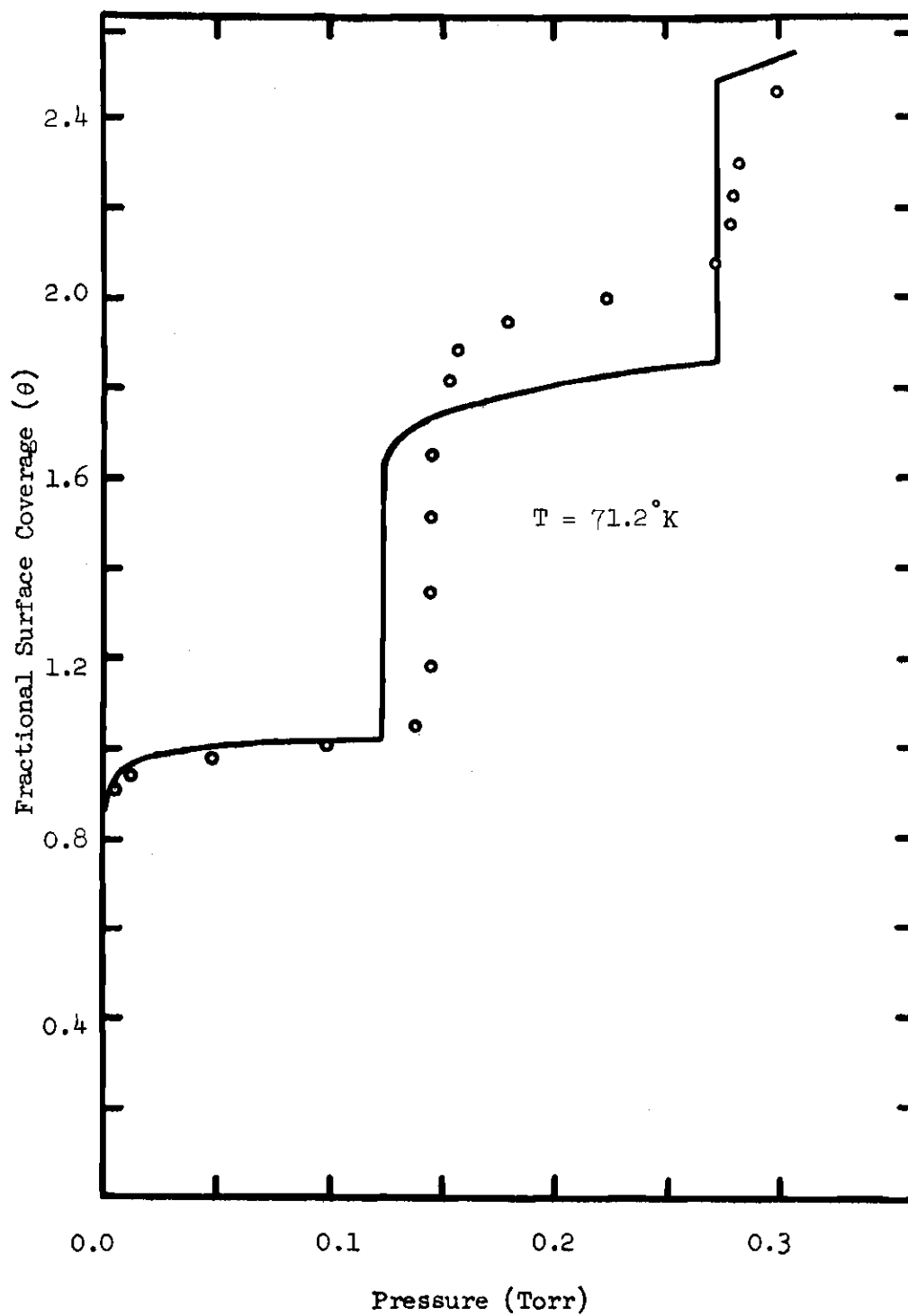


Figure 26. Comparison of the Experimental Data to the Significant Structures Multilayer Theory for Krypton on Graphite at 71.2 K.

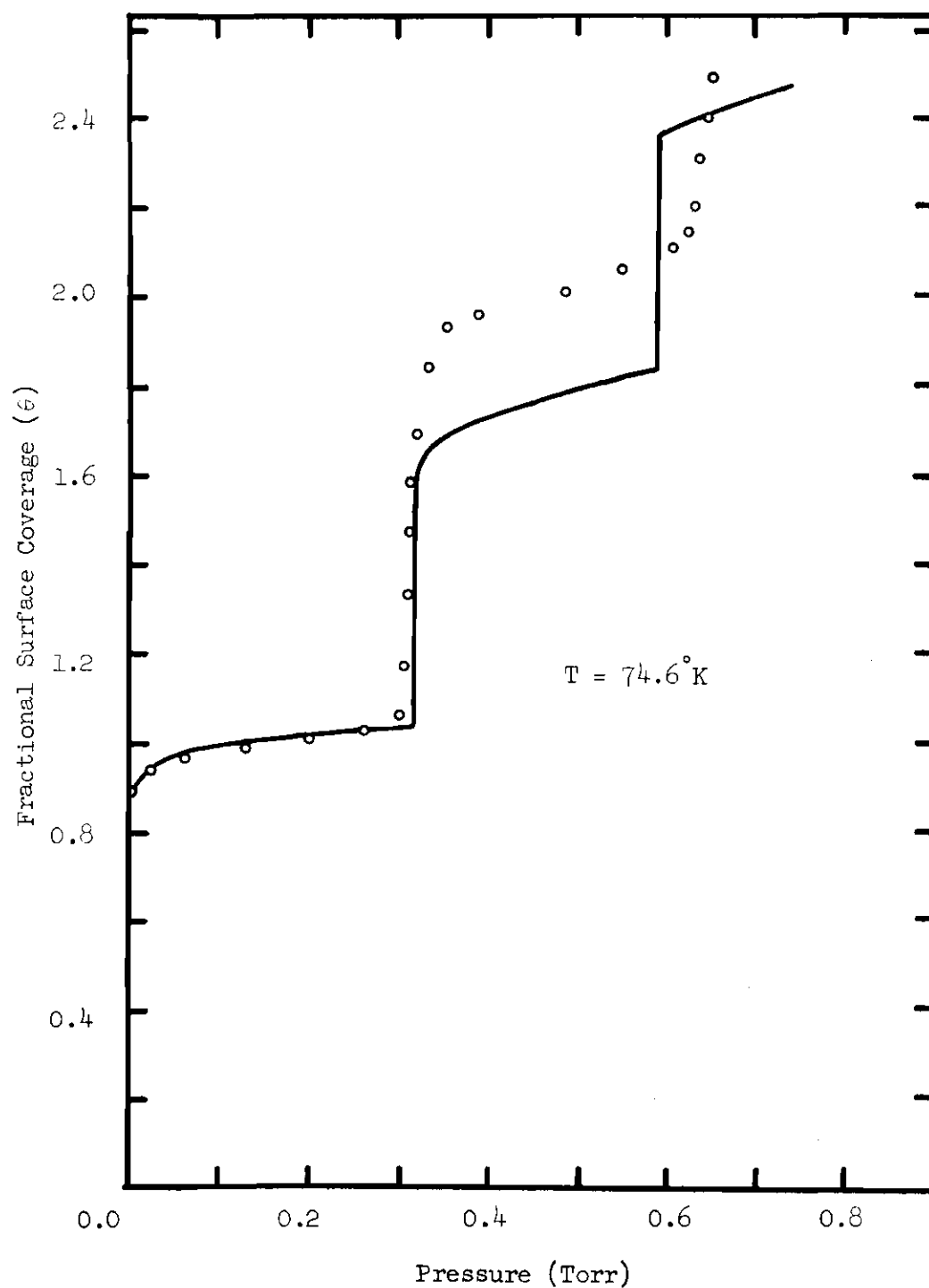


Figure 27. Comparison of the Experimental Data to the Significant Structures Multilayer Theory for Krypton on Graphite at 74.6°K .

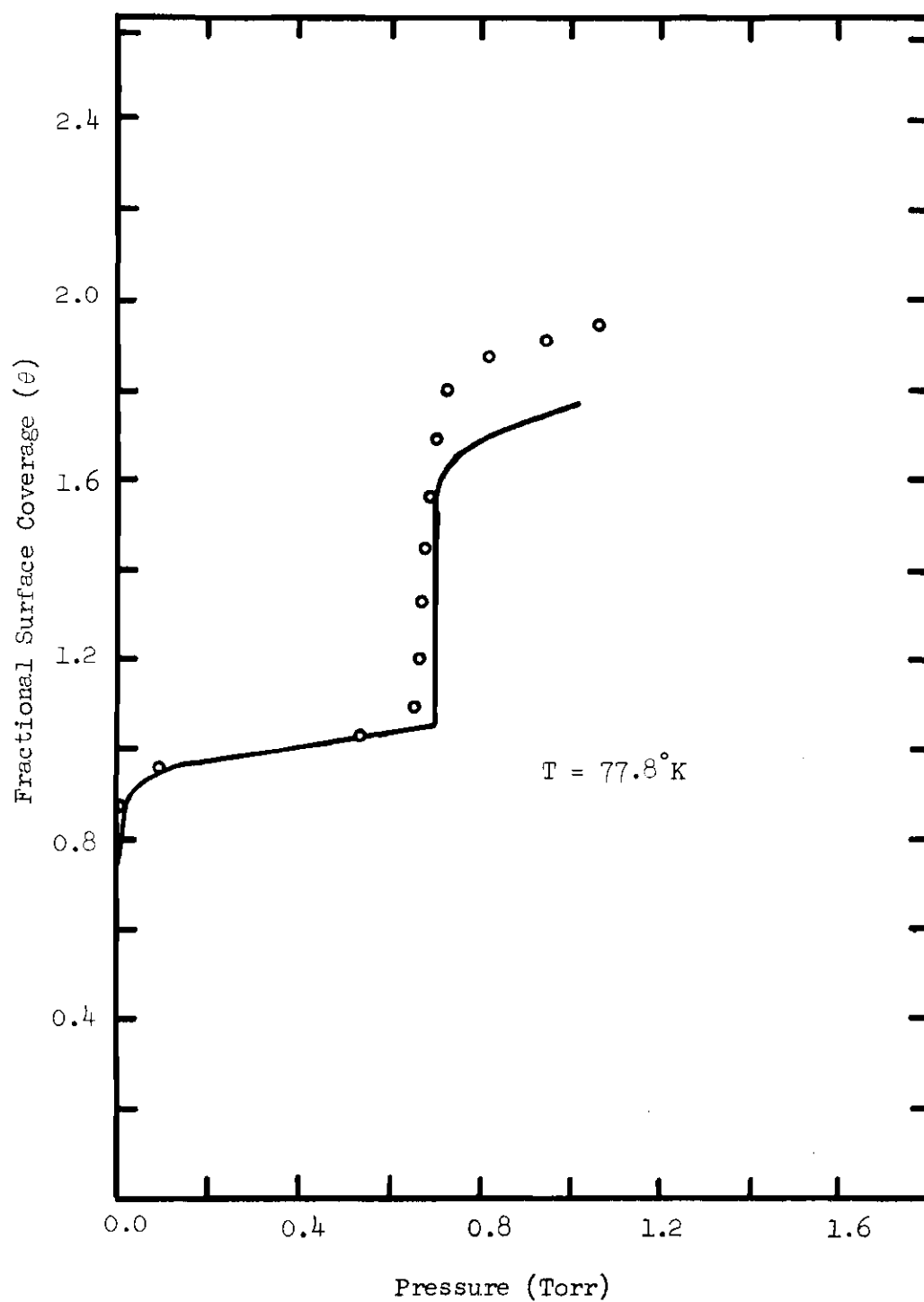


Figure 28. Comparison of the Experimental Data to the Significant Structures Multilayer Theory for Krypton on Graphite at 77.8 K.

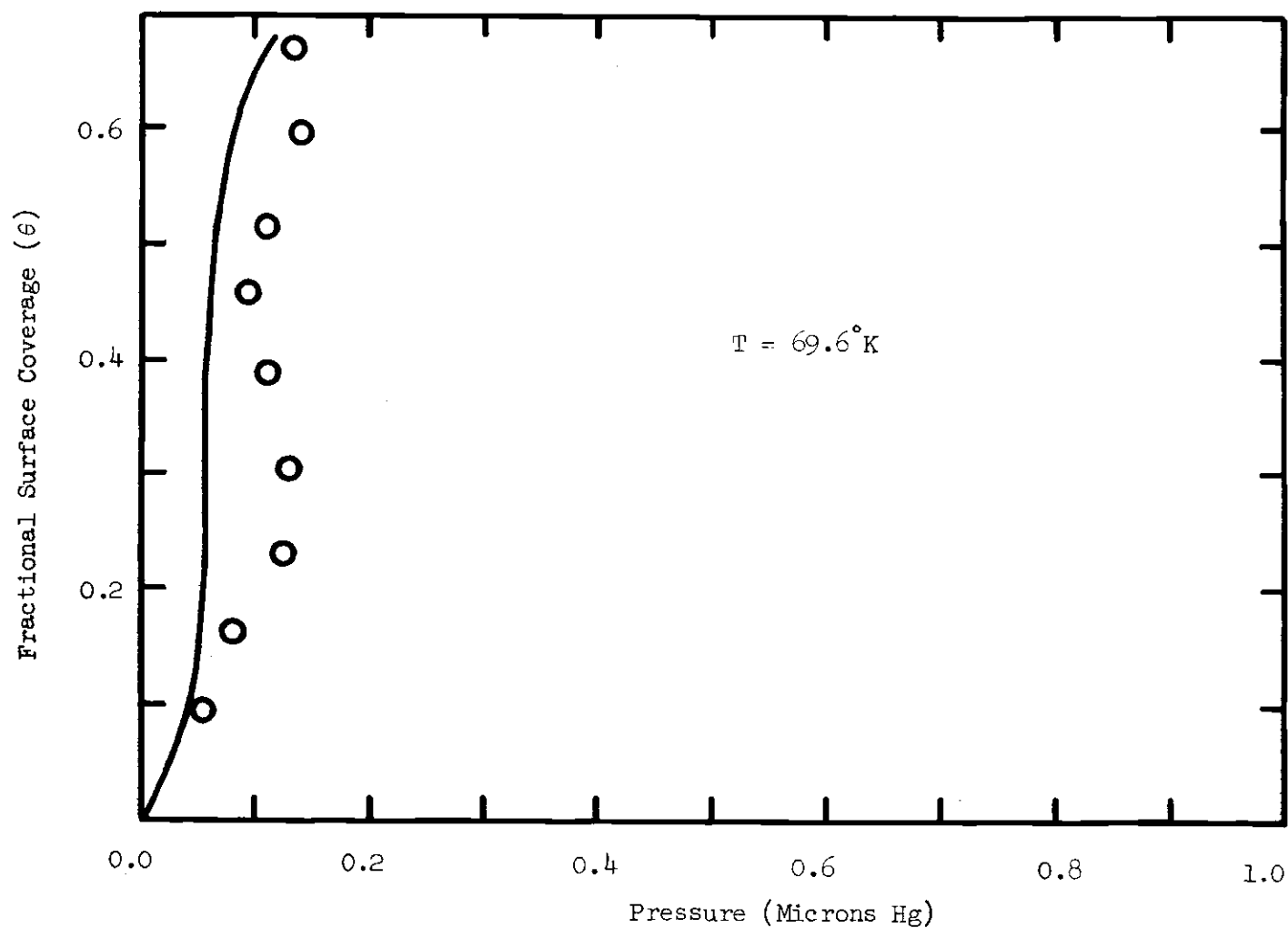


Figure 29. Comparison of the Experimental Data to the Significant Structures Multilayer Theory for Krypton on Graphite at 69.6 K; Submonolayer Region.

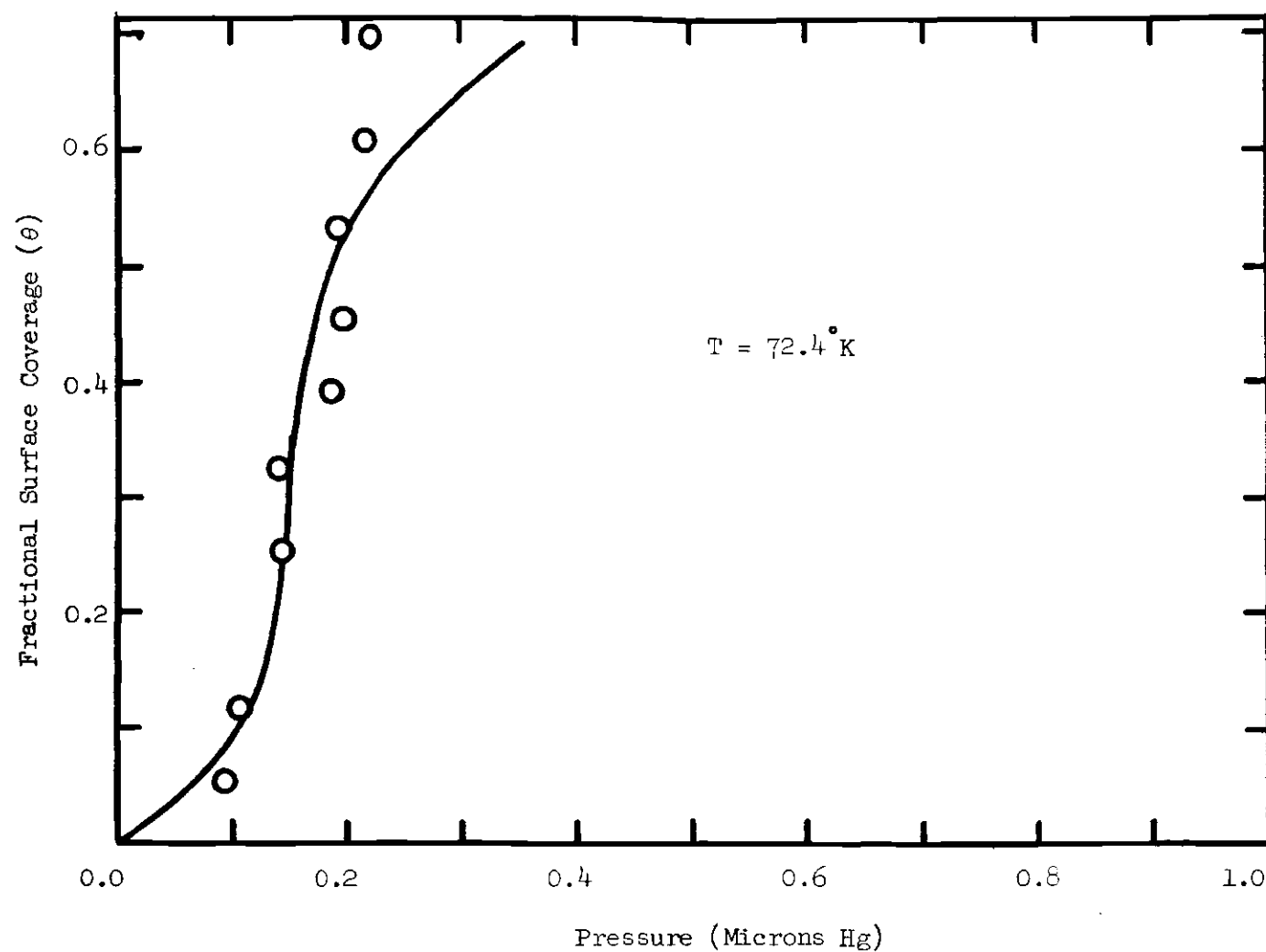


Figure 30. Comparison of the Experimental Data to the Significant Structures Multilayer Theory for Krypton on Graphite at 72.4 K; Submonolayer Region.

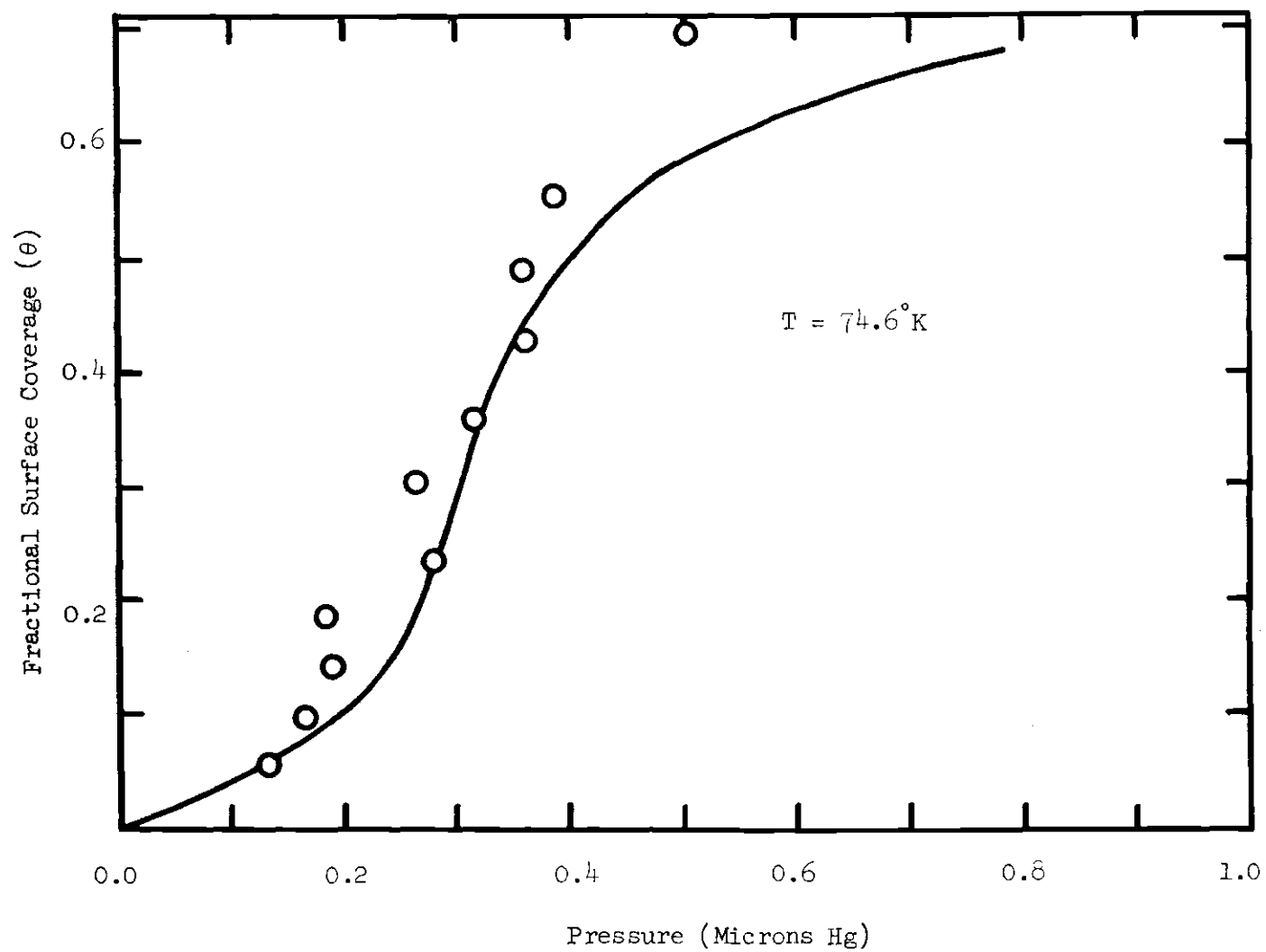


Figure 31. Comparison of the Experimental Data to the Significant Structures Multilayer Theory for Krypton on Graphite at 74.6°K ; Submonolayer Region.

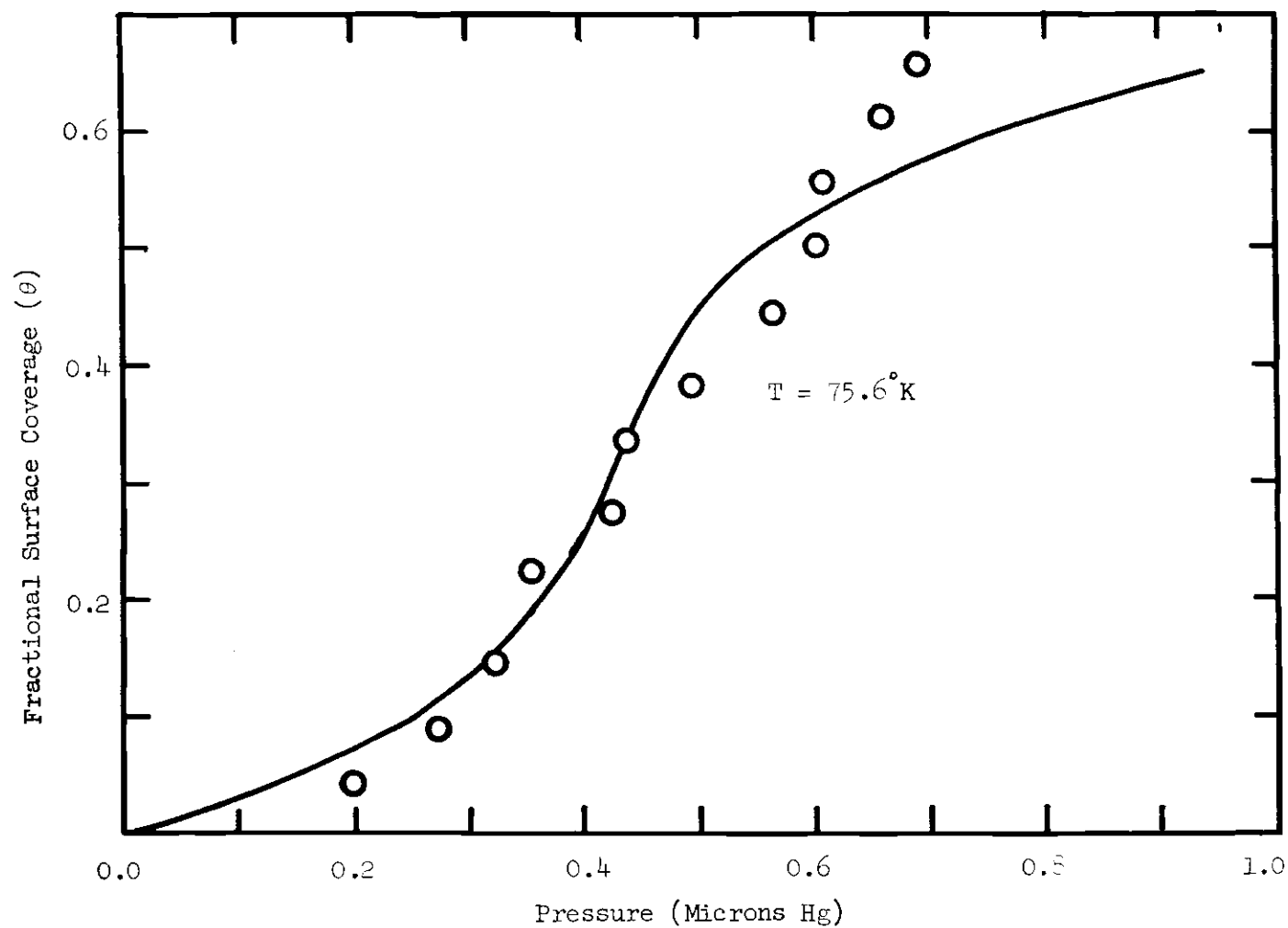


Figure 32. Comparison of the Experimental Data to the Significant Structures Multilayer Theory for Krypton on Graphite at 75.6 K; Submonolayer Region.

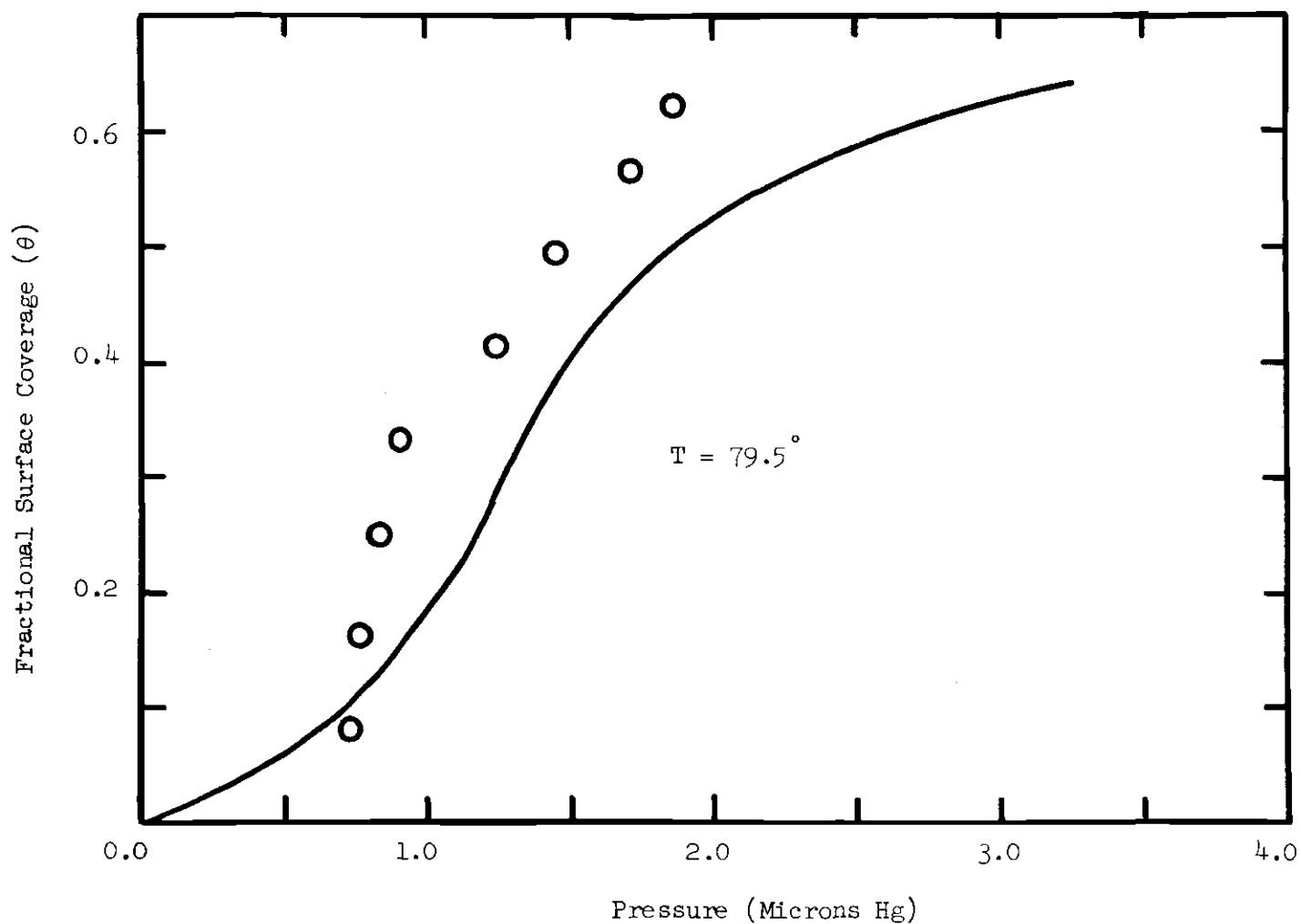


Figure 33. Comparison of the Experimental Data to the Significant Structures Multilayer Theory for Krypton on Graphite at 79.5 K; Submonolayer Region.

closely with the actual data. The worst fits for the submonolayer region are at the temperature extremes of 69.6°K and 79.5°K , and even here the shapes of the theoretical curves are correct.

The theory also predicts the two-dimensional submonolayer critical temperature to be about 69.6°K as is seen from the curves. It was concluded in Chapter V from an examination of the data that this was the approximate critical temperature.

The theoretical multilayer isotherms as compared to the data are seen in Figure 22 and Figures 24 through 28. Overall the model does a good job of predicting the positions of the steps. For example, in Figures 24 and 25, the isotherm pressures change tremendously from those in Figure 22 at 73.5°K . Yet the theory predicts these pressure changes admirably, particularly at 69.6°K . The fits in Figures 27 and 28 at 74.6°K and 77.8°K are equally impressive. The fit at 71.2°K , Figure 26, is not so good, strangely enough, but still satisfactory.

Isosteric Heats

The theoretical and experimental isosteric heats are shown in Figure 34 as a function of coverage. These heats are determined graphically from both the theoretical and experimental isotherm curves by using a Clausius-Clapeyron type expression and making a least squares fit of a plot of $\ln P$ versus $1/T$ for various values of θ .

The agreement between the theoretical and experimental heat curves is only fair. It is interesting to note that the calorimetric heats of adsorption for the krypton-P-33 (2700°) system obtained by Amberg, Spencer, and Beebe (35) and seen also in Figure 34 are located

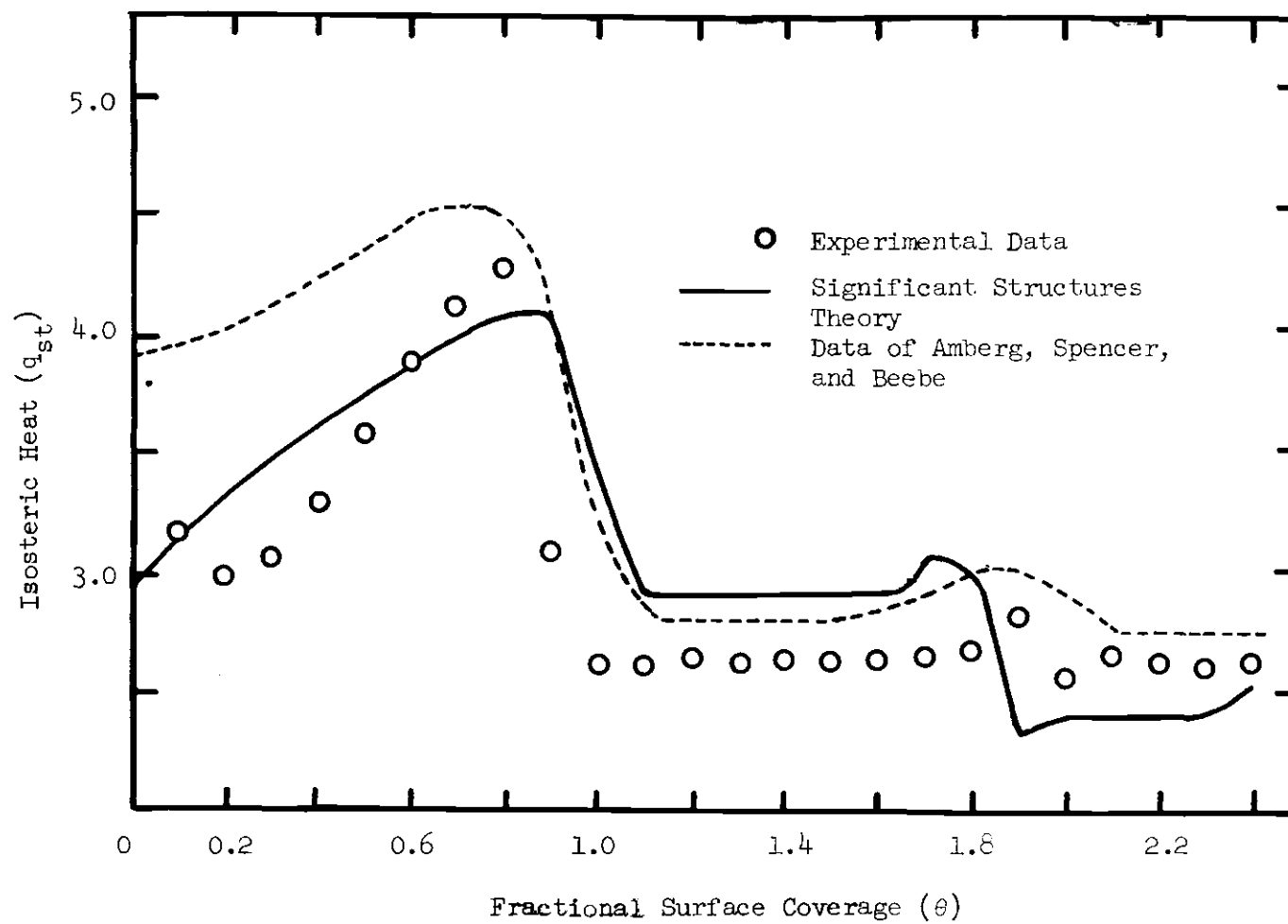


Figure 34. Theoretical and Experimental Isosteric Heats of Adsorption for Krypton on Graphite.

right in between our experimental and theoretical heat curves in the region of θ equal one to θ equal two. In addition, it is very interesting that Amberg et al. also obtained the flat portions of constant heat in their calorimetric study that were obtained in both our theoretical and experimental curves.

Discussion of Results

The molecular interaction parameters found in Table 3 and used to fit the theory to the experimental data will now be discussed in terms of other accepted values and in light of other theories.

The adsorbate-adsorbate interaction parameter is given a value of 130°K in the first adsorbed layer in the theory. This value is required to give the theoretical isotherm the correct shape, and also the correct critical temperature. The gas phase value for ϵ/k for krypton is 171°K (39); the interaction parameter is thus lowered about 24 per cent upon adsorption in the first layer. Using third order perturbation theory, Sinanoglu and Pitzer (40) have predicted just such a lowering of the gas-gas interaction parameter. They determined that, on adsorption, a repulsion is introduced between the molecules in the monolayer which amounts to about 20 to 40 per cent of their gas phase potential minimum. Our agreement here is therefore good.

The interaction of the surface with higher layers than the first drops off very rapidly. In fact, it is known that the adsorbate-adsorbent interaction in the second layer is only about 1/8 that of the first layer. For this reason the gas phase values of the interaction parameter are used for the lateral interaction in the second

and third layers of the theory.

The molar site energy determined for the first layer compares very favorably with values found by other workers. Using a virial approach Halsey and coworkers (20) determined that U_1 is 2901 calories per mole for krypton adsorbed on P-33 (2700[~]). The virial method is regarded as a very accurate approach to determine such parameters since the complication of lateral interactions is removed. The agreement with our U_1 is excellent.

If U_1 is regarded as being correct as given in Table 3, then we can estimate closely what U_2 should be by means of a lattice summation. Assume that the energies are pairwise additive between one isolated krypton molecule in the second layer and all the krypton molecules in the first layer. If a Lennard-Jones 6-12 type of potential is assumed, then the interaction energies between the second layer and the first layer can be found by equation (62).

$$E = R (\epsilon/k) \left[\left(\frac{r^*}{r} \right)^{12} - 2 \left(\frac{r^*}{r} \right)^6 \right] . \quad (62)$$

Here E equals the interaction energy, ϵ equals the depth of the potential well, r^* equals the internuclear distance at the potential minimum, and r equals the internuclear distance. Consider the interaction between the given krypton atom in the second layer and its three nearest neighbors in the first layer in Figure 35. Letting $r = r^*$ in equation (62) and multiplying the result by three, for the three neighbors, yields

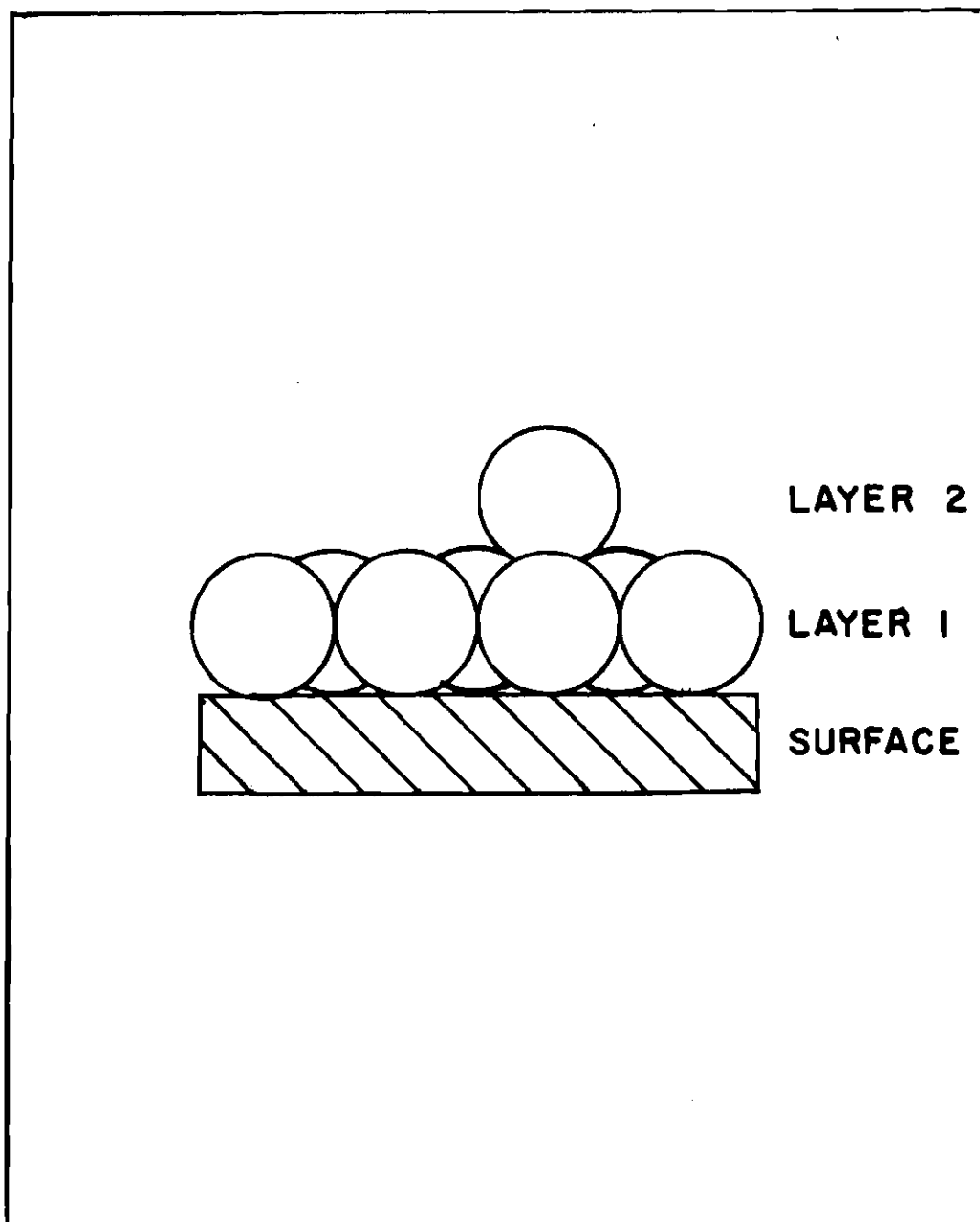


Figure 35. A Simple Model for the Packing of Krypton Atoms on the Graphite Surface in the First and Second Adsorbed layers.

$$E = R \left(\frac{\epsilon}{k} \right) (-1) \times 3 = -3R \left(\frac{\epsilon}{k} \right). \quad (63)$$

Now consider the next closest three neighbors to the given molecule in Figure 35. Equation (62) is again used and the result is equation (64).

$$E = R \left(\frac{\epsilon}{k} \right) \left[\left(\frac{1}{\sqrt{2}} \right)^{12} - 2 \left(\frac{1}{\sqrt{2}} \right)^6 \right] \times 3 = -0.70 R \left(\frac{\epsilon}{k} \right). \quad (64)$$

This process is continued for the nearest 48 neighbors in the first layer of the given krypton atom in the second layer. All the contributions are added with the result being that

$$E_{48} = -4.329 R \left(\frac{\epsilon}{k} \right) \quad (65)$$

for the total interaction of the given krypton atom in the second layer with its first 48 neighbors in the first layer. Equation (62) is integrated for the interaction past the first 48 neighbors, resulting in equation (66).

$$E_r = -0.016 R \left(\frac{\epsilon}{k} \right). \quad (66)$$

Adding equations (65) and (66), the total interaction between the krypton atom in the second layer and all the atoms in the first layer is E_T , where

$$E_T = 4.345 R \left(\frac{\epsilon}{k} \right). \quad (67)$$

The negative sign is dropped since these energies are usually given positive signs.

Another contribution to the site energy of the given molecule in the second layer is due to the solid surface. This contribution is approximated by the well known cube law. That is,

$$E_s = \frac{U_1}{\left(\frac{d_2}{d_1} \right)^3} \quad (68)$$

where E_s equals the site energy contribution from the solid surface, U_1 equals the adsorptive potential in the first layer, and d_2/d_1 equals the ratio of the distance of the first and second layers away from the surface. Here E_s is 364 calories per mole if the second layer is assumed to be twice as far from the surface as the first layer. Therefore, if a value is given to ϵ/k in equation (67), then U_2 can be estimated by letting

$$U_2 = E_s + E_T . \quad (69)$$

If a value of 130°K is given to ϵ/k , then

$$U_2 = 1486 \text{ cal/mole.}$$

This is the value of ϵ/k in the first layer as found from the best fit of the data. Sinanoglu and Pitzer (40) predict, however, that the interaction between molecules in adjacent layers should be greater than the interaction between molecules within a given layer. That is, the molecular interaction is lowered from the gas phase value within a given layer. But the interaction between molecules in adjacent layers should be raised above the gas phase value, and the gas phase value of ϵ/k would therefore perhaps be a better choice in equation (67). Letting ϵ/k be 171°K we find that

$$U_2 = 1840 \text{ cal/mole.}$$

Our theoretical value of 1670 calories per mole for U_2 lies between these two estimated values.

To estimate U_3 equation (67) is again used for the interaction between the second and third layer. If ϵ/k is 171°K then

$$E_T = 1476 \text{ cal/mole.}$$

The cube law is used to estimate the interaction between the third layer and all the molecules below the third layer. For this the theoretical value of 1670 calories per mole for U_2 is used, with the result being

$$E_S = 208 \text{ cal/mole.}$$

We thus estimate that

$$U_3 = E_T + E_S = 1684 \text{ cal/mole.}$$

This value compares very favorably with our theoretical value of 1625 calories per mole obtained from fitting the data.

CHAPTER VII

CONCLUSIONS AND RECOMMENDATIONS

It is concluded that the krypton-Sterling FT (2700°) adsorption system shows some very pronounced stepwise behavior. Two dimensional condensation is clearly seen in the first and second adsorbed layers with the two dimensional critical temperature occurring at about 69.6°K for adsorption in the submonolayer region.

It is possible that a liquidlike to solidlike surface phase transition may have been observed in one isotherm. This particular area deserves some very careful study, not only for the krypton-Sterling FT (2700°) system, but for other adsorption systems as well. It is also recommended that there be other measurements of the critical temperature of the krypton-Sterling FT (2700°) adsorption system.

The multilayer significant structures theory does many of the things one would hope a multilayer theory would do. It predicts stepwise adsorption, condensation, and critical temperatures. It fits the adsorption data of the krypton-Sterling FT (2700°) system fairly well and predicts molecular type parameters that have been shown to be very reasonable.

It is recommended that this theory be applied to several other adsorption systems. It is also recommended that the theory be extended to include polyatomic molecules.

APPENDIX A

UNCERTAINTIES IN THE THEORETICAL MOLECULAR PARAMETERS

The effects that occur in a particular theoretical isotherm upon changing the molecular parameters are now examined. Some uncertainty limits in the theoretical adsorption parameters are desired. Throughout this discussion the 73.5°K theoretical isotherm is used as an example. In Figures 36 and 37 the parameter U_1 is changed by 50 calories per mole in all three layers. The isotherm curve is translated along the pressure axis by changes in U_1 , but basically the isotherm shape remains the same. From Figures 36 and 37 we can make an estimate of the uncertainty in U_1 by the deviations of the experimental data in Chapter VI away from the theoretical curves. The uncertainty in U_1 is estimated to be 50 calories per mole, in U_2 , 20 calories per mole, and in U_3 , 10 calories per mole. These uncertainties, and those that follow, represent only the model's ability to fit the data.

In Figures 38 and 39 U_1 remains the same, but $(\epsilon/k)_1$ is changed in all three layers by 10°K. Changing $(\epsilon/k)_1$ affects not only the pressures, but the basic shape of the theoretical isotherm as well. This is very clearly seen in the submonolayer region, Figure 39. In the second layer, seen in Figure 38, lowering ϵ_2 raises the pressure, as expected, and also makes the region of vertical discontinuity somewhat less. In the third layer, lowering ϵ_3 raises

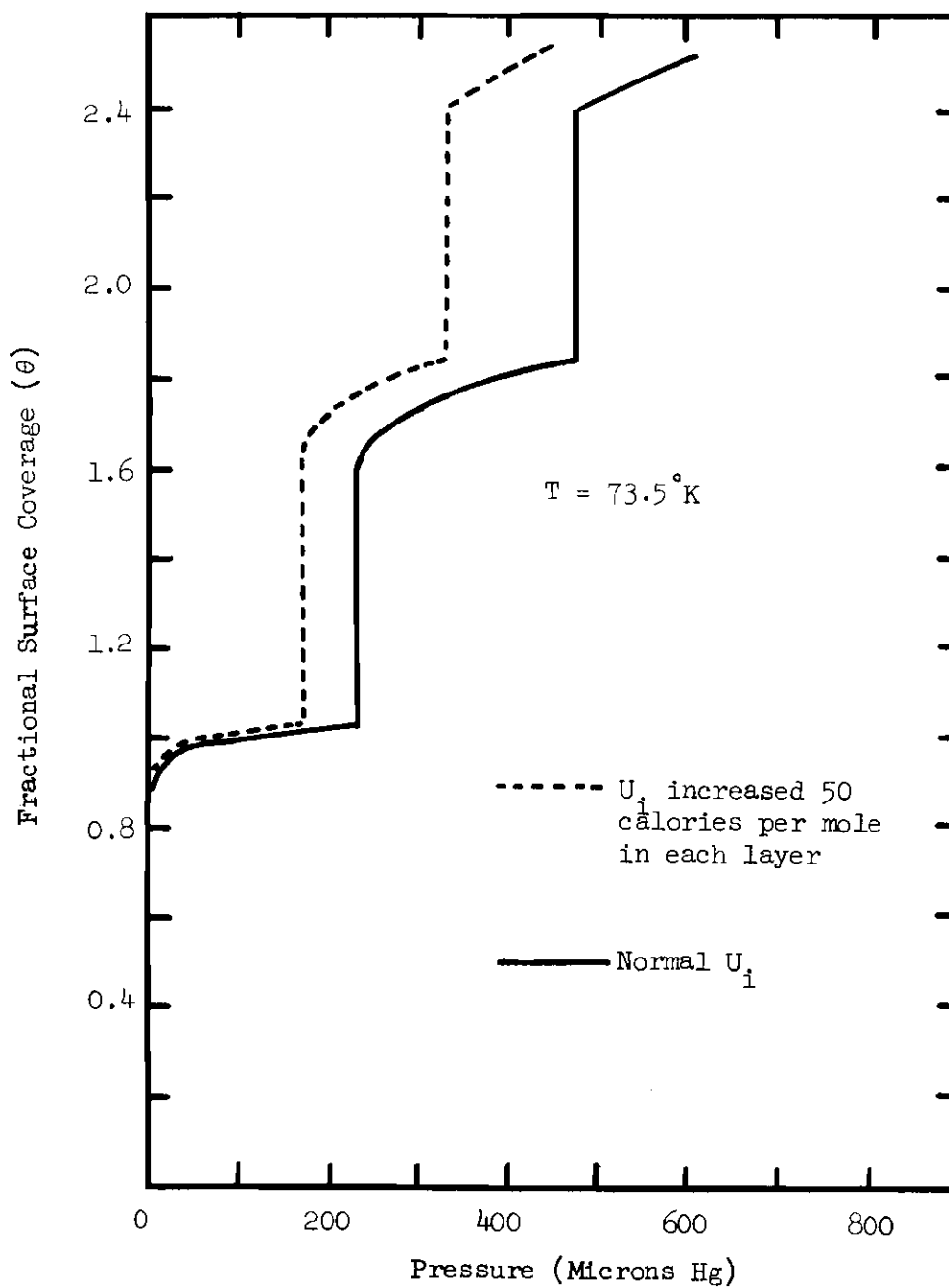


Figure 36. The Effect of Changes in U_i on the Position of the Isotherm.

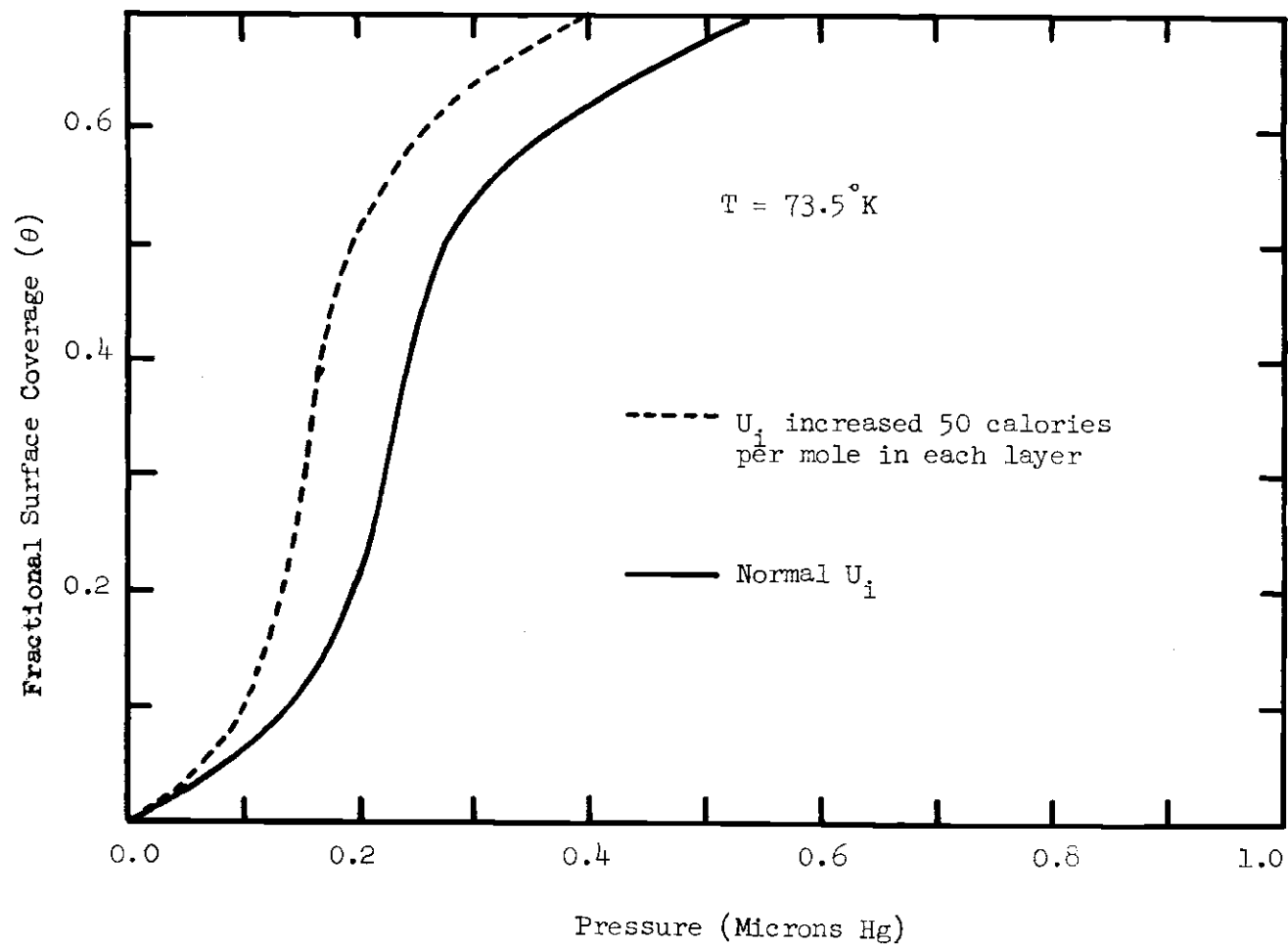


Figure 37. The Effect of Changes in U_i on the Position of the Isotherm; Submonolayer Region.

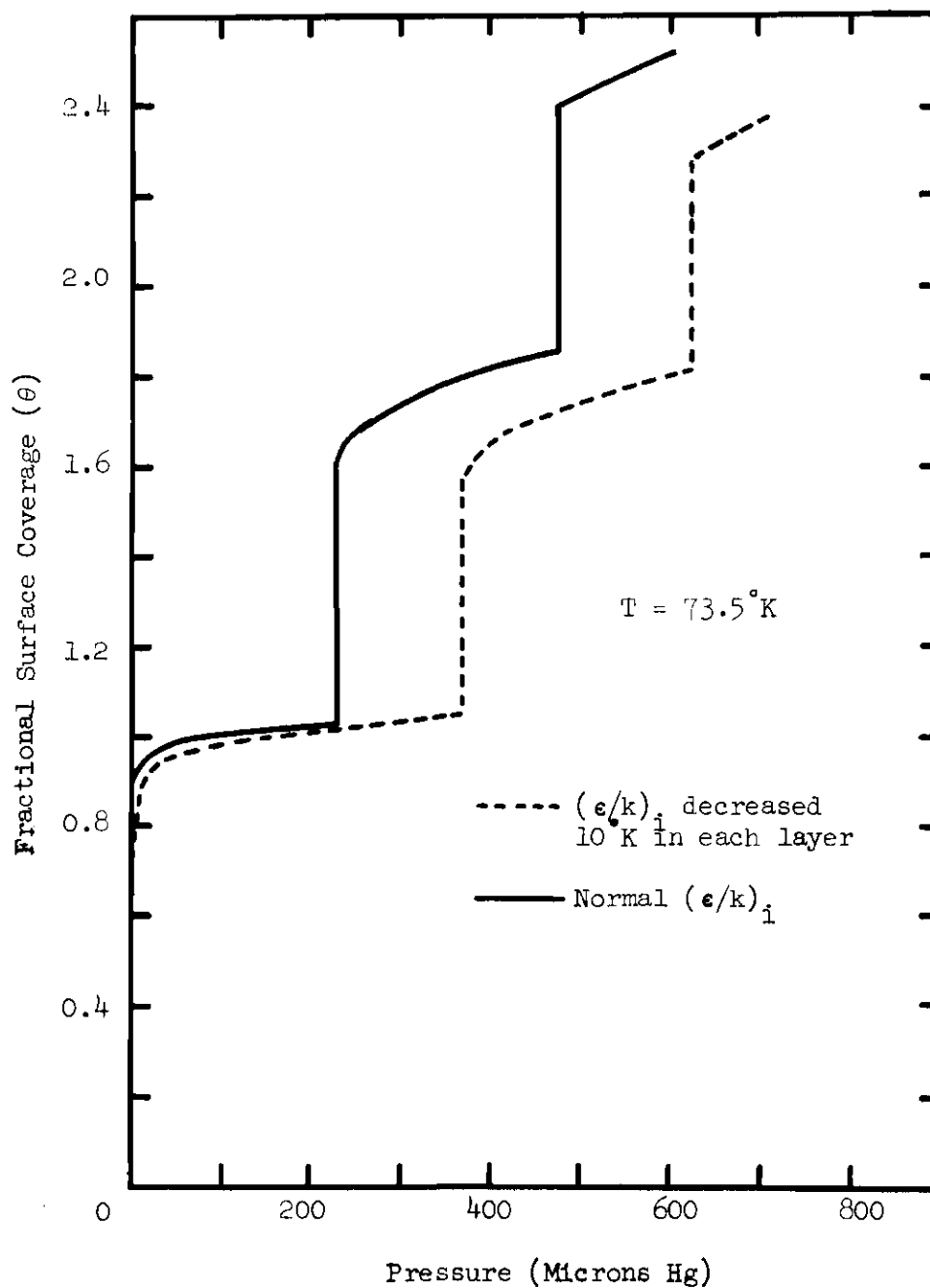


Figure 38. The Effect of Changes in ϵ_1 on the Position of the Isotherm.

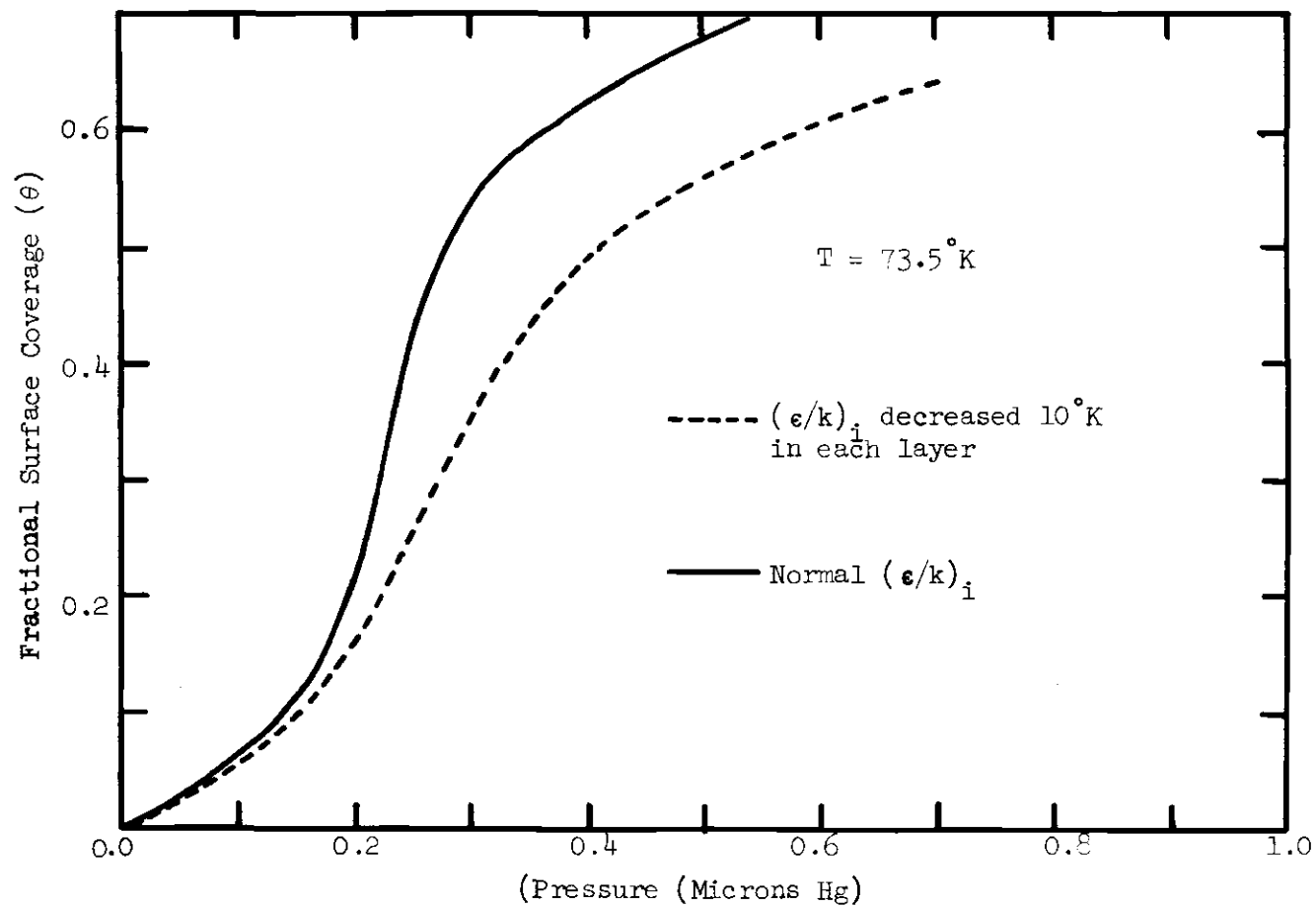


Figure 39. The Effect of Changes in ϵ_i on the Position of the Isotherm; Submonolayer Region.

the pressure and makes the formation of the third layer begin much sooner. It also causes the region of vertical discontinuity to be less in the third layer. The uncertainties in these parameters are very difficult to establish. Probably about 5°K is a fair estimate of the uncertainty in $(\epsilon/k)_1$.

This raises the question of how to fit the data if there are two parameters, ϵ_1 and U_1 , which change the isotherm pressures. We rely first on the shape of the isotherm to determine ϵ_1 . Of course ϵ_2 and ϵ_3 are more difficult and are given the gas phase value. The pressures in each layer are then adjusted to the data by means of U_1 .

The greatest deviation of the theoretical curves from the experimental data occurs at the flat plateau regions of the theoretical curve; that is, the theoretical curve bends over much too quickly from the vertical riser in Figures 22 through 28. One possible explanation for this deviation is that the packing of the krypton atoms in the second and third adsorbed layers is different than the packing in the first layer. Throughout the treatment thus far, it has been assumed that the area per molecule at capacity coverage and the amount of krypton needed to complete a layer were exactly the same for each layer; that is, A_1 is 19.5\AA^2 and V_m is 3.22cc(STP) per gram.

It is quite reasonable to let the packing be different in each layer, particularly considering the fact that the lateral interactions are so much greater in the second and third layers than in the first layer. A good approximation is to let the density of the krypton in the second and third layers be the same as that of bulk solid krypton.

For hexagonally packed solid krypton

$$\frac{V}{N} = \frac{a^3}{\sqrt{2}} \quad (70)$$

where a is the cell radius and V is the total volume of the N molecules in the system. For a two-dimensional triangular lattice of krypton

$$\frac{A}{N} = \frac{\sqrt{3}}{2} a^2 \quad (71)$$

where a is the cell radius and A is the total area occupied by the N atoms. If the density of krypton in the two-dimensional lattice is the same as the bulk solid krypton, then a is the same in equations (70) and (71). Thus

$$\frac{A}{N} = \frac{\sqrt{3}}{2} \left[2^{1/3} \left(\frac{V}{N} \right)^{2/3} \right] . \quad (72)$$

At 73.5°K the density of solid krypton is 2.95 grams per cubic centimeter (41). From this density V/N is determined, resulting in

$$\frac{A}{N} = 14.3A^2.$$

Thus

$$A_1^o = 19.5A^2$$

$$A_2^o = 14.3A^2$$

$$A_3^o = 14.3A^2$$

If these new values of A_i are substituted in the theoretical isotherm equations, it would seem that a whole new set of θ 's would result. This is not the case however, as the theoretical θ 's remain the same as a result of the way θ_i is defined. The number of sites in the i -th layer is defined as the number of molecules adsorbed in the $i-1$ layer; thus, N_i can never exceed N_{i-1} .

Since we know that the packing in the second and third layers can be greater than in the first layer, we can artificially force N_2 and N_3 in the theory to be greater by multiplying each by A_1^o/A_2^o , or 1.36. That is

$$N_1 = \theta_1 N_0,$$

$$N_2 = \theta_2 N_1 \times 1.36 = \theta_2 \theta_1 N_0 \times 1.36,$$

and

$$N_3 = \theta_3 N_2 \times 1.36 = \theta_3 \theta_2 \theta_1 N_0 \times 1.36.$$

Thus

$$\theta = \theta_1 + (\theta_1\theta_2) 1.36 + (\theta_1\theta_2\theta_3) 1.36 . \quad (73)$$

The isotherm at 73.5° K in Figure 22 is now adjusted with the new value of θ in equation (73) and the result is shown in Figure 40. The agreement between the theoretical curve and experimental data is greatly improved by this approximation. The fact that the data lies below the theoretical curve at the second plateau probably indicates that the density of the second adsorbed layer is somewhat less than that of bulk solid krypton.

The rest of the theoretical curves could obviously be treated in a similar manner, resulting in closer agreement between the theory and experiment. We decline to do this, however, since the idea of different packing in different layers is not really consistent with the present theoretical development.

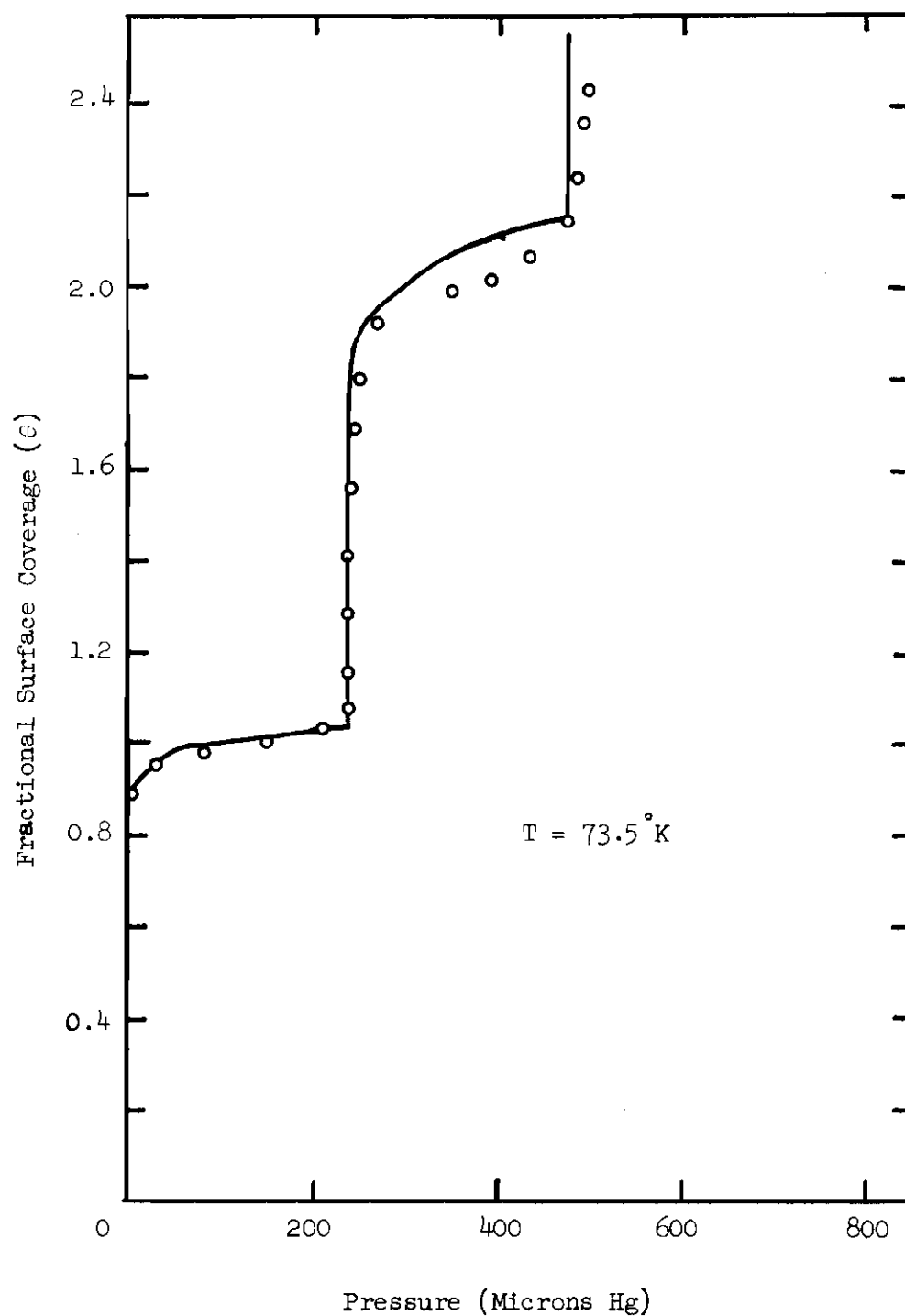


Figure 40. Comparison of the Experimental Data to the Theoretical Isotherm After Changing the Packing in the Second and Third Adsorbed Layers.

APPENDIX B

EXPERIMENTAL DATA

Table 4. Experimental Submonolayer Data for
Krypton on Graphite at 69.6° K.
 $V_m = 3.22$ STP cc/gm

V_{ads} (STP cc/gm)	P (microns Hg)	θ
0.310	0.053	0.096
0.525	0.081	0.163
0.733	0.126	0.228
0.972	0.128	0.302
1.25	0.111	0.387
1.47	0.094	0.457
1.65	0.110	0.513
1.92	0.139	0.595
2.17	0.133	0.672
2.43	0.152	0.755
2.65	0.194	0.824
2.86	0.818	0.887

Table 5. Experimental Submonolayer Data for
 Krypton on Graphite at 72.4 K.
 $V_m = 3.22$ STP cc/gm

V_{ads} (STP cc/gm)	P (microns Hg)	θ
0.174	0.093	0.054
0.379	0.106	0.118
0.818	0.143	0.254
1.04	0.138	0.324
1.26	0.186	0.391
1.46	0.196	0.452
1.71	0.191	0.530
1.95	0.215	0.607
2.24	0.221	0.697
2.52	0.256	0.782
2.84	0.654	0.882

Table 6. Experimental Submonolayer Data for
 Krypton on Graphite at 72.5 K.
 $V_m = 3.22$ STP cc/gm

V_{ads} (STP cc/gm)	P (microns Hg)	θ
0.174	0.096	0.054
0.310	0.132	0.096
0.515	0.173	0.160
0.702	0.189	0.218
1.07	0.192	0.331
1.26	0.199	0.391
1.45	0.211	0.450
1.63	0.234	0.506
1.96	0.235	0.609
2.59	0.320	0.803
2.84	0.654	0.882

Table 7. Experimental Submonolayer Data for
 Krypton on Graphite at 73.5 K. (Run #1)
 $V_m = 3.22$ STP cc/gm

V_{ads} (STP cc/gm)	P (microns Hg)	θ
0.177	0.121	0.055
0.379	0.130	0.118
0.549	0.188	0.171
0.740	0.214	0.230
0.924	0.230	0.287
1.10	0.214	0.339
1.29	0.263	0.399
1.49	0.268	0.462
1.69	0.254	0.523
1.88	0.278	0.582
2.02	0.280	0.628
2.23	0.297	0.693
2.40	0.314	0.747
2.58	0.357	0.802
2.75	0.502	0.854

Table 8. Experimental Submonolayer Data for
 Krypton on Graphite at 73.5 K. (Run #2)
 $V_m = 3.22$ STP cc/gm

V_{ads} (STP cc/gm)	P (microns Hg)	θ
0.177	0.121	0.055
0.385	0.129	0.120
0.604	0.158	0.188
0.791	0.177	0.246
0.965	0.182	0.300
1.13	0.196	0.352
1.30	0.199	0.403
1.49	0.207	0.464
1.69	0.234	0.523
1.87	0.267	0.581
2.10	0.286	0.651
2.27	0.306	0.704
2.43	0.378	0.753

Table 9. Experimental Submonolayer Data for
Krypton on Graphite at 74.6 K.
 $V_m = 3.22$ STP cc/gm

V_{ads} (STP cc/gm)	P (microns Hg)	θ
0.177	0.133	0.055
0.310	0.165	0.096
0.454	0.189	0.141
0.593	0.184	0.184
0.750	0.280	0.233
0.968	0.264	0.301
1.16	0.316	0.359
1.37	0.361	0.427
1.60	0.358	0.490
1.77	0.386	0.552
2.24	0.504	0.697
2.41	0.597	0.749
2.62	0.736	0.813
2.80	1.001	0.868
2.90	1.323	0.901

Table 10. Experimental Submonolayer Data for
 Krypton on Graphite at 75.6 K.
 $V_m = 3.22$ STP cc/gm

V_{ads} (STP cc/gm)	P (microns Hg)	θ
0.136	0.198	0.042
0.280	0.274	0.087
0.471	0.322	0.146
0.723	0.353	0.225
0.876	0.424	0.272
1.08	0.437	0.335
1.23	0.493	0.382
1.44	0.564	0.448
1.62	0.602	0.504
1.79	0.608	0.557
1.97	0.661	0.612
2.12	0.691	0.659
2.30	0.755	0.713
2.45	0.834	0.759
2.64	1.030	0.819

Table 11. Experimental Submonolayer Data for
Krypton on Graphite at 79.5° K.
 $V_m = 3.22$ STP cc/gm

V_{ads} (STP cc/gm)	P (microns Hg)	θ
0.261	0.719	0.081
0.518	0.754	0.161
0.811	0.819	0.252
1.07	0.902	0.333
1.34	1.24	0.416
1.60	1.45	0.496
1.82	1.71	0.566
2.00	1.86	0.621
2.23	2.25	0.692
2.42	2.34	0.752
2.59	2.31	0.805
2.76	2.37	0.858
2.94	2.87	0.914
3.15	3.96	0.979

Table 12. Experimental Multilayer Data for
Krypton on Graphite at 67.7 K.
 $V_m = 3.22$ STP cc/gm

V_{ads} (STP cc/gm)	P (microns Hg)	θ	V_{ads} (STP cc/gm)	P (microns Hg)	θ
2.19	0.118	0.68	5.13	55.5	1.59
2.45	0.118	0.76	5.42	55.6	1.68
2.72	0.134	0.84	5.65	57.4	1.76
2.96	1.30	0.92	5.90	52.7	1.83
3.22	27.4	1.00	6.17	57.4	1.92
3.26	37.9	1.01	6.33	68.9	1.97
3.29	43.1	1.02	6.44	81.9	2.00
3.33	48.6	1.04	6.48	87.7	2.01
3.38	53.4	1.05	6.52	91.3	2.03
3.43	53.7	1.06	6.57	99.2	2.04
3.47	53.0	1.08	6.68	106	2.08
3.60	52.6	1.12	6.82	111	2.12
3.84	51.9	1.19	7.05	111	2.19
4.08	53.3	1.27	7.26	114	2.25
4.33	53.0	1.35	7.49	116	2.33
4.59	51.5	1.43	7.79	117	2.42
4.85	51.8	1.51			

Table 13. Experimental Multilayer Data for
Krypton on Graphite at 69.6 K.
 $V_m = 3.22$ STP cc/gm

V_{ads} (STP cc/gm)	P (microns Hg)	θ	V_{ads} (STP cc/gm)	P (microns Hg)	θ
2.41	0.146	0.75	6.59	148	2.05
2.88	1.09	0.89	6.63	153	2.06
3.13	20.0	0.97	6.76	164	2.10
3.16	28.6	0.98	6.87	170	2.13
3.18	36.8	0.99	6.98	174	2.17
3.21	46.8	1.00	7.22	176	2.24
3.24	56.9	1.01	7.49	178	2.33
3.28	64.4	1.02	7.76	179	2.41
3.32	73.1	1.03	8.05	182	2.50
3.36	77.2	1.04	8.35	188	2.59
3.40	79.4	1.06	8.58	190	2.67
3.44	79.3	1.07	8.79	191	2.73
3.48	80.3	1.08	9.00	196	2.79
3.65	79.6	1.13	9.22	199	2.86
3.68	80.3	1.14	9.38	197	2.91
3.74	80.7	1.16	9.57	201	2.97
3.85	81.3	1.20	9.75	202	3.03
4.07	81.5	1.26	9.96	205	3.09
4.34	82.0	1.35	10.17	207	3.16
4.59	83.6	1.43	10.32	206	3.21
4.88	83.8	1.52	10.53	207	3.27
5.15	84.2	1.60	10.74	208	3.34
5.37	85.7	1.67	10.94	208	3.40
5.60	86.4	1.74	11.23	209	3.49
5.81	87.9	1.81	11.51	209	3.58
6.01	89.9	1.87	11.78	210	3.66
6.24	96.9	1.94	12.09	210	3.75
6.50	137	2.02	12.42	211	3.86
6.55	143	2.03	12.75	212	3.96

Table 14. Experimental Multilayer Data for
Krypton on Graphite at 71.2 K.
 $V_m = 3.22$ STP cc/gm

V_{ads} (STP cc/gm)	P (microns Hg)	θ	V_{ads} (STP cc/gm)	P (microns Hg)	θ
2.48	0.209	0.77	7.15	279	2.22
2.70	0.291	0.84	7.37	282	2.29
2.92	5.55	0.91	7.62	296	2.37
3.03	12.7	0.94	7.91	300	2.46
3.15	48.3	0.98	8.18	296	2.54
3.24	99.2	1.01	8.45	303	2.62
3.31	129	1.03	8.72	324	2.71
3.38	139	1.05	9.09	336	2.82
3.44	137	1.07	9.35	344	2.90
3.78	145	1.17	9.62	350	2.99
4.08	145	1.27	9.91	357	3.08
4.34	145	1.35	10.17	360	3.16
4.60	145	1.43	10.45	364	3.25
4.86	145	1.51	10.73	371	3.33
5.09	146	1.58	11.01	383	3.42
5.30	146	1.65	11.30	391	3.51
5.57	148	1.73	11.57	393	3.59
5.84	153	1.81	11.81	398	3.67
6.05	157	1.88	12.12	417	3.76
6.26	179	1.95	12.33	431	3.83
6.35	199	1.97	12.61	443	3.92
6.43	223	2.00	12.88	446	4.00
6.52	245	2.03	13.14	434	4.08
6.69	273	2.08	13.41	426	4.16
6.84	287	2.12	13.67	423	4.25
6.97	277	2.16			

Table 15. Experimental Multilayer Data for
Krypton on Graphite at 73.5 K.
 $V_m = 3.22$ STP cc/gm

V_{ads} (STP cc/gm)	P (microns Hg)	θ	V_{ads} (STP cc/gm)	P (microns Hg)	θ
2.19	0.869	0.68	4.13	237	1.28
2.41	0.950	0.75	4.33	236	1.34
2.65	0.997	0.82	4.56	236	1.42
2.87	4.44	0.89	4.78	238	1.49
2.94	10.7	0.91	5.00	240	1.55
2.98	12.8	0.93	5.21	240	1.62
3.01	16.5	0.94	5.42	243	1.68
3.04	20.5	0.94	5.60	244	1.74
3.06	29.6	0.95	5.79	248	1.80
3.09	39.6	0.96	5.96	251	1.85
3.11	52.2	0.97	6.17	268	1.92
3.13	65.8	0.97	6.27	294	1.95
3.15	81.9	0.98	6.39	348	1.98
3.17	106	0.99	6.42	364	1.99
3.19	121	0.99	6.44	373	2.00
3.21	137	1.00	6.47	381	2.01
3.22	151	1.00	6.49	391	2.02
3.25	172	1.01	6.53	401	2.03
3.27	188	1.02	6.55	411	2.04
3.30	201	1.03	6.59	421	2.05
3.33	213	1.03	6.61	427	2.05
3.35	225	1.04	6.64	433	2.06
3.38	228	1.05	6.66	436	2.07
3.41	232	1.06	6.69	442	2.08
3.43	236	1.07	6.71	447	2.08
3.46	236	1.08	6.75	454	2.10
3.55	237	1.10	6.90	473	2.14
3.70	237	1.15	7.05	481	2.19
3.93	237	1.22	7.18	483	2.23

Table 15. Continued

V_{ads} (STP cc/gm)	P (microns Hg)	θ	V_{ads} (STP cc/gm)	P (microns Hg)	θ
7.34	488	2.28	9.67	541	3.00
7.58	490	2.35	9.87	546	3.07
7.84	496	2.43	10.11	551	3.14
8.06	501	2.50	10.33	558	3.21
8.32	505	2.58	10.55	560	3.28
8.59	512	2.67	10.73	565	3.33
8.83	520	2.74	11.03	572	3.43
9.05	525	2.81	11.37	575	3.53
9.26	531	2.88	11.66	577	3.62
9.49	536	2.95	11.92	579	3.70

Table 16. Experimental Multilayer Data for
Krypton on Graphite at 74.6° K.
 $V_m = 3.22$ STP cc/gm

V_{ads} (STP cc/gm)	P (microns Hg)	θ	V_{ads} (STP cc/gm)	P (microns Hg)	θ
2.87	5.00	0.89	6.61	550	2.05
2.89	9.34	0.90	6.67	573	2.07
2.90	12.2	0.90	6.73	590	2.09
2.93	16.1	0.91	6.81	607	2.11
3.02	27.0	0.94	6.91	623	2.15
3.11	63.4	0.97	7.02	627	2.18
3.18	129	0.99	7.10	631	2.21
3.24	200	1.01	7.28	633	2.26
3.31	261	1.03	7.41	635	2.30
3.41	299	1.06	7.57	638	2.35
3.48	303	1.08	7.72	645	2.40
3.54	304	1.10	7.88	642	2.45
3.64	304	1.13	8.03	652	2.49
3.79	306	1.18	8.23	655	2.56
4.06	308	1.26	8.44	661	2.62
4.30	309	1.34	8.61	666	2.67
4.53	310	1.41	8.78	673	2.73
4.73	311	1.47	9.01	670	2.80
4.97	315	1.54	9.25	684	2.87
5.11	314	1.59	9.45	694	2.94
5.27	315	1.64	9.69	703	3.01
5.46	319	1.70	9.93	712	3.08
5.61	321	1.74	10.08	735	3.13
5.76	327	1.79	10.32	738	3.21
5.93	332	1.84	10.51	745	3.26
6.12	342	1.90	10.75	750	3.34
6.21	354	1.93	11.09	753	3.44
6.30	387	1.96	11.41	759	3.54
6.38	433	1.98	11.74	762	3.65
6.37	427	1.98	12.06	764	3.74
6.46	486	2.01	12.46	768	3.87
6.53	519	2.03			

Table 17. Experimental Multilayer Data for
Krypton on Graphite at 77.8 K.
 $V_m = 3.22$ STP cc/gm

V_{ads} (STP cc/gm)	P (microns Hg)	θ
2.80	3.05	0.87
3.07	93.3	0.96
3.31	533	1.03
3.51	651	1.09
3.68	657	1.14
3.87	661	1.20
4.09	664	1.27
4.28	666	1.33
4.47	670	1.39
4.67	673	1.45
4.83	674	1.50
5.04	683	1.56
5.15	687	1.60
5.26	693	1.64
5.45	699	1.69
5.63	710	1.75
5.78	725	1.80
5.92	745	1.84
6.03	816	1.87
6.14	946	1.91
6.13	914	1.90
6.25	1061	1.94
6.36	1117	1.98
6.50	1203	2.02
6.63	1270	2.06

LITERATURE CITED

1. J. H. de Boer and J. C. P. Broekhoff, Proc. Koninkl. Ned. Akad. Wetenschap, B 70, 326 (1967).
2. B. W. Davis and C. Pierce, J. Phys. Chem., 70, 1051 (1966).
3. C. F. Prenzlow and G. D. Halsey, Jr., J. Phys. Chem., 61, 1158 (1957).
4. B. J. Alder and T. E. Wainwright, Phys. Rev., 127, 359, (1962).
5. S. Ross and J. P. Olivier, "On Physical Adsorption," Interscience Publishers, New York, New York, 1964.
6. D. M. Young and A. D. Crowell, "Physical Adsorption of Gases," Butterworths, London, 1962.
7. J. J. McAlpin and R. A. Pierotti, J. Chem. Phys., 41, 68 (1964).
8. J. J. McAlpin and R. A. Pierotti, J. Chem. Phys., 42, 1842 (1965).
9. J. J. McAlpin, Ph.D. Thesis, Georgia Institute of Technology (1966).
10. S. Brunauer, P. H. Emmett, and E. Teller, J. Amer. Chem. Soc., 60, 309, (1938).
11. E. L. Pace, J. Chem. Phys., 27, 1341 (1957).
12. R. A. Pierotti and H. E. Thomas in Egon Matijevic, Ed., "Surface and Colloid Science," Vol. IV, Wiley-Interscience, New York, 1971, p. 93.
13. R. A. Pierotti, J. Phys. Chem., 66, 1810 (1962).
14. A. C. Levy, Masters Thesis, Georgia Institute of Technology, (1966).
15. T. L. Hill, "Introduction to Statistical Thermodynamics," Addison-Wesley Publishing Company, Reading, Mass., 1960, p. 291.
16. H. Eyring, T. Ree, and N. Hirai, Procedures National Acad. of Sciences U. S., 44, 683 (1958).
17. D. Henderson, J. Chem. Phys., 39, 1857 (1963).
18. H. Eyring and M. S. Jhon, "Significant Liquid Structures," Wiley, New York, 1969.

LITERATURE CITED (Continued)

19. H. Eyring and M. S. Jhon, "Significant Liquid Structures," Wiley, New York, 1969, p. 33.
20. J. R. Sams, G. Constabaris, and G. D. Halsey, Jr., J. Phys. Chem., 64, 1689 (1960).
21. S. Ross and J. P. Olivier, "On Physical Adsorption," Interscience Publishers, New York, New York, 1964, p. 123.
22. J. E. Lennard-Jones and A. F. Devonshire, Proc. Roy. Soc. (London) A 163, 53, (1937).
23. H. Eyring and M. S. Jhon, "Significant Liquid Structures," Wiley, New York, 1969, p. 32.
24. T. L. Hill, "Introduction to Statistical Thermodynamics," Addison-Wesley Publishing Company, Reading, Mass., 1960, p. 79.
25. D. M. Young and A. D. Crowell, "Physical Adsorption of Gases," Butterworths, London, 1962, p. 285.
26. H. Clark, J. Phys. Chem., 59, 1058 (1955).
27. F. W. Lytle and J. T. Stoner, Science, 148, 1721 (1965).
28. A. M. Clark, F. Din, and J. Robb, Physica, 17, 876 (1951).
29. S. Ross and J. P. Olivier, "On Physical Adsorption," Interscience Publishers, New York, New York, 1964, p. 41.
30. Ibid., p. 33.
31. J. H. Singleton and G. D. Halsey, Jr., J. Phys. Chem., 58, 330 (1954).
32. G. A. Miller, J. Phys. Chem., 67, 1359 (1963).
33. S. Ross and W. Winkler, J. Colloid Sci., 10, 330, (1955).
34. C. F. Prenzlow, H. R. Beard, and R. S. Brundage, J. Phys. Chem., 73, 969 (1969).
35. C. H. Amberg, W. B. Spencer, and R. A. Beebe, Can. J. Chem., 33, 305 (1955).
36. F. Tsien and G. D. Halsey, Jr., J. Phys. Chem., 71, 4012 (1967).
37. A. Thomy and X. Duval, Colloques Internationaux Du Center National de La Recherche Scientifique, No. 152, 1965.

LITERATURE CITED (Concluded)

38. A. P. Kharaukhov, Kinetika i Kataliz, 3, No. 4 (1962).
39. J. O. Hirschfelder, C. F. Curtiss, and R. B. Bird, "Molecular Theory of Gases and Liquids," Wiley, New York, 1954.
40. O. Sinanoglu and K. S. Pitzer, J. Chem. Phys., 32, 1279 (1960).
41. B. F. Figgins and B. L. Smith, Phil. Mag., 5, 186 (1960).

VITA

David Sanford Newsome was born April 13, 1943, in Charleston, South Carolina to Nellie Hayes and Mike Newsome. He was reared in North Charleston, South Carolina and graduated from North Charleston High School in June 1961. He entered the College of Charleston in September, 1961, and received the degree Bachelor of Science in chemistry in June 1965. After completion of his undergraduate work he entered the graduate division of Georgia Tech to study for the Doctor of Philosophy in the School of Chemistry. During his graduate work he held a NDEA fellowship for three years, received a Project THEMIS grant for one year, and was a teaching assistant for one year.